A Genome-Wide Arrayed CRISPR Screen Reveals PLSCR1 as an Intrinsic Barrier to SARS-CoV-2 Entry

Authors

Jérémie Le Pen[1,*], Gabrielle Paniccia[1,*], Michael Bauer[1,#], H.-Heinrich Hoffmann[1,#], Volker Kinast[2,3,#], Marcela Moncada-Velez[4,#], Ana Pinharanda[5,#], Inna Ricardo-Lax[1,#], Ansgar F. Stenzel[1,6,#], Edwin A. Rosado-Olivieri[7,8,#], Alison W. Ashbrook[1], Kenneth H. Dinnon[1], William C. Doyle[1,9], Catherine A. Freije[1], Seon-Hui Hong[1], Danyel Lee[4,10,11], Tyler Lewy[1], Joseph M. Luna[1,12], Avery Peace[1], Carltin Schmidt[4], William M. Schneider[1], Roni Winkler[1], Chloe Larson[13], Timothy McGinn[13], Miriam-Rose Menezes[13], Lavoisier Ramos-Espiritu[13], Priyam Banerjee[14], John T. Poirier[15], Francisco J. Sànchez-Rivera[16,17], Qian Zhang[4], Jean-Laurent Casanova[4,10,11,18,19], Thomas S. Carroll[20], J. Fraser Glickman[13], Eleftherios Michailidis[1,21,§], Brandon Razooky[1,22,§], Margaret R. MacDonald[1,§], Charles M. Rice[1,§]

[*] Contributed equally to this work
[#] Contributed equally to this work
[§] Contributed equally to this work

Correspondence: Jérémie Le Pen: jlepen@rockefeller.edu; Charles M. Rice: ricec@rockefeller.edu

Affiliations:
1. Laboratory of Virology and Infectious Disease, The Rockefeller University, New York, NY, USA.
2. Department of Medical Microbiology and Virology, Carl von Ossietzky University Oldenburg, Oldenburg, Germany.
3. Department for Molecular and Medical Virology, Faculty of Medicine, Ruhr University Bochum, Bochum, Germany.
4. St Giles Laboratory of Human Genetics of Infectious Diseases, Rockefeller Branch, The Rockefeller University, New York, NY, USA.
5. Department of Biological Sciences, Columbia University, New York, NY 10027, USA.
6. Present address: Department of Infectious Diseases, Molecular Virology, Heidelberg University, Heidelberg, Germany.
7. Laboratory of Synthetic Embryology, The Rockefeller University, New York, NY, USA.
8. Present address: Department of Molecular Pathobiology, New York University.
9. Present address: Laboratory of Host-Pathogen Biology, The Rockefeller University, New York, NY, USA.

10. Laboratory of Human Genetics of Infectious Diseases, Necker Branch, INSERM U1163, Paris, France, EU.
11. University of Paris, Imagine Institute, Paris, France, EU.
12. Present address: Department of Biochemistry and Center for RNA Science and Therapeutics, Case Western Reserve University, Cleveland, OH, USA.
13. Fisher Drug Discovery Resource Center, The Rockefeller University, New York, NY, USA.
14. Bio-Imaging Resource Center, The Rockefeller University, New York, NY, USA.
15. Laura and Isaac Perlmutter Cancer Center, New York University Grossman School of Medicine, NYU Langone Health, New York, NY.
16. Department of Biology, Massachusetts Institute of Technology, Cambridge, 02142, Massachusetts, USA.
17. David H. Koch Institute for Integrative Cancer Research, Massachusetts Institute of Technology, Cambridge, 02142, Massachusetts, USA.
18. Department of Pediatrics, Necker Hospital for Sick Children, Paris, France, EU.
19. Howard Hughes Medical Institute, New York, NY, USA.
20. Bioinformatics Resource Center, The Rockefeller University, New York, NY, USA.
21. Present address: Laboratory of Biochemical Pharmacology, Department of Pediatrics, Emory University School of Medicine, Atlanta, GA, USA.
22. Present address: National Resilience, Inc., La Jolla, CA, USA.

Abstract

Interferons (IFNs) play a crucial role in the regulation and evolution of host-virus interactions. Here, we conducted a genome-wide arrayed CRISPR knockout screen in the presence and absence of IFN to identify human genes that influence SARS-CoV-2 infection. We then performed an integrated analysis of genes interacting with SARS-CoV-2, drawing from a selection of 67 large-scale studies, including our own. We identified 28 genes of high relevance in both human genetic studies of COVID-19 patients and functional genetic screens in cell culture, with many related to the IFN pathway. Among these was the IFN-stimulated gene *PLSCR1*. PLSCR1 did not require IFN induction to restrict SARS-CoV-2 and did not contribute to IFN signaling. Instead, PLSCR1 specifically restricted spike-mediated SARS-CoV-2 entry. The PLSCR1-mediated restriction was alleviated by TMPRSS2 over-expression, suggesting that PLSCR1 primarily restricts the endocytic entry route. In addition, recent SARS-CoV-2 variants have adapted to circumvent the PLSCR1 barrier via currently undetermined mechanisms. Our study contributes to understanding the association between PLSCR1 variants and severe COVID-19 cases reported in a recent GWAS.

Introduction

Viruses maintain a complex relationship with their host cells, co-opting host factors for their replication while being targeted by cellular defense mechanisms. Such cellular defenses include the interferon (IFN) pathway, where the infected cell senses foreign molecules and secretes IFN to trigger an antiviral state in neighboring cells.

Approximately 1-5% of critical COVID-19 patients have mutations that compromise the production of or response to type I IFNs, while an additional 15% possess autoantibodies that neutralize type I IFNs [1-7]. This highlights the essential role of type I IFN in the defense against

77 the SARS-CoV-2 virus that caused the COVID-19 pandemic [8, 9]. Consequently, investigating IFN-
78 stimulated genes (ISGs) is crucial to our understanding of the remarkable antiviral systems that
79 evolved in nature. This knowledge could enhance our preparedness for future pandemics.
80 Several recent studies have identified ISGs restricting SARS-CoV-2. Most of these studies
81 involved gain-of-function genetic screens, over-expressing individual ISGs. The factors bone
82 marrow stromal cell antigen 2 (BST2), cholesterol 25-hydroxylase (CH25H), lymphocyte antigen 6
83 family member E (LY6E), 2'-5'-oligoadenylate synthetase 1 (OAS1), and receptor transporter
84 protein 4 (RTP4) were notably identified as SARS-CoV-2 antivirals in these studies [9-14]. One
85 advantage of the gain-of-function approach is that it circumvents potential genetic redundancies
86 between ISGs [15, 16]. However, this approach is biased towards ISGs that act autonomously
87 when over-expressed and does not mimic the cellular context of the IFN response, where
88 hundreds of genes and gene products are differentially regulated to establish an antiviral state.
89 To counter this limitation, two recent publications examined the effects of ISG loss of function in
90 IFN-treated cells. They conducted pooled CRISPR knockout (KO) screens in cells pre-treated with
91 IFN before SARS-CoV-2 infection [17, 18]. By sorting for cells with high SARS-CoV-2 viral load, they
92 identified SARS-CoV-2 restriction factors such as death domain associated protein (DAXX).
93 Here, we conducted a human whole-genome arrayed CRISPR KO screen to identify genes
94 that influence SARS-CoV-2 infection in cells with or without pretreatment with a low dose of IFN.
95 The arrayed approach, though logistically challenging, has advantages over the pooled format in
96 capturing both proviral and antiviral genes, genes affecting virus egress, and those coding for
97 secreted products that exert their impact on neighboring cells. It reliably captures genotype-
98 phenotype correlations while also unveiling the effects of single gene perturbation on cell growth
99 and death [19]. We then compiled a comprehensive list of genes interacting with SARS-CoV-2,
100 incorporating findings from our own screen as well as existing literature. This meta-analysis
101 revealed several host genes of interest, both previously described and novel. Notably, the ISG
102 product phospholipid scramblase 1 (PLSCR1) emerged as a prominent antiviral factor. PLSCR1 is
103 involved in several biological processes [20], including regulating the movement of phospholipids
104 between the two leaflets of a cell membrane (lipid scrambling) [21] and IFN signaling in the
105 context of virus infection [22]. Follow-up experiments revealed that PLSCR1 is a cell intrinsic factor
106 that restricts spike-mediated SARS-CoV-2 entry, independently of the IFN pathway, via currently
107 undetermined mechanisms. Our genetic screen data and meta-analysis provide a valuable
108 resource to broaden our understanding of coronavirus infection and innate immunity.
109 Furthermore, we extend the recent characterization of PLSCR1 as an antiviral against SARS-CoV-
110 2 impacting COVID-19 outcomes (**Fig. 1**)[18, 23, 24].

111 Results

112 A genome-wide arrayed CRISPR KO screen identifies known and novel factors influencing 113 SARS-CoV-2 infection.

114 While the liver is not the primary target organ of SARS-CoV-2 infection, human
115 hepatocellular carcinoma Huh-7.5 cells naturally express SARS-CoV-2 dependency factors,
116 including the receptor angiotensin converting enzyme 2 (ACE2), and proved unexpectedly useful
117 in SARS-CoV-2 research [18, 25-32]. Huh-7.5 cells do not produce IFN during SARS-CoV-2 infection,

but they do induce an antiviral state in response to IFN pretreatment (**Fig 2A-2C, Supp Tables 1-4**), making them a convenient model to control the exposure of the cells to IFN.

Using these cells, we conducted a whole-genome arrayed CRISPR KO screen designed to identify both SARS-CoV-2 proviral and antiviral genes, whose KO reduces or enhances SARS-CoV-2 infection, respectively. In particular, we aimed to identify factors involved in the IFN response, from IFN sensing to ISG induction, including effector ISGs that directly influence the virus life cycle. With this arrayed approach performed in 384-well plates, the cells in each well received a pool of four gRNAs targeting a single host gene. Each well was then either treated with 1 pM IFN-α2a or left untreated before being infected with SARS-CoV-2, followed by SARS-CoV-2 nucleoprotein (N) immunofluorescence staining and high content microscopy (**Fig 2D**). This low dose of IFN was chosen to mimic a cellular environment where IFN triggers an antiviral state before infection. We anticipated that a saturating amount of IFN would lead to high ISG transcription and functional redundancy between effectors, biasing hits towards factors in IFN signaling. In contrast, a low dose of IFN, around the IC50, might enable identification of the specific roles of individual effector ISGs.

Of the 16,790 screened genes, we selected 16,178 genes where KO did not lead to changes in cellular fitness assessed by nuclei count ($-2 \leq$ z-score ≤ 2)(**Supp Fig 1A**). Of these, we selected 12,119 genes expressed in three cell lines relevant for SARS-CoV-2 research (A549, Calu-3, Huh-7.5 cells) and human lung cells, the primary target cell type *in vivo*, for downstream analysis [33-35]. We then binned the genes into two groups for data visualization, depending on whether they were induced by IFN-α2a treatment in Huh-7.5 cells as determined by mRNA-seq (log 2 FC ≥ 2 and padj ≤ 0.05) (**Supp Fig 1B, Supp Tables 5-7**).

Our screen found known and previously unidentified host factors influencing SARS-CoV-2 infection (**Fig 2E**). As expected, positive regulators of IFN signaling, such as interferon-alpha/beta receptor alpha chain 1 and 2 (IFNAR1,2) [36-38], interferon regulatory factor 9 (IRF9) [39, 40], Janus kinase 1 (JAK1) [41], and signal transducer and activator of transcription 2 (STAT2) [42, 43] were antiviral only in IFN pretreated cells. Known negative regulators of IFN signaling, such as ISG15 ubiquitin-like modifier (ISG15) [44-46], suppressor of cytokine signaling 1 (SOCS1) [47], and ubiquitin specific peptidase 18 (USP18) [48, 49] were proviral only in IFN pretreated cells.

The SARS-CoV-2 receptor ACE2 was confirmed as proviral with or without IFN pretreatment. In our mRNA-seq analysis, IFN treatment was found to significantly upregulate ACE2 mRNA levels (**Supp Fig. 1B**). Prior studies indicate that IFN induces transcription of a truncated ACE2 isoform, rather than the full-length receptor for SARS-CoV-2 [50, 51].

The lysosomal cysteine protease cathepsin L (CTSL), required for SARS-CoV-2 spike protein activation [52-54], was a proviral hit in our screens. In contrast, KO of the cell-surface transmembrane serine protease 2 (TMPRSS2) did not influence infection, suggesting that SARS-CoV-2 particles primarily enter Huh-7.5 cells through the endocytic pathway that does not depend on TMPRSS2 (**Fig 1**) [55, 56].

The screen data likely contains false negatives. For example, STAT1 and tyrosine kinase 2 (TYK2) [57, 58] did not influence infection alongside other positive regulators of IFN signaling, which we attribute to the fact that some gRNAs in the library may have not efficiently directed Cas9 to cut at their respective target gene loci.

Collectively, the identification of known proviral and antiviral factors confirms the validity of our screening method.

We performed a Gene Set Enrichment Analysis (GSEA) to identify cellular pathways exhibiting proviral or antiviral properties in our screen. The full GSEA results, including the genes driving each pathway enrichment (so-called *leading edge*), can be found in **Supp Table 8**. Some top pathways ranked by adjusted p-value are summarized in **Fig 2F**. Notably pathways associated with RNA pol II transcription and mRNA maturation, as well as pathways related to cellular respiration, exhibited antiviral activity independent of IFN. Surprisingly, pathways associated with RNA pol III transcription, in part driven by the genes RNA polymerase III subunit A (*POLR3A*) and RNA polymerase III subunit B (*POLR3B*), were critical to the antiviral response mediated by IFN. Conversely, factors involved in translation, such as eukaryotic translation initiation factor 3 subunits F and G (EIF3G and EIF3F), likely co-opted for producing viral proteins, were identified as proviral. Similarly, factors regulating cholesterol homeostasis, likely crucial for SARS-CoV-2 entry [13, 59], were also identified as proviral. For instance, the gene sterol regulatory element binding transcription factor 2 (*SREBF2*) was one of the top proviral genes (**Fig 2E**).

Our arrayed CRISPR KO screen results thus constitute a valuable resource for research on coronavirus infection and innate immunity. These can be used to help characterize human genes influencing SARS-CoV-2 infection and the IFN response.

The ISG PLSCR1 is associated with COVID-19 outcomes and exhibits antiviral effects in functional SARS-CoV-2 genetic screens

To provide a thorough perspective on human genes that impact SARS-CoV-2 infection and to place our arrayed CRISPR KO screen results within the context of existing research, we have compiled a table that includes findings from a selection of 67 large-scale 'omic' studies related to SARS-CoV-2. This compilation encompasses this study and 25 other functional genetic screens for genes that influence SARS-CoV-2 infection [10-12, 14, 17, 18, 26, 29, 60-76], 24 human genetic studies that correlate certain alleles with severe COVID-19 outcomes [4, 5, 7, 23, 24, 77-95], ten publications detailing SARS-CoV-2 protein interactomes [96-105], six focusing on SARS-CoV-2 RNA interactomes [106-111], and one that examines proteins with altered phosphorylation states in SARS-CoV-2-infected cells [112] **(Supp Tables 9-10 for the full, and summary tables, respectively)**. This table highlights the depth of research in publications addressing SARS-CoV-2 infection: genes reported in several independent large-scale studies are more credible candidates for biological relevance (**Supp Fig 2**). As expected, genes associated with the IFN pathway, such as *IFNAR2*, *OAS1*, and *ZC3HAV1/ZAP*, frequently emerged as significant in SARS-CoV-2 studies.

We focused on 28 genes identified in both human genetic studies of COVID-19 patients and in functional genetic screens in cell culture, including our own (**Fig 3**). These genes are likely to have significant physiological relevance and to be well-suited for mechanistic studies in cell culture. Among these, the ISG *PLSCR1* stood out, being identified as one of the most potent antiviral genes in our screen (**Fig 2E**). *PLSCR1* variants have been linked to severe COVID-19 in a recent GWAS (listed in **Table 1**)[23, 24]. This was attributed to a role of PLSCR1 in regulating the IFN response in COVID-19 patients [24]. Indeed, a pioneering study showed that PLSCR1 potentiates the transcriptional response to IFN-β treatment in human ovarian carcinoma Hey1B cells [22]. However, PLSCR1 surprisingly appeared as a potent SARS-CoV-2 antiviral even in the absence of IFN in our screens, suggesting a cell intrinsic, IFN-independent function. In other words, baseline levels of PLSCR1 may be sufficient to restrict SARS-CoV-2, and IFN pretreatment could simply enhance this effect by elevating cellular PLSCR1 levels.

206

207 ## Intrinsic PLSCR1 restricts SARS-CoV-2 independently of the IFN pathway.

208 To better characterize the function of PLSCR1 during SARS-CoV-2 infection, we generated
209 and validated by western blot (WB) PLSCR1 KO bulk Huh-7.5 and A549-ACE2 lines (**Supp Fig 3A**).
210 As observed in the arrayed screen (**Supp Fig 1A**), PLSCR1 KO cells were viable (**Supp Fig 3B**).
211 PLSCR1 depletion increased susceptibility to SARS-CoV-2 independently of IFN pretreatment (**Fig**
212 **4A**). Cell treatment with a JAK-STAT inhibitor, which effectively abrogated IFN signaling, confirmed
213 that intrinsic PLSCR1 limits SARS-CoV-2 infection independently of the IFN signaling pathway (**Fig**
214 **4A**). SARS-CoV-2 susceptibility of PLSCR1 KO cells was reversed by the ectopic expression of
215 PLSCR1 (**Fig 4B, Supp Fig 3C**). Interestingly, while PLSCR1 tagged with an N-terminal FLAG tag
216 could rescue, PLSCR1 tagged with a C-terminal FLAG tag could not. The C-terminus of the protein
217 is extracellular, and previous research suggests that this region is important for the protein's
218 scramblase activity and Ca^{2+} binding [113]. It is possible that the addition of this FLAG-tag
219 impaired Ca^{2+} binding, affected PLSCR1's localization at the plasma membrane, or otherwise
220 disrupted the structure of this region, thereby abolishing PLSCR1's antiviral ability. We co-cultured
221 PLSCR1 reconstituted cells and PLSCR1 KO cells in the same well and infected them with SARS-
222 CoV-2. A higher proportion of PLSCR1 KO than PLSCR1 reconstituted cells were positive for SARS-
223 CoV-2 indicating that PLSCR1 acts in a cell autonomous manner (**Fig 4C**). Altogether, these data
224 suggest that intrinsic PLSCR1 contributes to the restriction of SARS-CoV-2, even without IFN.

225

226 ## IFN signaling is unaffected by the loss of PLSCR1 in A549-ACE2 and Huh-7.5 cells.

227 PLSCR1 has been shown to potentiate ISG transcription in IFN-treated Hey1B cells [22].
228 We thus hypothesized PLSCR1 might enhance the type I IFN response in A549-ACE2 and Huh-7.5
229 cells. We investigated PLSCR1's role in the IFN response by infecting Huh-7.5 cells with
230 chikungunya virus (CHIKV), which is unaffected by PLSCR1 KO without IFN (**Fig 5A**). PLSCR1
231 depletion did not functionally affect the antiviral effects of IFN treatment (**Fig 5B**). Furthermore,
232 IFN treatment induced *OAS1* and *IFI6*, two ISGs known to restrict SARS-CoV-2 [10, 12, 17, 91, 92,
233 94, 95], to a similar extent in both WT and PLSCR1 KO cells, indicating that the IFN signaling
234 pathway was unaffected by PLSCR1 depletion (**Fig 5C-J**). Finally, PLSCR1 depletion did not alter
235 basal ISG transcription in the absence of IFN (**Supp Fig 4**).

236 These findings indicate that PLSCR1 limits SARS-CoV-2 infection independently of the IFN
237 signaling pathway in A549-ACE2 and Huh-7.5 cells.

238

239 ## PLSCR1 restricts SARS-CoV-2 entry.

240 We hypothesized that PLSCR1 directly targets and inhibits a specific step of the SARS-CoV-
241 2 life cycle. PLSCR1 primarily localized at the plasma membrane in Huh-7.5 cells (**Fig 6A**).
242 Furthermore, PLSCR1 depletion led to increased SARS-CoV-2 foci formation (**Fig 6B,C**), and PLSCR1
243 KO cells did not show increased susceptibility to a SARS-CoV-2 replicon system that bypasses entry
244 (**Fig 6D**) [114]. In contrast, a single-cycle, replication-defective human immunodeficiency virus
245 type-1 (HIV-1) particles pseudo-typed with SARS-CoV-2 spike showed enhanced entry in PLSCR1
246 depleted cells (**Fig 6E, F**) [115]. This data indicates that PLSCR1 restricts SARS-CoV-2 spike-
247 mediated virion entry. Over-expression of TMPRSS2 lifted the PLSCR1-mediated restriction of
248 authentic SARS-CoV-2 (**Fig 6G-I**) and of SARS-CoV-2 spike pseudo-typed particles (**Fig 6J-M**),

249 indicating that PLSCR1 primarily restricts the endosomal entry route. It is possible that the
250 TMPRSS2-dependent entry near the cell surface provides SARS-CoV-2 with some level of evasion
251 from PLSCR1 restriction, as recently described for the ISG NCOA7 [116].
252 In addition to SARS-CoV-2, we also evaluated the antiviral activity of PLSCR1 against ten
253 viruses that utilize endosomal entry: CHIKV, human parainfluenza virus (hPIV), herpes simplex
254 virus 1 (HSV-1), influenza A virus (IAV), human coronavirus OC43 (hCoV-OC43), human
255 coronavirus NL63 (hCoV-NL63), human coronavirus 229E (hCoV-229E), Sindbis virus (SINV),
256 Venezuelan equine encephalitis virus (VEEV), and vesicular stomatitis virus (VSV). Only SARS-CoV-
257 2 showed a notable susceptibility to PLSCR1's inhibitory effects (**Supp Fig 5**).
258

259 ## Recent variants of SARS-CoV-2 are less restricted by PLSCR1

260 During the COVID-19 pandemic, SARS-CoV-2 variants evolved from the initial strain,
261 showing increased immune evasion and transmissibility [117-119]. To examine if these variants
262 could circumvent the antiviral action of PLSCR1, we infected WT and PLSCR1 KO Huh-7.5 cells with
263 an early strain isolated in July 2020 (NY-RU-NY1) and the Beta (B.1.352), Delta (B.1.617.2),
264 Omicron (BA.5), and Kraken (XBB.1.5) variants **(Fig 7A-E)**. Although PLSCR1 continued to restrict
265 these later variants, the discrepancy in infection rates between WT and PLSCR1 KO cells
266 diminished compared to the original strain, notably with the Omicron and its descendant, Kraken
267 **(Fig 7F)**. We then infected WT and PLSCR1 KO Huh-7.5 cells with the same focus-forming units
268 (FFU) of each virus, as determined in PLSCR1 KO cells, and conducted a focus forming assay. The
269 ratio of foci in WT cells relative to KO cells increased for later variants, especially for the Omicron
270 subvariant Kraken (XBB.1.5) **(Fig 7G)**. Our data suggests a diminished efficacy of PLSCR1 in
271 restricting the newer SARS-CoV-2 variants.
272

273 ## Association between PLSCR1 variants and severe COVID-19

274 PLSCR1 encodes a 318 amino acid protein containing a palmitoylation motif and a
275 transmembrane domain which regulate its plasma membrane localization, and a nuclear
276 localization signal (NLS) and transcriptional activation domain thought to be important for its
277 nuclear functions (**Fig 8A**)[20, 120-125].
278 A recent GWAS has identified an association between PLSCR1 variants and severe COVID-
279 19 outcomes, reporting an odds ratio of approximately 1.2 and a p-value of approximately 10^{-8}
280 (**Table 1**)[23, 24]. In other words, the GWAS suggests that PLSCR1 has a small, but significant effect
281 on severe COVID-19 risks.
282 GWAS typically identify variants associated with increased odds of a disease, but these
283 variants are not necessarily causative. Among the PLSCR1 variants identified in the COVID-19
284 GWAS cited above, only rs343320 results in a protein-coding change, specifically His262Tyr,
285 located in the NLS (**Fig 8A**, **Table 1**). Although we cannot dismiss the possibility that (i) some non-
286 coding variants identified in the GWAS could influence the regulation of *PLSCR1* mRNA,
287 potentially leading to functional outcomes, and (ii) the GWAS might have missed nonsynonymous
288 variants impacting PLSCR1 function, we thought to investigate the functional effects of the
289 His262Tyr variant in cell culture. We ectopically expressed PLSCR1 His262Tyr or PLSCR1 WT in
290 A549-ACE2 cells from a lentiviral vector [126]. PLSCR1 His262Tyr and PLSCR1 WT were expressed
291 at similar levels in this system (**Supp Fig 6**). PLSCR1 His262Tyr did not fully rescue the PLSCR1 KO

292 (**Fig 8B**), indicating that the His262Tyr variant is hypomorphic. Additionally, introducing PLSCR1
293 His262Tyr into cells already expressing PLSCR1 WT increased their susceptibility to SARS-CoV-2
294 infection (**Fig 8B**), suggesting a dominant effect. However, this effect might be attributed to the
295 overexpression of PLSCR1 His262Tyr from the transgene, compared to the natural expression
296 levels of PLSCR1 WT from the endogenous locus. To counter this, we examined patient-derived
297 SV40-immortalized fibroblasts expressing ACE2 that were heterozygous for His262Tyr. These cells
298 were hyper-susceptible to SARS-CoV-2 infection compared to PLSCR1 WT control SV40-fibroblasts
299 (**Fig 8C**), further suggesting that His262Tyr is dominant. We cannot formally rule out that the
300 examined SV40-fibroblasts may carry other mutations influencing SARS-CoV-2 infection.
301 Our data collectively highlight PLSCR1's function in restricting SARS-CoV-2 entry in cell
302 culture, thereby clarifying the association between PLSCR1 variants and severe COVID-19
303 outcomes [23, 24]. Future human genetic studies are crucial for determining if certain PLSCR1
304 variants in the population cause increased risks of severe COVID-19. Our results highlight the
305 variant rs343320 (His262Tyr) as a potential causative candidate, as it caused increased SARS-CoV-
306 2 infection in cell culture.

307 Discussion

308 Here, we conducted an unbiased arrayed CRISPR KO screen on Huh-7.5 cells infected with
309 SARS-CoV-2. The screen revealed novel aspects of SARS-CoV-2 and IFN biology while also
310 confirming previously known facets. Pathways related to mRNA transcription and maturation
311 were identified as antiviral. This observation may stem from the conflict between the host cell
312 and SARS-CoV-2, where the host attempts to export mRNAs from the nucleus to facilitate antiviral
313 responses while the virus replicates in the cytoplasm, impeding nuclear export [127-130]. RNA
314 Pol III transcription was specifically essential for the IFN-mediated antiviral response, through
315 mechanisms that are yet to be determined. Interestingly, inborn errors in POLR3A and POLR3C
316 have been previously described in patients with severe varicella zoster virus infections [131].
317 Cellular respiration was identified as a key IFN-independent antiviral pathway. Furthermore,
318 mitophagy was identified as proviral. This may indicate the infected cell's increased demand for
319 energy and ATP to combat the virus. Alternatively, cellular respiration may have other, yet-to-be-
320 identified, IFN-independent antiviral roles. Conversely, translation and cholesterol homeostasis
321 emerged as the foremost proviral pathways. These findings underscore the complex, dualistic
322 nature of the interactions between SARS-CoV-2 and host cells.
323 Our screen notably identified the ISG zinc-finger antiviral protein (*ZC3HAV1*/*ZAP*) as a
324 proviral factor in IFN-treated cells. Initially, ZC3HAV1/ZAP gained attention as an antiviral factor
325 that targets the SARS-CoV-2 RNA genome [111] and prevents programmed ribosomal
326 frameshifting [132]. Yet, a recent study demonstrated that ZC3HAV1/ZAP also promotes the
327 formation of SARS-CoV-2 non-structural proteins 3 and 4-induced double-membrane vesicles,
328 essential for virus replication [68]. SARS-CoV-2 may have adapted to exploit certain ISG products,
329 such as ZC3HAV1/ZAP, within the cellular environment it encounters. It is still unclear if the
330 seemingly contradictory roles of ZC3HAV1/ZAP – both proviral and antiviral – are caused by
331 distinct isoforms.
332 Many other ISG products influenced SARS-CoV-2 infection, PLSCR1 being the most potent
333 restriction factor. PLSCR1 did not influence ISG induction as previously reported [22], but rather
334 inhibited spike-mediated SARS-CoV-2 entry through the endocytic route. Our results corroborate

335 a recent study from Xu et al [18] and provide an explanation for the enrichment for PLSCR1 SNPs
336 observed in a GWAS on severe COVID-19 [23, 24].
337 The molecular mechanisms of PLSCR1-mediated restriction of SARS-CoV-2 entry remain
338 to be elucidated. PLSCR1 could be altering the lipid composition at the contact site between the
339 virus and endosomal membranes, akin to the ISG IFITM3 for influenza A virus [133-136]. PLSCR1
340 was first identified as a Ca^{2+}-dependent phospholipid scramblase [21], but it is unclear whether
341 PLSCR1 depletion affects the bidirectional movement of phospholipids *in vivo* [137-139]. A C-
342 terminal FLAG-tag abolished the antiviral ability of reconstituted PLSCR1, possibly by interfering
343 with the function of the Ca^{2+} binding domain. In contrast, inhibiting PLSCR1's phospholipid
344 scramblase activity did not alleviate SARS-CoV-2 restriction [18].
345 Intriguingly, PLSCR1 specifically restricted SARS-CoV-2 in Huh-7.5 and A549-ACE2 cells but
346 it did not show similar inhibitory effects on other viruses that enter cells via endocytosis. Future
347 studies will investigate the mechanisms behind this specificity. PLSCR1 has been described to
348 inhibit a range of viruses in various cell lines, such as encephalomyocarditis virus, vesicular
349 stomatitis virus, Epstein-Barr virus, hepatitis B virus, hepatitis C virus, human cytomegalovirus,
350 human immunodeficiency virus 1, human T-cell lymphotropic virus type 1, and influenza A virus
351 [22, 140-146]. It has been proposed that PLSCR1 directly binds viral proteins and impairs their
352 functions to restrict the non-coronaviruses cited above, reviewed in [147]. However, it seems
353 unlikely that PLSCR1 has evolved to interact directly with such a diverse set of viral proteins. An
354 alternative explanation is that diverse viral proteins convergently evolved to bind PLSCR1 as a
355 mechanism of immune evasion. Meanwhile, overexpressing PLSCR1 in cell culture could act *like*
356 *a sponge*, absorbing these viral proteins and thereby hindering viral function. We searched for
357 PLSCR1 interactions in ten SARS-CoV-2 proteins interactome studies, relying on ectopic expression
358 of individual viral proteins [96-98, 100-105, 148], and no interaction was reported in two or more
359 independent studies. Two interactions were reported in a single study: (i) PLSCR1-ORF7b [98],
360 and (ii) PLSCR1-ORF8 [101], both by proximity biotinylation, which was less stringent compared
361 to affinity purification-mass spectrometry (AP-MS) and yeast two-hybrid (Y2H) techniques (**Supp**
362 **Fig 7**). To date, there is no strong evidence of a direct interaction between a SARS-CoV-2 protein
363 and PLSCR1, although we cannot rule out that such interactions may occur or even appear in the
364 future as SARS-CoV-2 evolves.
365 Recent SARS-CoV-2 variants, including Omicron (BA.5) and Kraken (XBB.1.5), showed
366 reduced sensitivity to PLSCR1-mediated restriction compared to the New York 2020 strain which
367 served as a reference in our study. Previous research suggests that Omicron, in particular, has
368 developed increased resistance to IFN [149, 150], a trait associated with its highly-mutated spike
369 protein [151]. Omicron's relative resistance to IFN may be due to alternative entry routes that
370 alleviate the restrictions from antiviral ISGs targeting endocytosis, such as PLSCR1 (**Fig 1**). While
371 Omicron favors endocytic entry over TMPRSS-2-dependent entry near the cell-surface [152, 153],
372 recent findings suggest that Omicron can also utilize cellular metalloproteinases for near cell-
373 surface entry, enhancing its infectivity in nasal epithelia [151]. Future research should investigate
374 how SARS-CoV-2 variants evade PLSCR1 and whether this evasion is primarily due to mutations in
375 the spike protein facilitating alternative entry mechanisms or to other factors.
376 Several PLSCR1 variants were enriched in a GWAS on severe COVID-19, with a relatively
377 low odds ratio of approximately 1.2 [23, 24]. Considering the complex redundancies within
378 antiviral defenses, from innate immunity featuring multiple effector ISGs that restrict SARS-CoV-

379 2 [9-14, 17, 18], to adaptive immunity [154], the modest odds ratio associated with a single
380 effector ISG not involved in IFN signaling may not be unexpected. However, for these very reasons,
381 the identification of PLSCR1 in the GWAS remains noteworthy. Of these enriched PLSCR1 variants,
382 only rs343320 resulted in a protein-coding change, His262Tyr. Our findings indicate that His262Tyr
383 exhibits a hypomorphic and dominant effect in cell culture, leading to increased SARS-CoV-2
384 infection. Future research should aim to ascertain whether rs343320, or potentially other PLSCR1
385 variants, are directly responsible for elevated risks of severe COVID-19 in patients. It is also
386 noteworthy to mention the presence of a loss-of-expression/loss-of-function variant in PLSCR1,
387 specifically p.Ile110AsnfsTer6 (rs749938276). This variant exhibits a minor allele frequency (MAF)
388 of 0.0003 in the general population, yet it is notably more prevalent among the Ashkenazi Jewish
389 population, with a maximum MAF (MAFmax) of 0.01. The identification of at least one
390 homozygous individual in the gnomAD database underscores the viability of individuals deficient
391 in PLSCR1 [155]. This suggests a potential enrichment of this variant within specific populations,
392 an aspect that merits further epidemiological and functional exploration to understand its impact
393 on susceptibility to SARS-CoV-2.
394 Our findings show that baseline levels of PLSCR1 are effective in limiting SARS-CoV-2
395 infection. This is in line with other studies where ISGs like *DAXX* and *LY6E* were shown to inhibit
396 SARS-CoV-2 independently of IFN [17, 156, 157]. mRNA-seq analyses of Huh-7.5 cells and primary
397 human hepatocytes, as well as data from the GTEx consortium on various human tissues [35,
398 158], revealed that many ISGs are constitutively expressed, even without IFN stimulation (**Supp**
399 **Fig 8**). This supports the idea that the IFN-induced antiviral state results more from enhanced
400 expression of antiviral genes rather than a binary ON/OFF switch. In future studies, it will be
401 interesting to explore whether intrinsically expressed ISGs also carry out cellular functions beyond
402 pathogen defense.

403 Materials and Methods

404 Plasmids, oligos, and primers

405 The plasmids, gene fragments, and primers used in this study are listed in **Supp Tables**
406 **11, 12, and 13**, respectively.
407

408 Cell Lines

409 Huh-7.5 (human hepatocellular carcinoma) [159], A549-ACE2 (human lung carcinoma,
410 generously provided by the laboratory of Brad R. Rosenberg), Lenti-X 293T (Takara, cat. #632180),
411 Caco2, Vero E6 (*Chlorocebus sabaeus* kidney epithelial cells, ATCC cat. #CRL-1586), BHK-21
412 (hamster kidney) cells, and SV40-Fribroblasts were cultured in Dulbecco's Modified Eagle Medium
413 (DMEM, Fisher Scientific, cat. #11995065) supplemented with 0.1 mM nonessential amino acids
414 (NEAA, Fisher Scientific, cat. #11140076) and 10% fetal bovine serum (FBS, HyClone Laboratories,
415 Lot. #KTH31760) at 37°C and 5% CO2. All cell lines tested negative for mycoplasma.
416

417 Virus stocks

418 **CHIKV-181/25-mKate2:** the infectious clone was a kind gift from Mark Heise (University
419 of North Carolina, USA) [not published yet]. 20 µg of infectious clone DNA was linearized with
420 NotI-HF at 37°C overnight. Complete digestion was confirmed by running a sample of the digested

421 DNA on a 1% agarose gel. After confirmation, linearized DNA was cleaned via phenol-chloroform
422 extraction, and then ethanol precipitated. The precipitated DNA was resuspended in 20 µL of
423 RNase-free H_2O and in vitro transcribed with an SP6 mMessage mMachine In Vitro Transcription
424 Kit (ThermoFisher, cat. AM1340). The generated RNA was electroporated into 1.2 x 10^7 BHK-21
425 cells, and the produced virus was harvested once approximately 80% of the electroporated cells
426 lifted or showed signs of cytopathic effects and 100% of the cells were positive for mKate2 signal.
427 The titer of the virus was 8.5 x 10^6 focus-forming units (FFU) on Huh-7.5 cells.
428 **hCoV-NL63:** was generously provided by Volker Thiel (University of Bern) and amplified at
429 33°C in Huh-7.5 cells as in [29].
430 **hCoV-OC43**: was obtained from ZeptoMetrix (cat. #0810024CF) and amplified at 33°C in
431 Huh-7.5 cells as in [29].
432 **hPIV3-GFP** [160]: stock (based on strain JS) grown in VeroE6 cells as in [161].
433 **HSV-1-GFP**: stock made by passage on VeroE6 cells. 2 x 10^7 cells seeded in a T175 flask
434 were infected at an MOI of 0.01 PFU/ml of HSV-1-GFP virus engineered and provided by Ian Mohr
435 [162]. After a one-hour incubation at 37°C, the inoculum was removed, and 20 ml of DMEM
436 supplemented to contain 10% FBS and NEAA was added. Cells were incubated at 37°C for 24 h or
437 until CPE was evident. Cell supernatant containing progeny virus was harvested and titrated on
438 Vero E6 cells (2.4% avicel, fix 2 dpi) at 2.4 x 10^8 PFU/ml.
439 **IAV WSN (H1N1):** was generated in MDCK cells. Cells were inoculated at MOI 0.01 in
440 DMEM supplemented with NEAA, 0.2% BSA, 0.1% FCS, 50 mM Hepes, and 1 µg/ml TPCK-trypsin.
441 Virus-containing culture supernatant was harvested at 52 h post-infection and cleared by
442 centrifugation.
443 **SARS-CoV-2:** unless otherwise stated, the isolate SARS-CoV-2/human/USA/NY-RU-
444 NY1/2020 was used in this study [163]. The virus was sourced from the saliva of a deidentified
445 patient in New York City, collected on July 28, 2020. Its sequence is publicly accessible (GenBank
446 OM345241). The virus isolate was amplified in Caco-2 cells. The passage 3 stock employed had a
447 titer of 3.4 × 10^6 PFU/ml, as measured on Vero E6 cells using a 1% methylcellulose overlay,
448 according to previously described methods [164]. The Beta (B.1.351), Delta (B.1.617.2), Omicron
449 (BA.5), and Kraken (XBB.1.5) variants were obtained from BEI resources (cat. # NR-54008, NR-
450 55611, NR-58616, and NR-59104, respectively), amplified in Vero E6 cells engineered to stably
451 express TMPRSS2, and titer was determined as described above.
452 **SINV Toto1101** [165]: expressing an nsP3-mScarletI fusion reporter was generated by
453 cloning the sequence encoding mScarletI in frame into a unique SpeI restriction site in the
454 pToto1101 infectious clone plasmid as previously described [166]. *In vitro* transcribed, capped
455 RNA was generated from the pToto1101-nsP3-mScarletI plasmid (Invitrogen mMessage
456 mMachine SP6 kit, AM1340) and electroporated into BHK-J cells, a derivative of BHK-21 cells
457 (ATCC, CCL-10) as previously described [166]. 24 hours post electroporation, centrifuge clarified
458 supernatants were aliquoted and stored at -80C. BHK-J cells were cultured and virus stocks
459 generated in MEM supplemented with 7.5% FBS.
460 **VEEV-dsEGFP** [15, 167]: the infectious clone plasmid was linearized (MluI) and transcribed
461 *in vitro* using an mMessage mMachine SP6 transcription kit (Ambion). BHK-21 cells were
462 electroporated with viral RNA, and supernatant containing progeny virus was harvested after
463 incubation at 37°C for 30 h or until CPE was evident. Virus was titrated by plaque assay on BHK-
464 21 cells (2.4% avicel, fix 2 dpi). BHK-21: 1.45 x 10^9 FPU/ml.

465 **VSV-GFP** [168]: grown in BHK-21 cells as in [161].
466 **YFV 17D:** was generated via transfection of Huh-7.5 with in vitro transcribed RNA from
467 pACNR-FLYF-17D plasmid as described in [161].
468

469 mRNA-seq

470 mRNA-seq on SARS-CoV-2-infected cells

471 **Cell culture and infection:** 75,500 Huh-7.5 cells or 150,000 Calu-3 cells were seeded in
472 each well of a 12-well plate with 1 mL media. Media: DMEM with 5% FBS and 1% NEAA for Huh-
473 7.5 cells or EMEM (ATCC, 30-2003) with 10% FBS for Calu-3 cells. The next day, cells were infected
474 by removing 500 µL of media and adding 500 µL of media with SARS-CoV-2 strain USA-WA1/2020
475 (BEI Resources, NR-52281) at 5,000 PFU/well (virus titer determined in Huh-7.5 cells). After one
476 day, the wells were washed with PBS and cells were harvested in 1 mL TRIzol (Invitrogen, cat.
477 15596-018). N = 3 replicates (separate wells) per sample.
478 **RNA extraction:** 2 ml MaXtract High Density tubes (Qiagen, 129056) were centrifugated
479 at 12,000–16,000 x g for 20-30 second centrifugation. A volume of 750 µL TRIzol-prepared sample
480 was combined with 150 µL chloroform in these tubes and hand-shaken vigorously. Phase
481 separation was accomplished by centrifugation at 1500 x g for 5 min at 4°C. The aqueous phase
482 was then mixed with 400 µL ethanol 95-100% in a separate tube. These preparations were then
483 transferred to Zymo Research RNA clean and concentrator-25 kit columns (Zymo Research, cat.
484 R1018) and subjected to multiple wash and centrifugation steps as recommended by the
485 manufacturer. An in-column DNase I treatment was performed using Qiagen DNase (Qiagen,
486 79254). Finally, RNA was eluted with 50 µL DNase/RNase-Free water and stored at -80°C.
487 **Sequencing:** Poly-A enriched libraries were made using the TruSeq stranded mRNA LT kit
488 (Illumina, Cat# 20020594) and sequenced on a NovaSeq SP with PE150 read length.
489

490 mRNA-seq on IFN-treated cells

491 **Cell culture and treatment:** 75,500 Huh-7.5 or 200,000 Calu-3 cells were seeded in each
492 well of a 12-well plate with 1 mL media. Two days later, the media was replaced with 1 mL of
493 DMEM with 5%FBS, 1% NEAA in Huh-7.5 or EMEM (ATCC, cat. 30-2003) with 10% FBS for Calu-3
494 cells with IFN-α2a (PBL, cat. 11101-2) and incubated at 37°C. 24 h later, cells were harvested in
495 500 µL TRIzol. N = 3 replicates (separate wells) per sample.
496 **RNA extraction** as described above.
497 **Sequencing:** Poly A-enriched libraries were made using the NEBNext Ultra II RNA Library
498 Prep Kit for Illumina (NEB, cat. E7770) and sequenced on a NovaSeq SP with PE150 read length.
499

500 mRNA-seq on PLSCR1 KO cells

501 **Cell culture and CRISPR KO:** 30,000 Huh-7.5 cells were seeded in five wells of a 24-well
502 plate with 480 uL media. The cells were reverse transfected with 120 uL of a transfection mixture
503 composed of 250 nM of pooled anti-PLSCR1 or non-targeting Edit-R crRNAs from Horizon
504 Discovery (cat. CM-003729-01-0002, CM-003729-02-0002, CM-003729-03-0002, and CM-
505 003729-04-0002 or U-007501-01-05, U-007502-01-05, U-007503-01-05, and U-007504-01-05,
506 respectively) which had been resuspended with an equimolar amount of Edit-R tracrRNA
507 (Horizon, cat. U-002005-20) and a 1:200 dilution of Dharmafect 4 (Horizon, cat. T-2004-01). The

508 following day, the media was changed, and the cells were progressively scaled up to a 6-well plate
509 over the next 4 days. When the cells were confluent in the 6-well plate, the media was removed
510 from four of the wells. They were then washed with 1x PBS (cat. 14190-144) and lysed with 1 mL
511 TRIzol (Life Technologies, cat. 15596-018) for 5 minutes at room temperature before transferring
512 to an Eppendorf tube and freezing at -80°C to await RNA extraction. The remaining well was lysed
513 with 300 µL of RIPA buffer (Thermo cat. 89900) supplemented with 1x protease inhibitor (Thermo
514 cat. 87786) and 1x EDTA and prepared for western blot as described below, in the "Western Blots"
515 section.
516 **RNA extraction** as described above.
517 **Sequencing:** Poly A-enriched libraries were made using the NEBNext Ultra II RNA Library
518 Prep Kit for Illumina (NEB, cat. E7770) and sequenced on a NovaSeq SP with PE150 read length.
519

520 ### mRNA-seq analysis

521 mRNA-seq reads were first quality-filtered and adapter-trimmed using Trim Galore with
522 parameters -q 20 -e 0.1 --length 20 --paired and Cutadapt. Reads were then mapped to the human
523 genome GRCh38 or to a combined SARS-CoV-2 MN985325.1/human genome GRCh38 using STAR
524 [169] with settings including --runThreadN 8 --outFilterMultimapNmax 1 --twopassMode Basic.
525 Feature counting was performed using the featureCounts function from the Rsubread package
526 [170], with strandness specified depending on the sequencing and other parameters as default.
527 The resulting counts were imported into a DESeqDataSet object using the DESeq2 package [171]
528 with a design formula of ~Group. Size factors were estimated and normalized counts were
529 extracted and saved. Differential expression analysis was performed using DESeq with the created
530 DESeqDataSet object, contrasted by sample groups, cooksCutoff and independentFiltering
531 disabled, and otherwise default parameters.
532

533 ## Unbiased arrayed CRISPR KO screening

534 ### Screen overview

535 The content of each gRNA 384-well plate constituting the whole-genome library (61
536 library plates total) was transfected to 16 assay 384-well plates (976 assay plates total). Positive
537 and negative control gene gRNAs were incorporated into vacant wells of each assay plate as
538 described below. Huh-7.5 cells were subsequently seeded into these assay plates. The 16 assay
539 plates served as replicates for three distinct experimental conditions: 4 replicates for mock
540 treatment followed by mock infection, 5 replicates for IFN-α2a treatment followed by SARS-CoV-
541 2 infection, and 7 replicates for mock treatment followed by SARS-CoV-2 infection. Each day, three
542 library 384-well plates were processed, along with their corresponding 48 assay plates. The full
543 gRNA library, distributed across 61 384-well plates, was completed over a span of 21 days. For
544 each set of plates, cell seeding was conducted on day 0, IFN-α2a treatment on day 4, SARS-CoV-
545 2 infection on day 5, and cell fixation on day 6.

546 ### gRNA library preparation

547 A 0.1 nmol Edit-R Human Whole Genome crRNA Library (Horizon, cat. GP-005005-01)
548 containing four crRNAs per gene and one gene per well (total 0.1 nmol crRNA/well) was
549 resuspended in 80 µL of a 1.25 µM tracrRNA (Horizon, cat. U-002005-1000) 10 mM Tris-HCL pH
550 7.4 solution to create a 1.25 µM gRNA solution. The library was then aliquoted in 10 mM Tris-HCL

pH 7.4 in several 96-well plate and 384-well plate copies using a Tecan Freedom EVO liquid handler. A single-use library copy containing a 40 µL/well of a 312.5 nM gRNA solution in the 384-well plate format was used in this study.

gRNA reverse transfection (day 0)

In each well of the 384-well assay plates, 40 µL of a transfection solution was prepared by combining 2% DharmaFect-4 transfection reagent (Horizon, cat. GP-T-2004-07A) in Opti-MEM (Gibco, cat. 31985070). This was added to 40 µL of a 312.5 nM gRNA library using a Thermofisher Multidrop Reagent Dispenser, yielding an 80 µL/well transfection mixture. The mixture was left to incubate at room temperature for 20 minutes. Simultaneously, assay plates were preloaded with 11 µL/well of serum-free media, which was formulated from DMEM, 1X Antibiotic-Antimycotic solution (Gibco, cat. 15240-062), and 1X NEAA, dispensed via a Thermofisher Multidrop Reagent Dispenser. Subsequently, 4 µL/well of the transfection mixture was dispensed into each of the assay plates (16 assay plates per library plate) using a Tecan Freedom EVO liquid handler. During this time, Huh-7.5 cells were prepared in media containing 25% FBS, 1X Antibiotic-Antimycotic solution, and 1X NEAA. A volume of 10 µL cells/well was added to the assay plates, again using a Thermofisher Multidrop Reagent Dispenser. Ultimately, each well contained 1,250 cells in a 25 µL final volume, with a composition of 25 nM gRNA, 10% FBS, 0.8X Antibiotic-Antimycotic, and 0.8X NEAA. Plates were then span at 200 g for 5 minutes. To minimize evaporation, plates were sealed with Breathe-Easy sealing membranes (Sigma-Aldrich, cat. Z380059) and placed in humid chambers constructed from a 245 mm x 245 mm dish containing a paper towel moistened with 15 mL of 1X Antibiotic-Antimycotic solution. Four assay plates were placed in each humid chamber and incubated at 37°C.

IFN-α2a treatment (day 1)

Each well received 5 µL of IFN-α2a (PBL, cat. 11101-2) in media (DMEM, 20% FBS, 1X Antibiotic-Antimycotic solution, 1X NEAA), using a Thermofisher Multidrop Reagent Dispenser, for a final concentration of 1 pM IFN-α2a in a final volume of 30 µL. Plates were then span at 200 g for 5 minutes and incubated at 37°C.

SARS-CoV-2 infection (day 5)

Each well received 212.5 PFU SARS-CoV-2 virus (titer determined on Vero E6 cells, see Virus Stocks section above) diluted in 5 µL of media (DMEM, 20% FBS, 1X Antibiotic-Antimycotic solution, 1X NEAA) for a final volume of 35 µL in the BSL3. Plates were then span at 200 g for 5 minutes and incubated at 37°C.

Fixing (day 6)

Each well received 50 µL of 20% neutral buffered formalin (Azer Scientific, cat. 20NBF-4-G) and plates were incubated overnight. The formalin mixture was then removed and each well received 50 µL of PBS.

IF staining

For IF staining of SARS-CoV-2 infected cells in the arrayed CRISPR KO screen (**Fig 1E)**, as well as some focused experiments (**Fig 3B**, **Fig 3C**, **Fig 4B,C**, **Fig 8C)**: the following solutions were prepared for both 96-well plate (96-wp) and 384-well plate (384-wp): PBS (Phosphate Buffered Saline), Perm Solution: Comprised of PBS with an added concentration of 0.1% Triton X100, Blocking Solution: PBS was mixed with 1% BSA. This solution was prepared a day in advance and filtered before use, PBST: PBS with 0.1% of Tween 20, Primary Antibody Solution: Genetex anti

SARS-CoV-2 N poly rabbit antibody (GTX135357) at a dilution of 1:3000, Secondary Antibody Solution: AF647 anti-rabbit antibodies at a dilution of 1:3000 and Hoechst 33342 (10 mg/ml) at 1:10,000. Plates were stained on a Biotek EL406 Microplate Washer Dispenser using the following steps: 1. Priming: The washer was primed with 200 ml of each buffer: PBS, Perm Solution, Blocking Solution, and PBST. 2. First Washing Phase: Contents of the plates were aspirated. Plates were then washed with 50 µL/well (384-wp) or 200 µL/well (96-wp) of Perm Solution, followed by a slow shake for 3 seconds. 3. Permeabilization: A delay of approximately 1 minute was implemented for permeabilization, in addition to the time required to process all the plates (around 1 minute per plate). 4. Second Washing Phase: Plates were washed with 50 µL/well (384-wp) or 200 µL/well (96-wp) of PBS. Subsequently, 50 µL/well (384-wp) or 200 µL/well (96-wp) of Blocking Solution was added to the plates, followed by a slow shake for 3 seconds. 5. Blocking, autoclean, and Primary Antibody Priming: The washer was set to undergo an autoclean cycle with PBS for 30 minutes. Simultaneously, the syringe containing the Primary Antibody Solution was primed with 16 ml. 6. Third Washing Phase and First Antibody Dispensing: After aspirating the contents of the plates, 15 µL/well (384-wp) or 60 µL/well (96-wp) from the Primary Antibody Solution was added, followed by a slow shake for 3 seconds. 7. Primary Antibody Incubation, autoclean, and Secondary Antibody Priming: The washer was subjected to another autoclean cycle using PBS for 2 hours and 5 minutes. The syringe containing the Secondary Antibody Solution was primed with 16 ml during this period. 8. Fourth Washing Phase and Second Antibody Dispensing: Plates were washed with 50 µL/well (384-wp) or 200 µL/well (96-wp) of PBST, followed by a 2-second slow shake and aspiration. Then, 15 µL/well (384-wp) or 60 µL/well (96-wp) from the Secondary Antibody Solution was added, accompanied by a 3-second slow shake. 9. Secondary Antibody Incubation and autoclean: An autoclean cycle with PBS was initiated and lasted for 1 hour. 10. Final Washing Phase: Plates were washed with 50 µL/well (384-wp) or 200 µL/well (96-wp) of PBST. This was followed by two consecutive washes with 50 µL/well (384-wp) or 200 µL/well (96-wp) of PBS, incorporating a 2-second slow shake in each cycle. Finally, plates were left with 50 µL/well (384-wp) or 200 µL/well (96-wp) of PBS.

Imaging

Plates were imaged with a ImageXpress micro-XL and analyzed with MetaXpress (Molecular Devices).

Analysis

Analysis was conducted in R.

Data Omission: We excluded five library plates, constituting 8% of the total library, due to insufficient infection levels for accurate quantification.

Normalization: Two variables were subject to normalization—percentage of SARS-CoV-2 positive cells and the count of nuclei. The normalization steps were applied separately for the three screening conditions: mock treatment followed by mock infection, IFN-α2a treatment followed by SARS-CoV-2 infection, and mock treatment followed by SARS-CoV-2 infection. Data was first Z-scale normalized within assay plates:

$$Scale(x) = \frac{x - mean(x)}{sd(x)}$$

And then Z-scale normalized per row and per column to remove any spatial effects.

Statistics: a robust statistic accounting for technical and biological variability was applied using the below formula within the replicates of each gene**:**

$$Stat\ score(x) = \frac{mean(x)}{sd(x)}$$

This statistic was further standardized by Z-scaling across all genes to produce our final z-score.

Exclusion of genes influencing cell proliferation: 224 genes with nuclei count z-score ≥ 2 and 388 genes with nuclei count z-score ≤ 2 in the mock treatment followed by mock infection condition were deemed to influence cell proliferation and excluded from subsequent analyses.

Exclusion of genes not expressed in cell lines of interest (A549, Calu-3, Huh-7.5 cells) and in human lung cells. Expression data from cell lines from [33, 34]. Expression data from tissues from [35]. Genes were considered expressed if they had at least one read count within exons.

Gene set enrichment analysis

For the pathway analysis, we leveraged the FGSEA package [172] to perform Gene Set Enrichment Analysis (GSEA) using gene sets found in the Molecular Signatures Database (MSigDB) [173]: Reactome [174], KEGG [175], Wikipathways [176], Pathway Interaction Database [177], and Biocarta [178]. The analysis was conducted separately for two conditions: IFN-α pretreated SARS-CoV-2 infection and non-pretreated SARS-CoV-2 infection. We attributed a score to each pathway for both conditions:

$$Score = -log10(padj) \times sign(Normalized\ Enrichment\ Score)$$

Each pathway was then attributed to one of nine quadrants (as in **Fig 2F**) based on its score in the IFN-α pretreated condition (axis x) versus non-pretreated condition (axis y), using padj ≤ 0.05 as a cutoff.

Compilation of published large-scale omic studies on SARS-CoV-2

As a rule, we listed the genes classified as 'hits' by the authors of the respective studies. Below are some exceptions or clarifications:

Functional genetic screens

Baggen, et al. [76]: we used the “low stringency adjusted” analysis in Suppl Table 11. Proviral: p_value_neg ≤ 0.05 and log2 FC ≥ 1. Antiviral: p_value_pos ≤ 0.05 and log2 FC ≤ -1. We also used “High stringency” analysis in Suppl Table 7. Proviral: Gene is TMEM106B (log2 FC = 3.8 and p_value_neg = 0.08) or p_value_neg ≤ 0.05 and log2 FC ≥ 1 (no gene matched this criteria). Antiviral: p_value_pos ≤ 0.05 and log2 FC ≤ -1 (no gene matched this criteria). **Biering, et al. [75]:** in Supplementary Table 1, in Tab 1: LOF-enriched screen analysis, for proviral genes, we used FDR ≤ 0.05. In Tab 2: GOF-depleted screen analysis, proviral: FDR ≤ 0.05. In Tab 3: GOF-enriched screen analysis, for antiviral genes, we used FDR ≤ 0.05. **Chan, et al. [74]:** in Multimedia component 6, for Vero E6 (T16); UM-UC-4 (T23); HEK293+A+T (T12); HuH-7 (T15) and Calu-3 (T43), we considered gene as hits at FDR < 0.1 (as in Figure 4A). We listed the genes as proviral if differential ≥ 0 or antiviral if differential ≤ 0. **Daniloski, et al. [73]:** we used Table S1. FDR MOI1 ≤ 0.05 or FDR MOI3 ≤ 0.05. **Danziger, et al. [10]:** in S1 Table, we used the genes annotated as proviral or antiviral by the authors. **Gordon, et al. [72]:** for A549 +ACE2 in Table S6 or Caco2 in Table S7, for proviral

genes, we used Averaged z-scores ≤ 2 and for antiviral genes, we used Averaged z-scores ≥ 2. **Grodzki, et al. [71]:** for VeroE6 in additional file 4, tab 4, we used FDR <0.25. For HEK293T +Cas9 Study 1 in additional file 6, tab17, we used FDR <0.25. For HEK293T +Cas9 Study 1 in additional file 7, tab7, we used FDR <0.25. **Hoffmann, et al. [26]:** for 37°C (Table S1E) and for 33°C (Table S1C), we selected proviral genes if FDR ≤ 0.05 and z-score ≥ 0 and antiviral genes if FDR ≤ 0.05 and z-score ≤ 0. **Hossain, et al. [65]:** in Figure 3E, we selected the top 15 genes in the spike-mNG axis by negative log robust rank aggregation. **Israeli, et al. [70]:** we used Supplementary Data 1. **Kaur, et al. [14]:** we used the genes labelled in Figure 1. **Le Pen et al. (this study):** we used z-score ≥ 2 for antiviral genes and ≤ 2 for proviral genes, see Unbiased arrayed CRISPR KO Screen analysis section above for more details. **Loo, et al. [69]:** we used the genes labelled in Figure 2. **Mac Kain, et al. [17]:** in Electronic Supplementary Material 5, for antiviral genes, we used the filter: pos|rank ≤13, for proviral genes, we used neg|rank ≤13. **Martin-Sancho, et al. [11]:** we used Table S3, "Lentivirus validated hits". **Pahmeier, et al. [68]:** we used the genes labelled in Figure 6. **Rebendenne, et al. [67]:** for Calu3_Gattinara, we used for proviral genes: residual_z-score_avg ≥ 2.5 and for antiviral genes: residual_z-score_avg ≤ 2.5 (no gene). For VeroE6, proviral: residual_z-score_avg ≥ 2.5, and antiviral: residual_z-score_avg ≤ 2.5. For Caco2, proviral: residual_z-score_avg ≥ 2.5 and antiviral: residual_z-score_avg ≤ 2.5. For Calu3_Calabrese, proviral: residual_z-score_avg ≤ 2 and antiviral: residual_z-score_avg ≥ 2. **Rehfeld, et al. [66]:** In Table S1, we considered genes as hits for PRF-1 top eGFP-mCh or PRF-1 bottom eGFP-mCh if FDR ≤ 0.05. **Schneider, et al. [29]:** for both 37°C (Table_S1A) and 33°C (Table_S1B), we listed the gene as proviral if FDR ≤ 0.05 and z-score ≥ 0 and antiviral if FDR ≤ 0.05 and z-score ≤ 0. **Wang, et al. [63]:** we used Table S1. Proviral: Enrichment score ≤ 10^(-4). **Wei, et al. 2021 [62]:** we used Table S1. For proviral genes, we used Cas9-v1 Avg. ≥ 2.5 & Cas9-v2 Avg. ≥ 2.5. Average between Cas9-v1 Avg. and Cas9-v2 Avg. is given in the table. For antiviral genes, we used Cas9-v1 Avg. ≤ -2.5 & Cas9-v2 Avg. ≤ -2.5. Average between Cas9-v1 Avg. and Cas9-v2 Avg. is given in the table. **Wei, et al. 2023 [61]:** in Table S1, for Day 7 or Day 14, we used fdr ≤ 0.05 for positive regulators of ribosomal frameshifting or negative regulators of ribosomal frameshifting. **Wickenhagen, et al. [12]:** we used the genes labelled in Figure 1B. **Xu, et al. [18]:** in Huh-7.5 or A549-ACE2 cells, in untreated or in IFN-gamma treatment, we used Log10 p-value (mNG-High vs. mNG-Low Enrichment) ≥ 3. **Zhu et al. [60]:** In Supplementary Data 1 , SARS-CoV-2 WT and 2 VOCs tested, for proviral genes, we used pos.score_wt ≤ 0.0005 or pos.score_alpha ≤ 0.0005 or pos.score_beta ≤ 0.0005.

Human genetic studies

Degenhardt, et al. [86]: we used Table 2 and added KANSL1 and TAC4, based on new analysis by Pairo-Castineira et al. 2023 [23]. **Kousathanas, et al. [24]:** we used Table 1 from Pairo-Castineira, et al. 2023 [23]. **Pairo-Castineira, et al. 2021 [94]**: we used Table 1 from Pairo-Castineira, et al. 2023 [23]. **Pairo-Castineira, et al. 2023 [23]**: we only considered variants near annotated genes (i.e., we excluded rs1073165). **Roberts, et al. [79]:** we used Supplementary Table 4. **Zhou, et al. [91]**: we used Table 1 and the p-values from COVID-19 hospitalization (European ancestry only).

SARS-CoV-2 protein interactomes

Davies, et al. [105], Laurent, et al. [98], Li, et al. [104], Samavarch-Tehrani, et al. [96], St-Germain, et al. [99], Stukalov, et al. [103]: we used the Supplementay Table 3 from [25]**. Gordon,**

720 **et al. [97]:** we used the genes listed in Table S2. **Liu, et al. [100] and May, et al. [101]:** we used
721 the genes listed in May, et al. [101] Table S5-new. **Zhou, et al. [102]:** we used the genes listed in
722 Table S1. "SARS-CoV-2-human protein-protein interactions identified in this study."

723 ### SARS-CoV-2 RNA interactomes

724 **Flynn, et al. [110], Kamel, et al. [109], Labeau, et al. [108], Lee, et al. [111], Schmidt, et**
725 **al. 2021 [107]:** we used the Supplementay Table 3 from [25]**. Schmidt, et al. 2023 [106]:** we used
726 Table S2, "Huh-7 interactome comparison tab", genes listed in the following categories: "Huh-7
727 gRNA FDR5 HS" and "Huh-7 sgmRNA FDR5 HS".

728 ### Altered phosphorylation states in SARS-CoV-2-infected cells.

729 **Bouhaddou, et al. [112]:** for Vero E6 cells, we used Table S1, tab 1 "PhosphoDataFull" and
730 filtered for adj.pvalue ≤ 0.05 & log2FC ≥ 1 or adj.pvalue ≤ 0.05 & log2FC ≤ -1 in at least three
731 different time points.
732

733 ## Generation of PLSCR1 KO cells

734 ### CRISPR KO

735 KO Huh-7.5 and A549-ACE2 cells were generated using two anti-PLSCR1 Edit-R crRNAs
736 from Horizon Discovery (cat. CM-003729-02-0002 and CM-003729-04-0002) or non-targeting
737 controls (cat. U-007501-01-05 and U-007502-01-05) resuspended with an equimolar amount of
738 Edit-R tracrRNA (Horizon, cat. U-002005-20) to form sgRNAs. The sgRNAs were then co-
739 transfected with Cas9-mKate2 mRNA (Horizon, cat. CAS12218) according to the manufacturer's
740 protocol. 24 to 48 hours after transfection, cells were examined for mKate2 signal and FACS sorted
741 into bulk and single cell populations, gating on mKate2 signal. Bulk and single cell populations
742 were then assessed for PLSCR1 expression by western blot to confirm KO.

743 ### Amplicon sequencing

744 Genomic DNA was isolated from a frozen cell pellet using the Qiagen DNeasy kit (Qiagen,
745 cat. 69504) and treated with RNAse A in the optional RNA digestion step. The region of interest
746 was then amplified using Q5 2x mastermix (New England Biolabs, cat. M0492S), 500 ng of
747 template DNA, 0.5 µM of forward and reverse primers, and the following PCR conditions: 98°C
748 for 30 seconds, followed by 98°C for 5 seconds, 64°C for 15 seconds, and 72°C for 20 seconds,
749 repeating those steps 30 times before holding at 72°C for 2 minutes. The primers used when
750 amplifying PLSCR1 genomic DNA from WT and KO Huh-7.5 and A549+ACE2 cells were RU-O-
751 32687 (5' AACATAGAGGTGATTATGATTTCGTCT) and RU-O-32526 (5'
752 GGAGGAGCTTGGATTTCTATCTAC). PCR reactions were run on a 1% agarose gel to confirm
753 amplification. Amplicons were purified with a Zymo DNA clean and concentrator kit (Zymo, cat.
754 D4013) before sending to Genewiz for amplicon sequencing.

755 ### Western Blots

756 Cell pellets were collected and lysed in RIPA buffer (Thermo, catalog number 89900) with
757 1x Halt protease inhibitor cocktail and 1x EDTA (Thermo, catalog number 87786). Cell lysates were
758 spun down in a refrigerated centrifuge at 15,000 g at 4°C for 15 minutes to pellet any cell debris,
759 and the supernatant was collected and transferred to another tube. The collected samples were
760 quantified by BCA assay (Thermo Scientific, cat. #23225). Before loading into the gel, we added
761 sample buffer (Thermo, catalog number NP0007) with β-mercaptoethanol and heated the sample
762 at 95°C for 10 minutes. Samples were allowed to cool back to room temperature before loading

763 into 12% Bis-Tris 1.0 mm gels (Invitrogen, cat. #NP0321BOX). Proteins were electrophoretically
764 transferred onto nitrocellulose membranes. Membranes were blocked with 5% fat-free milk in 1X
765 TBS (Thermo, catalog number NP00061) and then incubated with primary antibody at 4°C
766 overnight in 5% fat-free milk in 1x TBS with 0.5% Tween-20 (TBST). Primary antibody: rabbit anti-
767 PLSCR1 polyclonal antibody (Proteintech, cat. #11582-1-AP) and mouse anti-β-actin antibody
768 (Millipore Sigma, cat. A5316-100UL) as a loading control. After incubation, membranes were
769 washed three times with 1x TBST and then incubated with fluorescently conjugated secondary
770 antibodies for 2 hours at room temperature. Secondary antibodies: LI-COR IRDye goat anti-rabbit
771 800 and goat anti-mouse 680 (LI-COR cat. 926-32211 and 926-68070, respectively). Membranes
772 were washed three times with 1X TBST, once with 1X TBS, then imaged on an Azure 600. For the
773 western blot in Supplementary Figure 4, this protocol was modified slightly: proteins were
774 electrophoretically transferred onto 0.22 µm polyvinylidene difluoride (PVDF) membranes,
775 incubated with a primary antibody solution of rabbit anti-PLSCR1 polyclonal antibody
776 (Proteintech, cat. #11582-1-AP) and polyclonal rabbit anti-RPS11 antibody (Abcam, cat.
777 ab157101), a secondary antibody solution of goat anti-rabbit HRP (Invitrogen, cat. 31462) and
778 visualized using a SuperSignal West Femto Maximum Sensitivity Substate kit (Thermo, cat.
779 #34096).
780

781 ## Cell viability assay

782 4,000 A549-ACE2 cells/well or 8,000 Huh-7.5 cells/well were seeded on day 0 in 100 µL
783 media (DMEM, 10% FBS, 1X NEAA, 1X Penicillin-Streptomycin) in a 96-well plate. The next day,
784 blasticidin selection was added as indicated in the figure to serve as a control for reduced cell
785 viability. On day 4, cell viability was assessed by resazurin assay (Abcam, cat. ab129732) according
786 to the manufacturer's protocol.
787

788 ## JAK-STAT inhibitor treatment

789 InSolution (Millipore, cat. 420097-500UG) was used according to the manufacturer's
790 instructions.
791

792 ## Titration of IFN-a2a in CHIKV-infected cells

793 6,000 Huh-7.5 cells/well were seeded in 100 µL media (DMEM, 10% FBS, 1X NEAA). The
794 following day, we treated cells with one of twelve concentrations of IFN-a2a (PBL, cat. 11101-2):
795 64 pM, 32 pM, 16 pM, 8 pM, 4 pM, 2 pM, 1 pM, 0.5 pM, 0.25 pM, 0.125 pM, 0.0625 pM, and 0
796 pM. The following day, the cells were infected with 2 µL of CHIKV-181/25-mKate2 (approximately
797 17,000 FFU per well, titer determined on Huh-7.5 cells) and fixed after 12 hours. Plates were
798 stained with a 1:1000 dilution of Hoechst for at least 10 minutes before washing with PBS and
799 imaging for mKate2 signal.
800

801 ## RT-qPCRs on ISGs

802 Huh-7.5 and A549-ACE2 cells were seeded at densities of 36,000 or 18,000 cells/well,
803 respectively, in 500 µL of media (DMEM, 10% FBS, 1X NEAA) in 24-well plates. The following day,
804 a dilution series of IFN-α2a (PBL, cat. 11101-2) or IFN-β (PBL, cat. #11415) was prepared (64 pM,
805 32 pM, 16 pM, 8 pM, 4 pM, 2 pM, 1 pM, 0.5 pM, 0.25 pM, 0.125 pM, 0.0625 pM, and 0 pM) and

806 50 µL of each dilution added to the cells in duplicate. After 24 hours, the media was removed and
807 the cells were washed with 1 mL of ice-cold PBS. 200 µL of RNA Lysis Buffer (Zymo Research, cat.
808 #R1060-1-100) was added to the cells, and the plates were frozen at -20°C before RNA isolation.
809 RNA was extracted using the Zymo Quick RNA 96-kit (Zymo Research, cat. R1052) including
810 DNaseI treatment, followed by cDNA synthesis using the SuperScript™ IV VILO™ Master Mix
811 (Invitrogen, cat. 11756050) according to manufacturers' instructions. qPCRs were conducted on
812 a QuantStudio 3 cycler using the Taqman Fast Advance master mix (Life Technologies Corporation,
813 cat. 4444965) and the following assays: *RPS11* (ThermoFisher 4331182; Hs01574200_gH), *IFI6*
814 (ThermoFisher 4331182; Hs00242571_m1), *OAS1* (ThermoFisher 4331182; Hs00973635_m1).
815 *IFI6* and *OAS1* were normalized to *RPS11* mRNA levels using the deltaCt method [179].
816

817 ## PLSCR1 subcellular localization

818 ### IF staining

819 A549-ACE2 cells were plated onto #1.5, 12mm glass coverslips (Fisher Scientific, cat.
820 #1254581) placed at the bottom of the wells of a 24-well plate. When confluent, the cells were
821 fixed, permeabilized with 1% Triton X-100 for 5 minutes and blocked for 1 hour at room
822 temperature with 1 mL of PBS-BGT (1x PBS with 0.5% bovine serum albumin, 0.1% glycine, 0.05%
823 Tween 20). Afterward, the cells were incubated in a 1:500 dilution of 4D2 mouse anti-PLSCR1
824 antibody (Millipore Sigma, cat. #MABS483) in PBS-BG (1x PBS with 0.5% bovine serum albumin
825 and 0.1% glycine) overnight at 4C with rocking. The cells were then washed twice with PBS-BGT
826 before incubation with a secondary antibody solution of 1:1000 anti-mouse 588 (ThermoFisher,
827 cat. #A-11001) and 1:1000 Hoechst dye (ThermoFisher, cat. #62249) in PBS-BG for two hours at
828 room temperature, followed by three washes with PBS-BGT.

829 ### Imaging

830 The coverslips were mounted onto slides (Fisher Scientific, cat. #1255015) with Invitrogen
831 ProLong Gold Antifade Mountant (Fisher Scientific, cat. # P36930). The slides were allowed to
832 cure for 24 hours before the edges of the coverslips were sealed, and the cells were imaged by
833 confocal microscopy. Confocal images were acquired using Zeiss Zen Blue (v3.5) software on a
834 LSM 980 point scanning confocal microscope (Zeiss) hooked to a Axio Observer.Z1 / 7 stand
835 equipped with C Plan-Apochromat 63X/1.40 oil (RI:1.518 at 23°C) objective lens (Zeiss). CW
836 excitation laser lines 405 nm and 488 nm were used to excite the fluorescence of DAPI and AF488
837 labeled samples. Emitted fluorescence were spectrally grated (410-483 nm for DAPI, 499-552 nm
838 for AF488) to avoid fluorescence bleed through and were detected in MA-PMT (DAPI), and GaAsP-
839 PMT (AF488). The confocal pinhole was set to 1AU for AF488, and the detector master gains were
840 set within the linear range of detection (550-750V). Scanned images were saved as .czi files.
841

842 ## Focus-forming assay on SARS-CoV-2-infected cells

843 In **Fig 6B**, Huh-7.5 and A549-ACE2 cells were cultured in media (DMEM with 5% FBS) and
844 seeded at densities of 2 x 10^5 and 1 x 10^5 cells per well, respectively, in collagen-coated 12-well
845 plates to reach 80-90% confluency by the day of infection. A 1:10 serial dilution of virus stock was
846 made in Opti-MEM in five separate tubes. Media was aspirated from the cells, and the wells were
847 washed with 1 ml of PBS before adding 200 µL of each virus dilution to the cells in triplicate. Plates
848 were incubated at 37°C with 5% CO2 for 1 hour, rocking every 15 minutes for even virus

849 distribution. A 1% methylcellulose overlay medium was prepared and mixed with complete
850 growth media at 37°C; 2 ml of this overlay was added to each well after removing the virus
851 inoculum. Plates were then incubated at 37°C with 5% CO2 for 48 for Huh-7.5 cells or 72 hours
852 for A549-ACE2 cells. Cells were then fixed in final 10% neutral buffered formalin and IF stained as
853 described in the Unbiased Arrayed CRISPR screen section. PLSCR1 KO and WT cells were
854 compared at similar virus dilutions.
855 In **Fig 7G**, the above protocol was followed to titer SARS-CoV-2 strains on Huh-7.5 PLSCR1
856 KO cells. Then, Huh-7.5 WT and KO cells were seeded at 2 x 10^5 cells per well in 1 mL of media
857 (DMEM, 10% FBS, 1X NEAA) in 12-well plates to reach 80-90% confluency the next day. Media
858 was aspirated from the cells, the wells were washed with 1mL of PBS, and then the cells were
859 infected with 50 FFU of SARS-CoV-2 (for each strain) diluted in 200 µL of Opti-MEM. Plates were
860 then incubated, overlayed with methylcellulose, fixed, and stained as described above.
861

862 ## Transfection with SARS-CoV-2 replicon system

863 The SARS-CoV-2 replicon and the method for electroporation has been described
864 previously [114]. Briefly, 6 x 10^6 Huh-7.5 WT and PLSCR1 KO cells were electroporated at 710 V
865 with 2 µg of SARS-CoV-2 N mRNA and 5 µg of replicon RNA. The cells rested for 10 minutes at
866 room temperature before resuspending to a concentration of 300,000 cells/mL and plating 100
867 µL of cells into each well of a 96-well plate. After 24 hours, supernatant was collected from the
868 replicon-transfected cells and assayed for *Renilla* luciferase activity according to kit instructions
869 (Promega, cat. E2810).
870

871 ## Infection with SARS-CoV-2 spike/VSV-G-pseudotyped, single-cycle, replication-defective
872 HIV-1 viruses.

873 ### Virus preparation

874 SARS-CoV-2 spike/VSV-G-pseudotyped, single-cycle, replication-defective HIV-1 viruses
875 (pCCNanoLuc/GFP) were prepared as in [115]. Plasmids were a kind gift of Theodora Hatziioannou
876 and Paul D. Bieniasz (The Rockefeller University, NY, USA) [115]. One day before the transfection,
877 4 x 10^6 293T cells were seeded in a 10 cm dish. One hour prior to transfection, the growth media
878 in the dish was replaced with 9 mL of fresh media containing 2% serum. A 1,000 µL transfection
879 mixture was prepared, comprising the diluent (a 150 mM NaCl solution prepared with sterile cell
880 culture water), 5 µg of HIV GP plasmid, 5 µg of pCLG plasmid, and either 2.5 µg of SARS-CoV-2
881 spike Δ19 or 1 µg of pHCMV.G plasmid, ensuring the total plasmid content did not exceed 12.5
882 µg. After brief vortexing, 50 µL of PEI (1 mg/mL, Polysciences cat. 23966) was added to achieve a
883 1:4 DNA/PEI ratio. The mixture was vortexed for 5 seconds and then allowed to sit for 20 minutes
884 in a hooded environment. Following gentle mixing by pipetting, 1 mL of the transfection mixture
885 was added to the 10 cm dish. Media was changed 12 hours post-transfection, and the supernatant
886 was harvested and filtered through a 0.2-micron filter 48 hours post-transfection, then stored at
887 -80°C.

888 ### Infection of PLSCR1 KO or WT cells

889 Seeded in 96-well plates, 6,000 A549+ACE2 cells per well were cultured in 100 µL of
890 media. After two days, either 10 µL of SARS-CoV-2 spike pseudotyped virus or 0.01 µL of VSV-G
891 pseudotyped virus were diluted in a final volume of 100 µL of media and added to the wells to

892 yield comparable NanoLuc signals. Plates were then spun at 200 g for 5 minutes and incubated at
893 37°C. Two days post-infection, the media was aspirated and replaced with 50 µL of NanoGlo
894 solution, sourced from the Promega Nano-Glo Luciferase Assay kit (Promega, N1110), with a
895 substrate to buffer ratio of 1:100. NanoLuc signal was subsequently quantified using a Fluostar
896 Omega plate reader.

897 ### Infection of siRNA-treated cells

898 Seeded in 96-well plates, 1,600 HEK293T, HEK293T-ACE2, or HEK293T-ACE2-TMPRSS2 cells
899 were cultured in 80 µL of media. The next day, a 20 µL transfection mixture made of Opti-MEM,
900 1% DharmaFECT1 (Horizon, T-2001-03), and 250 nM siRNA, PLSCR1 ON-TARGETplus SMARTpool
901 siRNA (Horizon, cat. L-003729-00-0005) or non-targeting control (Horizon, cat. D-001810-10-05)
902 was added to the cells. The final concentration of siRNAs was 25 nM. After two days, either 2 µL
903 of SARS-CoV-2 spike pseudotyped virus or 0.2 µL of VSV-G pseudotyped virus were diluted in a
904 final volume of 100 µL of media and added to the wells to yield comparable NanoLuc signals.
905 Plates were then span at 200 g for 5 minutes and incubated at 37°C. Two days after infection,
906 NanoLuc signal was quantified as described in the "Infection of PLSCR1 KO or WT cells" section.
907

908 ## Infection of siRNA-treated cells with SARS-CoV-2

909 Seeded in 96-well plates, 1,000 A549, A549-ACE2, or A549-ACE2-TMPRSS2 cells were
910 cultured in 80 µL of media. On the same day, a 20 µL transfection mixture made of Opti-MEM, 1%
911 DharmaFECT1 (Horizon, T-2001-03), and 250 nM siRNA, PLSCR1 ON-TARGETplus SMARTpool
912 siRNA (Horizon, cat. L-003729-00-0005) or non-targeting control (Horizon, cat. D-001810-10-05)
913 was added to the cells. The final concentration of siRNAs was 25 nM. Three days after
914 transfection, the cells were infected by adding 34,000 PFU of SARS-CoV-2 (titer determined on
915 Vero E6 cells) diluted in 10 µL media to each well. Plates were then spun at 200 g for 5 minutes
916 and incubated at 37°C. Staining and readout as described above in the "Unbiased arrayed CRISPR
917 KO screening" section.
918

919 ## Pan-virus infection of PLSCR1 KO cells

920 A549-ACE2 cells were seeded at a density of 6,000 cells/well in 96-well plates in 90 µL
921 media. The following day, 10 µL diluted virus was added to each well. Virus concentrations as
922 follow: CHIKV-mKate, 0.05 µL virus stock per well (titer 8.5 x 10^6 PFU/mL determined in Huh-7.5
923 cells); hCoV-NL63, 10 µL virus stock per well (titer 1.4 x 10^5 PFU/mL); hCoV-OC43, 10 µL virus stock
924 per well (titer 1.06 x 10^7 PFU/mL); hPIV-GFP, 0.05 µL virus stock per well; HSV1-GFP, 0.5 µL virus
925 stock per well (titer 2.4 x 10^8 PFU/mL determined on Vero E6 cells); IAV WSN, 0.5 µL virus stock
926 per well; SARS-CoV-2, 0.5 µL virus stock per well (titer 3.4 x 10^6 PFU/mL determined on Vero E6
927 cells); SINV-Toto1101-mScarletI, 10 µL virus stock per well; VEEV-EGFP, 0.005 µL virus stock per
928 well (titer 1.45 x 10^9 PFU/mL determined on BHK-21); VSV-GFP, 0.05 µL virus stock per well;
929 YFV_17D, 5 µL virus stock per well. The cells were fixed, stained and imaged as described in the
930 *Unbiased arrayed CRISPR KO screen* section. Fluorescent viruses were not stained: the fluorescent
931 signal was used as a reporter. We used the following primary antibodies when applicable: anti-
932 dsRNA (J2) mouse (Nordic MUbio, cat. 10010200) diluted 1:500 was used for hCoV-NL63 and
933 hCoV-OC43, anti-IAV mouse (Millipore, cat. MAB8257) diluted 1:3000, anti-YFV mouse (Santa

934 Cruz Biotechnology, cat# sc-58083) diluted 1:500, anti-SARS2-S rabbit (Genetex, cat. GTX135357)
935 diluted 1:3000.
936 Huh-7.5 cells were transfected with a 1:200 dilution of Dharmafect 4 (Horizon, cat. T-2004-
937 01) and 25 nM ON-TARGETplus SMARTpool siRNAs (Horizon Discovery) in 96-well plates. The cells
938 were infected three days after siRNA transfection with hCoV-NL63 or hCoV-OC43 or four days
939 after siRNA transfection with SARS-CoV-2 or hCoV-229E. IF and imaging as described above.
940

941 ## Reconstitution of WT and mutant PLSCR1

942 ### Plasmid cloning

943 N-terminal 3x FLAG-tagged PLSCR1, C-terminal 3x FLAG-tagged PLSCR1, and PLSCR1
944 H262Y were generated by designing and ordering large dsDNA gene blocks of PLSCR1 that
945 contained the desired mutations from IDT. These gene blocks were cloned into the PLSCR1-
946 SCRPSY vector [180] and confirmed by sequencing (see Supplementary Table 12 for sequences).

947 ### Lentivirus production

948 Lentivirus were generated in Lenti-X 293T cells by transfecting 200 ng VSV-G plasmid, 700
949 ng Gag-Pol plasmid, and 1100 ng plasmid of interest with lipofectamine 2000 in DMEM
950 supplemented with 5% FBS. Media was changed 4-6 hours later, and lentivirus harvested at 24
951 and 48 hours. Lentivirus from both timepoints was pooled, then filtered through a 0.45 µM filter
952 before aliquoting into 2 mL tubes and freezing at -80°C until use.

953 ### Cell transduction

954 0.3 million cells were transduced in suspension in a 12-well plate. Cells received 8 µg/mL
955 polybrene and 80 mM Hepes in addition to the lentivirus. Cells were then spinoculated at 37°C
956 for 1 hour at 1000 x g. The following day, cells were split into two, 6-well plates, then 24 hours
957 later one of the duplicates was treated with 2 µg/mL puromycin (when using SCRPSY-based
958 lentiviruses) to select for transduced cells. Further experiments were carried out using the cells
959 that had approximately 30% transduction before selection.

960 ### SARS-CoV-2 infection

961 In **Fig 8B**, Huh-7.5 and A549+ACE2 cells were plated at 6,000 cells/well and 3,000
962 cells/well, respectively, in 100 µL of media (DMEM, 10% FBS, 1X NEAA) in 96-well plates. The
963 following day, cells were treated with IFN (10pM for Huh-7.5 cells and 20pM for A549+ACE2 cells).
964 On the third day, the Huh-7.5 cells were infected with 0.1 µL of virus per well and the A549+ACE2
965 cells with 1 µL of virus per well, then spun at 200 g for 5 minutes and incubated at 37°C. Plates
966 were harvested the next day by fixing and staining as described above. For Figure 7A-E, Huh-7.5
967 cells were plated at 7,500 cells/well in 100µL of media (DMEM, 10% FBS, 1X NEAA) in 96-well
968 plates. The next day, cells were infected with quantities of virus that yielded comparable percent
969 infections in the WT cells, then spun at 200 g for 5 minutes and incubated at 33°C. The quantities
970 of virus used were as follows: 0.1 µL/well for parental, 0.05 µL/well for beta, 1 µL/well for delta,
971 0.5 µL/well for omicron, and 0.05 µL/well for kraken. The infected cells were fixed after 24 hours
972 and stained as described previously.

973 ### IF staining and imaging

974 In **Fig 8B**, cells were stained for IF as described in the *Unbiased arrayed CRISPR KO*
975 *screening* section, with different primary and secondary antibody solutions. The primary antibody
976 solution was a 1:3000 dilution of rabbit anti-SARS-CoV-2 nucleocapsid polyclonal antibody

977 (Genetex, cat. #GTX135357) in PBS-BGT, and the secondary antibody solution was 1:1000 goat
978 anti-rabbit 594 (ThermoFisher, cat. #A-11012) or 1:1000 goat anti-rabbit 647 (ThermoFisher, cat.
979 #A-21245), and 1:1000 Hoechst dye (ThermoFisher, cat. #62249) in PBS-BGT.
980

981 ## SARS-CoV-2 infection of human SV40-fibroblasts-ACE2

982 ### Generation of human SV40-fibroblasts ACE2 stable cell lines

983 *ACE2* cDNA was inserted with In-Fusion cloning kit (Takara Bio) and using the XhoI and
984 BamHI restriction sites into linearized pTRIP-SFFV-CD271-P2A in accordance with the
985 manufacturers' instructions. We checked the entire sequence of the *ACE2* cDNA in the plasmid
986 by Sanger sequencing. Then, HEK293T cells were dispensed into a six-well plate at a density of
987 8 x10^5 cells per well. On the next day, cells were transfected with pCMV-VSV-G (0.2 µg), pHXB2-
988 env (0.2 µg; NIH-AIDS Reagent Program; 1069), psPAX2 (1 µg; Addgene plasmid no. 12260) and
989 pTRIP-SFFV-CD271-P2A-ACE2 (1.6 µg) in Opti-MEM (Gibco; 300 µL) containing X-tremeGene-9
990 (Sigma Aldrich; 10 µL) according to the manufacturers' protocol. After transfection for 6 h, the
991 medium was replaced with 3 mL fresh culture medium, and the cells were incubated for a further
992 24 h for the production of lentiviral particles. The viral supernatant was collected and passed
993 through a syringe filter with 0.2 µm pores (Pall) to remove debris. Protamine sulfate (Sigma;
994 10 µg/mL) was added to the supernatant, which was then used immediately or stored at −80 °C
995 until use.
996 For the transduction of SV40-fibroblasts with ACE2, 5 x10^5 cells per well were seeded in
997 six-well plates. Viral supernatant was added (500 µL per well). The cells were then further
998 incubated for 48 h at 37 °C. Cells were keep in culture and after 8 days, transduction efficiency
999 was evaluated by CD271 surface staining with CD271 AlexaFluor 647, 1:200 dilution (BD
1000 Pharmigen 560326). MACS-sorting was performed with CD271 positive selection beads (Miltenyi
1001 Biotec) if the proportion of CD271-positive cells was below 80% [7, 163].

1002 ### Infection

1003 5,000 cells per well were seeded in a 96-well plate and infected the next day with SARS-
1004 CoV-2 at MOI = 0.05, using a titer determined on Vero E6 cells. Cells were fixed at 2 dpi, stained
1005 and imaged as described in the *Unbiased arrayed CRISPR KO screen* section.
1006

1007 # Acknowledgments

1008 We thank Georgia McClain for reading and editing this manuscript. We thank the staff at
1009 the Laboratory of Virology and Infectious Disease: Ellen Castillo, Michela De Santis, Arnella Norris,
1010 Aileen O'Connell, Santa Maria Pecoraro Di Vittorio, Glen Santiago, and Sonia Shirley. Ching-Wen
1011 Chang and Lihong Liu (Columbia University, NY, USA), and Theodora Hatziioannou and Paul D.
1012 Bieniasz (The Rockefeller University, NY, USA) generously provided plasmids and instructions to
1013 generate SARS-CoV-2 spike-pseudotyped, single-cycle, replication-defective HIV-1 viruses [115].
1014 Oded Danziger and Brad R. Rosenberg (Department of Microbiology at the Icahn School of
1015 Medicine at Mount Sinai, NY, USA) kindly provided the A549-ACE2 cells [10] used in this study.
1016 FACS was conducted at the Flow Cytometry Resource Center at Rockefeller University. mRNA-seq
1017 was performed by the Genomics Resource Center at The Rockefeller University and by Novogene.

Confocal microscopy was performed in the Rockefeller University's Bio-Imaging Resource Center, RRID:SCR_017791. We thank Ankit Patel, Sales Manager at Horizon Discovery.

Trim Galore was developed at The Babraham Institute by @FelixKrueger, now part of Altos Labs. The Genotype-Tissue Expression (GTEx) Project [35] was supported by the Common Fund of the Office of the Director of the National Institutes of Health, and by NCI, NHGRI, NHLBI, NIDA, NIMH, and NINDS. The data used for the analyses described in this manuscript were obtained from the EMBL-European Bioinformatics Institute portal, "https://www.ebi.ac.uk/gxa/experiments/E-MTAB-5214/Results", on October 1st, 2020.

Work in the Laboratory of Virology and Infectious Disease was supported by NIH grants P01AI138398-S1, 2U19AI111825, R01AI091707-10S1, and R01AI161444; a George Mason University Fast Grant; the G. Harold and Leila Y. Mathers Charitable Foundation; the Meyer Foundation; the Pilot Project Robertson Therapeutic Development Fund at The Rockefeller University; and the Bawd Foundation. J.L.P. was supported by the Francois Wallace Monahan Postdoctoral Fellowship at The Rockefeller University and the European Molecular Biology Organization Long-Term Fellowship (ALTF 380-2018). G.P. was supported by the James H. Gilliam Fellowship for Advanced Study from the Howard Hughes Medical Institute and the Graduate Research Fellowship Program from the National Science Foundation (FAIN 1946429). M.B. was supported by a Swiss National Science Foundation fellowship (P500PB_203007).

Data and code availability

To be determined.

Tables

Table 1. PLSCR1 variants associated with severe COVID-19 in GWAS [23, 24]

GWAS p-value	rsID	Genomic Coordinate (GRCh38)	Nucleotide Change	Gene	Functional Consequence
7.52E-07	rs116553931	chr3:146430956	C:T	PLSCR2	intron variant
1.08E-07	rs454645	chr3:146514682	C:T	PLSCR1	Downstream transcript variant
5.43E-08	rs343320	chr3:146517122	G:A	PLSCR1	His262Tyr
8.21E-08	rs343318	chr3:146518204	T:C	PLSCR1	intron variant
1.52E-07	rs343317	chr3:146518374	A:G	PLSCR1	intron variant
1.00E-07	rs186910	chr3:146520241	A:G	PLSCR1	intron variant
1.13E-07	rs173150	chr3:146520256	A:T	PLSCR1	intron variant

1.35E-07	rs71302408	chr3:146520389	T:C	PLSCR1	intron variant
7.06E-08	rs343316	chr3:146521151	A:G	PLSCR1	intron variant
4.64E-08	rs343314	chr3:146522652	C:T	PLSCR1	intron variant
7.46E-08	rs343312	chr3:146522970	G:A	PLSCR1	intron variant

Figure Legends

Figure 1. Known ISGs restricting SARS-CoV-2 entry.

A schematic of SARS-CoV-2 entry and the sites where known ISG entry restriction factors function is shown. CD74 suppresses endolysosomal cathepsins, enzymes that process certain viral glycoproteins to make them fusion-competent [181, 182]. CH25H facilitates the sequestration of accessible cholesterol, which results in decreased virus-cell membrane fusion and viral entry [13, 59]. NCOA7 accelerates the acidification of the lysosome, leading to the degradation of viral antigens [116, 183]. LY6E and PLSCR1 restrict virus-cell membrane fusion at the endosome through unknown mechanisms, see [18, 157] and this study.

Figure 2. Unbiased arrayed CRISPR KO screens reveal IFN-dependent and independent genes influencing SARS-CoV-2 infection.

A. mRNA-seq comparison between Huh-7.5 and Calu-3 cells, focusing on a subset of 224 ISGs, in response to 24 h SARS-CoV-2 infection MOI 0.03. Red diamond, PLSCR1 RNA level. Viral RNA levels were comparable in both cell lines (not shown). ****, $p<0.0001$; two-tailed t-test.
B. Cells were treated with 0.5 nM IFN-α2a for 24 h. mRNA-seq analysis as in **(A)**.
C. Huh-7.5-Cas9 cells were pretreated with different amounts of IFN-α2a, then infected with SARS-CoV-2 for 24 h followed by IF staining for SARS-CoV-2 N protein; $n = 6$; error bars represent SEM. ****, $p<0.0001$; two-tailed t-test.
D. Diagram of the arrayed CRISPR KO screen method.
E. The virus level (percentage infected cells was determined by IF staining, then normalized and z-score was calculated) is plotted for 24 h 0 pM (y axis) or 1 pM (x axis) IFN-α2a pretreatment followed by 24 h infection ($n \geq 5$). The genes were categorized as ISG or other based on mRNA-seq of IFN-α2a-treated cells as in **(B)**. ISGs were defined by a fold change ≥ 2 and padj ≤ 0.05 in the IFN-treatment versus untreated pairwise comparison.
F. Gene set enrichment analysis conducted on the arrayed CRISPR KO screens data represented in **(E)**. Description of the top pathways ranked by p-value for each quadrant. Databases: [1]Reactome; [2]WikiPathways; [3]Pathway Interaction Database; [4]KEGG; [5]Biocarta.

1073 Figure 3. Human genes significant in human genetics studies on COVID-19 patients and in
1074 functional genetic screens in cell culture
1075

1076 Figure 4. PLSCR1 is a highly effective anti-SARS-CoV-2 effector ISG contributing to intrinsic
1077 immunity in the absence of IFN.

1078 A. Cells were pretreated with a JAK-STAT inhibitor (InSolution 1 µM) for 2 h, followed by IFN-
1079 α2a (10 pM Huh-7.5 or 20 µM A549-ACE2) for 24 h and were infected with SARS-CoV-2 for
1080 24 h followed by IF staining for viral N protein. Huh-7.5 infection using an MOI of 0.5 (titer
1081 determined by focus forming assay on Huh-7.5 WT cells). A549-ACE2 infection using an
1082 MOI of 0.01 (titer determined by focus forming assay on A549-ACE2 WT cells). The
1083 percentage of SARS-CoV-2 positive cells is plotted.
1084 B. Cells were reconstituted with the indicated proteins by stable transduction with
1085 lentiviruses, then infected as in **(A)**.
1086 C. Cells were co-cultured as indicated (50:50 mix), then infected as in **(A)** and the % infection
1087 of each cell type was determined. n = 6; error bars represent sd. ****, p<0.0001; two-
1088 tailed t-test.
1089

1090 Figure 5. PLSCR1 is not important for IFN signaling.

1091 A. Huh-7.5 WT and PLSCR1 KO cells were infected with 17,000 FFU of CHIKV 181/25 mKate2
1092 for 12 or 24 hours, then fixed, IF stained for nuclei, and the percentage of positive cells
1093 determined by imaging for mKate2 reporter signal. n = 12 independent infections
1094 (separate wells). Error bars represent sd. ns, non-significant; two-way ANOVA.
1095 B. Huh-7.5 cells, PLSCR1 KO as indicated, were pretreated with different amounts of IFN-
1096 α2a, then infected with 17,000 FFU of CHIKV-mKate for 12 h; n = 7; error bars represent
1097 sd.
1098 C-J. Cells were treated for 24 h by IFN, as indicated, followed by RT-qPCRs on ISGs.
1099

1100 Figure 6. PLSCR1 restricts spike-mediated SARS-CoV-2 entry.

1101 A. A549-ACE2 cells were IF stained using an anti-PLSCR1 antibody (white) and Hoechst
1102 33342 nuclear staining (blue) and imaged at 63X magnification on a confocal microscope.
1103 B. Focus forming assays: SARS-CoV-2 N IF (red) and Hoechst 33342 nuclear staining (blue)
1104 on similarly infected WT or PLSCR1 KO Huh-7.5 and A549-ACE2 cells after 2 and 3 d,
1105 respectively.
1106 C. Quantification of **(B)**.
1107 D. Huh-7.5 WT and PLSCR1 KO cells electroporated with SARS-CoV-2 replicon which
1108 produces a secreted luciferase. Luciferase activity assayed 24 hours after electroporation.
1109 n = 36 (separate wells from single electroporation). Error bars represent sd. Ns = non-
1110 significant; two-tailed t-test.
1111 E-F. Transduction of A549-ACE2 cells with an HIV-based replicon expressing the
1112 nanoluciferase pseudotyped with VSV-G or SARS-CoV-2 spike, respectively. n = 5
1113 independent infection (separate wells). Nanoluciferase signal measured 2 dpi. Error bars
1114 represent sd. ns, non-significant, **, p<0.01; two-tailed t-test.

1115 G-I. A549 cells WT, expressing ACE2, or expressing ACE2-TMPRSS2 as indicated were
1116 transfected with PLSCR1 or non-template control (NTC) siRNAs as indicated for 3 d and
1117 infected with SARS-CoV-2 for 1 d. SARS-CoV-2 N was stained by IF and the percentage of
1118 positive cells was determined by imaging. n = 6 independent infection (separate wells).
1119 Error bars represent sd. ns, non-significant, **, p<0.01, ***, p<0.001; two-tailed t-test.
1120 J-M. HEK293T cells expressing ACE2 or ACE2-TMPRSS2, as indicated, were transfected with
1121 siRNA knockdown of PLSCR1 or non-template control (NTC), as indicated, for 3 d and
1122 transduced with an HIV-based replicon expressing the nanoluciferase pseudotyped with
1123 VSV-G or SARS-CoV-2 spike, as indicated for 2 d. n = 3 independent infection (separate
1124 wells). Error bars represent sd. ns, non-significant, **, p<0.01; two-tailed t-test.
1125

1126 ### Figure 7. Newer variants of SARS-CoV-2 are less restricted by PLSCR1

1127 A-E. Infection of Huh-7.5 cells with SARS-CoV-2 (parental) or its descendant variants, Beta,
1128 Delta, Omicron, and Kraken for 24 hours. SARS-CoV-2 N was stained by IF and the
1129 percentage of positive cells determined by imaging. n = 10 independent infection
1130 (separate wells). Error bars represent sd. ****, p < 0.0001; two-tailed t-test.
1131 F. Ratio of WT/KO percent infection from A-E. Error bars represent sd. ns, non-significant.
1132 ***, p<0.001, ****, p<0.0001; one-way ANOVA.
1133 G. Huh-7.5 WT and PLSCR1 KO cells were infected with 50 FFU of virus as titered on PLSCR1
1134 KO cells in a focus-forming assay. Plaques were counted, and then a ratio of WT-to-KO
1135 plotted for each SARS-CoV-2 variant. n = 6 independent infection (separate wells). Error
1136 bars represent sd. **, p<0.01; one-way ANOVA.
1137

1138 ### Figure 8. PLSCR1 His262Tyr, which associates with severe COVID-19, leads to higher SARS-
1139 CoV-2 infection in cell culture.

1140 A. Protein diagram of PLSCR1. Domain coordinates from UniProt.
1141 B. Huh-7.5 cells, WT and PLSCR1 KO, stably expressing N-terminal FLAG-tagged Firefly
1142 Luciferase (Fluc), N-terminal FLAG-tagged PLSCR1, or N-terminal FLAG-tagged PLSCR1
1143 H262Y mutant and infected with SARS-CoV-2 for 24 hours. SARS-CoV-2 N was stained by
1144 IF and the percentage of positive cells determined by imaging. n = 15 independent
1145 infection (separate wells). Error bars represent sd. ****, p<0.0001; two-tailed t-test.
1146 C. SV40-Fibroblast-ACE2 cells, genotype as indicated, infected for two days with SARS-CoV-
1147 2. N = eight independent infection in separate wells. ns, non-significant, **, p<0.01, ***,
1148 p<0.001; two-tailed t-test.

1149 ## Supplementary Figure Legends

1150 ### Supplementary Figure 1.

1151 A. Nuclei count (z-score) in arrayed genetic screen. Examples of VCP (essential gene) and
1152 PLSCR1 (SARS-CoV-2 antiviral hit) are plotted.
1153 B. Volcano plot of Huh-7.5 cells mRNA-seq treated with 0.5 nM IFN-α2a for 24 h as in **Fig 2B**.
1154

1155 ## Supplementary Figure 2
1156 A. Occurrence of human genes interacting with SARS-CoV-2 drawn from a selection of 67
1157 large-scale studies. The occurrence reflects the number of independent studies finding
1158 each gene as significant.
1159 B. Upset plot on data as in **(A)**, showing the overlap in significant genes in large-scale SARS-
1160 CoV-2 studies by category.
1161
1162 ## Supplementary Figure 3.
1163 A. Western blot on PLSCR1 KO cells against PLSCR1 (green) and ß-actin (red).
1164 B. Cells as indicated were seeded at similar density, treated or not with Blasticidin (used here
1165 as a control to decrease cell viability), and cultured for 4 days before resazurin cell viability
1166 assay. n = 4 independent wells.
1167 C. Western blot on PLSCR1 WT and KO A549-ACE2 cells against PLSCR1 (green) and ß-actin
1168 (red).
1169
1170 ## Supplementary Figure 4.
1171 A. Western blot against PLSCR1 and RPS11. Cas-9-expressing Huh-7.5 cells were transfected
1172 with 4-gRNA pools targeting PLSCR1 or non-template control (as indicated) and cells were
1173 in culture for 7 d.
1174 B. Quantification of bands intensity in **(A)**.
1175 C. mRNA-seq on cells as in **(B)**.
1176
1177 ## Supplementary Figure 5.
1178 A-I. Infection of A549-ACE2 cells with viruses as indicated. IF staining was used for IAV WSN,
1179 hCoV-OC43 and SARS-CoV-2, otherwise a fluorescent reporter was used. Percentage of
1180 virus positive cells was determined by imaging. N = six replicates (independent
1181 infections in separate wells), error bars represent SD.
1182 J-M. Infection of Huh-7.5 cells with viruses as indicated. siRNA knockdown of PLSCR1 vs non-
1183 template control (NTC). ****, $p<0.0001$; ns, non-significant; two-tailed t-test.
1184
1185 ## Supplementary Figure 6.
1186 Western Blot against PLSCR1 and β-actin (loading control). Huh-7.5 PLSCR1 KO cells were stably
1187 transduced with FLAG-tagged Fluc, FLAG-tagged PLSCR1, or FLAG-tagged PLSCR1 H262Y.
1188
1189 ## Supplementary Figure 7.
1190 Comparison between selected SARS-CoV-2 protein interactome studies [96-98, 100-105, 148].
1191
1192 ## Supplementary Figure 8.
1193 Comparison between the relative mRNA levels of 97 hallmark IFN-α-stimulated genes and the
1194 remaining transcriptome in cell lines as indicated. Red diamond, *PLSCR1* RNA level. For Huh-7.5
1195 cells mRNA-seq, cells treated with 0.5 nM IFN-α2a for 24 h as in **Fig 2B**. For primary human

hepatocytes, cells were treated with 0.1 nM IFN-α2a for 24 h (full data and methods to be released elsewhere). For the human tissues, data from [35].

Supplementary Material

Supplementary Table 1.

mRNA-seq on SARS-CoV-2 infected cells, Normalized reads, related to **Fig 2A**.

Supplementary Table 2.

mRNA-seq on SARS-CoV-2 infected cells, Differential Gene Expression.

Supplementary Table 3.

mRNA-seq on IFN treated cells, Normalized reads, related to **Fig 2B**, and **Supp Fig 8.**

Supplementary Table 4.

mRNA-seq on IFN treated cells, Differential Gene Expression, related to **Fig 2E** and **Supp Fig 1B**.

Supplementary Table 5.

Arrayed CRISPR KO screen, raw data.

Supplementary Table 6.

Arrayed CRISPR KO screen, analyzed data. Related to **Fig. 2E** and **Supp Fig 1A**.

Supplementary Table 7.

Arrayed CRISPR KO screen, summary table.

Supplementary Table 8.

GSEA on arrayed CRISPR KO screen. Related to **Fig. 2F**.

Supplementary Table 9.

Consolidated list of human genes classified as hits in selected SARS-CoV-2 studies, full table. Related to **Fig 3** and **Supp Fig 2.**

Supplementary Table 10.

Consolidated list of human genes classified as hits in selected SARS-CoV-2 studies, summary table. Related to **Fig 3** and **Supp Fig 2.**

Supplementary Table 11.

Plasmids used in this study.

1235 Supplementary Table 12.
1236 Gene fragments used in this study.
1237
1238 Supplementary Table 13.
1239 Primers used in this study.
1240

1241 ## References

1242 1. Bastard P, Zhang Q, Zhang SY, Jouanguy E, Casanova JL. Type I interferons and SARS-CoV-
1243 2: from cells to organisms. Curr Opin Immunol. 2022;74:172-82. Epub 20220125. doi:
1244 10.1016/j.coi.2022.01.003. PubMed PMID: 35149239; PubMed Central PMCID:
1245 PMCPMC8786610.
1246 2. Bastard P, Gervais A, Le Voyer T, Rosain J, Philippot Q, Manry J, et al. Autoantibodies
1247 neutralizing type I IFNs are present in ~4% of uninfected individuals over 70 years old and
1248 account for ~20% of COVID-19 deaths. Sci Immunol. 2021;6(62). Epub 2021/08/21. doi:
1249 10.1126/sciimmunol.abl4340. PubMed PMID: 34413139.
1250 3. Lopez J, Mommert M, Mouton W, Pizzorno A, Brengel-Pesce K, Mezidi M, et al. Early
1251 nasal type I IFN immunity against SARS-CoV-2 is compromised in patients with autoantibodies
1252 against type I IFNs. J Exp Med. 2021;218(10). Epub 20210806. doi: 10.1084/jem.20211211.
1253 PubMed PMID: 34357402; PubMed Central PMCID: PMCPMC8352718.
1254 4. Asano T, Boisson B, Onodi F, Matuozzo D, Moncada-Velez M, Maglorius Renkilaraj MRL,
1255 et al. X-linked recessive TLR7 deficiency in ~1% of men under 60 years old with life-threatening
1256 COVID-19. Sci Immunol. 2021;6(62). doi: 10.1126/sciimmunol.abl4348. PubMed PMID:
1257 34413140; PubMed Central PMCID: PMCPMC8532080.
1258 5. Zhang Q, Bastard P, Liu Z, Le Pen J, Moncada-Velez M, Chen J, et al. Inborn errors of type
1259 I IFN immunity in patients with life-threatening COVID-19. Science. 2020;370(6515). Epub
1260 20200924. doi: 10.1126/science.abd4570. PubMed PMID: 32972995; PubMed Central PMCID:
1261 PMCPMC7857407.
1262 6. Bastard P, Rosen LB, Zhang Q, Michailidis E, Hoffmann HH, Zhang Y, et al. Autoantibodies
1263 against type I IFNs in patients with life-threatening COVID-19. Science. 2020;370(6515). Epub
1264 20200924. doi: 10.1126/science.abd4585. PubMed PMID: 32972996; PubMed Central PMCID:
1265 PMCPMC7857397.
1266 7. Zhang Q, Matuozzo D, Le Pen J, Lee D, Moens L, Asano T, et al. Recessive inborn errors of
1267 type I IFN immunity in children with COVID-19 pneumonia. J Exp Med. 2022;219(8). Epub
1268 20220616. doi: 10.1084/jem.20220131. PubMed PMID: 35708626; PubMed Central PMCID:
1269 PMCPMC9206114.
1270 8. Zhou P, Yang XL, Wang XG, Hu B, Zhang L, Zhang W, et al. A pneumonia outbreak
1271 associated with a new coronavirus of probable bat origin. Nature. 2020;579(7798):270-3. Epub
1272 20200203. doi: 10.1038/s41586-020-2012-7. PubMed PMID: 32015507; PubMed Central
1273 PMCID: PMCPMC7095418.
1274 9. Savan R, Gale M, Jr. Innate immunity and interferon in SARS-CoV-2 infection outcome.
1275 Immunity. 2023;56(7):1443-50. doi: 10.1016/j.immuni.2023.06.018. PubMed PMID: 37437537;
1276 PubMed Central PMCID: PMCPMC10361255.

1277 10. Danziger O, Patel RS, DeGrace EJ, Rosen MR, Rosenberg BR. Inducible CRISPR activation
1278 screen for interferon-stimulated genes identifies OAS1 as a SARS-CoV-2 restriction factor. PLoS
1279 Pathog. 2022;18(4):e1010464. Epub 20220414. doi: 10.1371/journal.ppat.1010464. PubMed
1280 PMID: 35421191; PubMed Central PMCID: PMCPMC9041830.
1281 11. Martin-Sancho L, Lewinski MK, Pache L, Stoneham CA, Yin X, Becker ME, et al. Functional
1282 landscape of SARS-CoV-2 cellular restriction. Mol Cell. 2021;81(12):2656-68 e8. Epub 20210413.
1283 doi: 10.1016/j.molcel.2021.04.008. PubMed PMID: 33930332; PubMed Central PMCID:
1284 PMCPMC8043580.
1285 12. Wickenhagen A, Sugrue E, Lytras S, Kuchi S, Noerenberg M, Turnbull ML, et al. A
1286 prenylated dsRNA sensor protects against severe COVID-19. Science. 2021;374(6567):eabj3624.
1287 Epub 20211029. doi: 10.1126/science.abj3624. PubMed PMID: 34581622.
1288 13. Zang R, Case JB, Yutuc E, Ma X, Shen S, Gomez Castro MF, et al. Cholesterol 25-
1289 hydroxylase suppresses SARS-CoV-2 replication by blocking membrane fusion. Proc Natl Acad Sci
1290 U S A. 2020;117(50):32105-13. Epub 20201125. doi: 10.1073/pnas.2012197117. PubMed PMID:
1291 33239446; PubMed Central PMCID: PMCPMC7749331.
1292 14. Kaur R, Tada T, Landau NR. Restriction of SARS-CoV-2 replication by receptor transporter
1293 protein 4 (RTP4). mBio. 2023;14(4):e0109023. Epub 20230629. doi: 10.1128/mbio.01090-23.
1294 PubMed PMID: 37382452; PubMed Central PMCID: PMCPMC10470548.
1295 15. Schoggins JW, Wilson SJ, Panis M, Murphy MY, Jones CT, Bieniasz P, et al. A diverse range
1296 of gene products are effectors of the type I interferon antiviral response. Nature.
1297 2011;472(7344):481-5. Epub 20110410. doi: 10.1038/nature09907. PubMed PMID: 21478870;
1298 PubMed Central PMCID: PMCPMC3409588.
1299 16. Schoggins JW. Interferon-Stimulated Genes: What Do They All Do? Annu Rev Virol.
1300 2019;6(1):567-84. Epub 2019/07/10. doi: 10.1146/annurev-virology-092818-015756. PubMed
1301 PMID: 31283436.
1302 17. Mac Kain A, Maarifi G, Aicher SM, Arhel N, Baidaliuk A, Munier S, et al. Identification of
1303 DAXX as a restriction factor of SARS-CoV-2 through a CRISPR/Cas9 screen. Nat Commun.
1304 2022;13(1):2442. Epub 20220504. doi: 10.1038/s41467-022-30134-9. PubMed PMID:
1305 35508460; PubMed Central PMCID: PMCPMC9068693.
1306 18. Xu D, Jiang W, Wu L, Gaudet RG, Park ES, Su M, et al. PLSCR1 is a cell-autonomous
1307 defence factor against SARS-CoV-2 infection. Nature. 2023;619(7971):819-27. Epub 20230712.
1308 doi: 10.1038/s41586-023-06322-y. PubMed PMID: 37438530; PubMed Central PMCID:
1309 PMCPMC10371867.
1310 19. Kim HS, Lee K, Kim SJ, Cho S, Shin HJ, Kim C, et al. Arrayed CRISPR screen with image-
1311 based assay reliably uncovers host genes required for coxsackievirus infection. Genome Res.
1312 2018;28(6):859-68. Epub 20180430. doi: 10.1101/gr.230250.117. PubMed PMID: 29712754;
1313 PubMed Central PMCID: PMCPMC5991512.
1314 20. Kodigepalli KM, Bowers K, Sharp A, Nanjundan M. Roles and regulation of phospholipid
1315 scramblases. FEBS Lett. 2015;589(1):3-14. Epub 20141203. doi: 10.1016/j.febslet.2014.11.036.
1316 PubMed PMID: 25479087.
1317 21. Zhou Q, Zhao J, Stout JG, Luhm RA, Wiedmer T, Sims PJ. Molecular cloning of human
1318 plasma membrane phospholipid scramblase. A protein mediating transbilayer movement of
1319 plasma membrane phospholipids. J Biol Chem. 1997;272(29):18240-4. doi:
1320 10.1074/jbc.272.29.18240. PubMed PMID: 9218461.

1321 22. Dong B, Zhou Q, Zhao J, Zhou A, Harty RN, Bose S, et al. Phospholipid scramblase 1
1322 potentiates the antiviral activity of interferon. J Virol. 2004;78(17):8983-93. doi:
1323 10.1128/JVI.78.17.8983-8993.2004. PubMed PMID: 15308695; PubMed Central PMCID:
1324 PMCPMC506946.
1325 23. Pairo-Castineira E, Rawlik K, Bretherick AD, Qi T, Wu Y, Nassiri I, et al. GWAS and meta-
1326 analysis identifies 49 genetic variants underlying critical COVID-19. Nature. 2023;617(7962):764-
1327 8. Epub 20230517. doi: 10.1038/s41586-023-06034-3. PubMed PMID: 37198478; PubMed
1328 Central PMCID: PMCPMC10208981.
1329 24. Kousathanas A, Pairo-Castineira E, Rawlik K, Stuckey A, Odhams CA, Walker S, et al.
1330 Whole-genome sequencing reveals host factors underlying critical COVID-19. Nature.
1331 2022;607(7917):97-103. Epub 20220307. doi: 10.1038/s41586-022-04576-6. PubMed PMID:
1332 35255492; PubMed Central PMCID: PMCPMC9259496.
1333 25. Baggen J, Vanstreels E, Jansen S, Daelemans D. Cellular host factors for SARS-CoV-2
1334 infection. Nat Microbiol. 2021;6(10):1219-32. Epub 20210901. doi: 10.1038/s41564-021-00958-
1335 0. PubMed PMID: 34471255.
1336 26. Hoffmann HH, Sanchez-Rivera FJ, Schneider WM, Luna JM, Soto-Feliciano YM, Ashbrook
1337 AW, et al. Functional interrogation of a SARS-CoV-2 host protein interactome identifies unique
1338 and shared coronavirus host factors. Cell Host Microbe. 2021;29(2):267-80 e5. Epub 20201216.
1339 doi: 10.1016/j.chom.2020.12.009. PubMed PMID: 33357464; PubMed Central PMCID:
1340 PMCPMC7833927.
1341 27. Li Q, Wu J, Nie J, Zhang L, Hao H, Liu S, et al. The Impact of Mutations in SARS-CoV-2
1342 Spike on Viral Infectivity and Antigenicity. Cell. 2020;182(5):1284-94 e9. Epub 20200717. doi:
1343 10.1016/j.cell.2020.07.012. PubMed PMID: 32730807; PubMed Central PMCID:
1344 PMCPMC7366990.
1345 28. Riva L, Yuan S, Yin X, Martin-Sancho L, Matsunaga N, Pache L, et al. Discovery of SARS-
1346 CoV-2 antiviral drugs through large-scale compound repurposing. Nature. 2020;586(7827):113-
1347 9. Epub 20200724. doi: 10.1038/s41586-020-2577-1. PubMed PMID: 32707573; PubMed
1348 Central PMCID: PMCPMC7603405.
1349 29. Schneider WM, Luna JM, Hoffmann HH, Sanchez-Rivera FJ, Leal AA, Ashbrook AW, et al.
1350 Genome-Scale Identification of SARS-CoV-2 and Pan-coronavirus Host Factor Networks. Cell.
1351 2021;184(1):120-32 e14. Epub 20201209. doi: 10.1016/j.cell.2020.12.006. PubMed PMID:
1352 33382968; PubMed Central PMCID: PMCPMC7796900.
1353 30. Xia S, Lan Q, Su S, Wang X, Xu W, Liu Z, et al. The role of furin cleavage site in SARS-CoV-2
1354 spike protein-mediated membrane fusion in the presence or absence of trypsin. Signal
1355 Transduct Target Ther. 2020;5(1):92. Epub 20200612. doi: 10.1038/s41392-020-0184-0. PubMed
1356 PMID: 32532959; PubMed Central PMCID: PMCPMC7289711.
1357 31. Xia S, Liu M, Wang C, Xu W, Lan Q, Feng S, et al. Inhibition of SARS-CoV-2 (previously
1358 2019-nCoV) infection by a highly potent pan-coronavirus fusion inhibitor targeting its spike
1359 protein that harbors a high capacity to mediate membrane fusion. Cell Res. 2020;30(4):343-55.
1360 Epub 20200330. doi: 10.1038/s41422-020-0305-x. PubMed PMID: 32231345; PubMed Central
1361 PMCID: PMCPMC7104723.
1362 32. Yan Y, Chang L, Wang L. Laboratory testing of SARS-CoV, MERS-CoV, and SARS-CoV-2
1363 (2019-nCoV): Current status, challenges, and countermeasures. Rev Med Virol.

1364 2020;30(3):e2106. Epub 20200417. doi: 10.1002/rmv.2106. PubMed PMID: 32302058; PubMed
1365 Central PMCID: PMCPMC7235496.
1366 33. Barretina J, Caponigro G, Stransky N, Venkatesan K, Margolin AA, Kim S, et al. The Cancer
1367 Cell Line Encyclopedia enables predictive modelling of anticancer drug sensitivity. Nature.
1368 2012;483(7391):603-7. Epub 20120328. doi: 10.1038/nature11003. PubMed PMID: 22460905;
1369 PubMed Central PMCID: PMCPMC3320027.
1370 34. Klijn C, Durinck S, Stawiski EW, Haverty PM, Jiang Z, Liu H, et al. A comprehensive
1371 transcriptional portrait of human cancer cell lines. Nat Biotechnol. 2015;33(3):306-12. Epub
1372 20141208. doi: 10.1038/nbt.3080. PubMed PMID: 25485619.
1373 35. Consortium GT. Human genomics. The Genotype-Tissue Expression (GTEx) pilot analysis:
1374 multitissue gene regulation in humans. Science. 2015;348(6235):648-60. Epub 20150507. doi:
1375 10.1126/science.1262110. PubMed PMID: 25954001; PubMed Central PMCID:
1376 PMCPMC4547484.
1377 36. de Weerd NA, Samarajiwa SA, Hertzog PJ. Type I interferon receptors: biochemistry and
1378 biological functions. J Biol Chem. 2007;282(28):20053-7. Epub 20070514. doi:
1379 10.1074/jbc.R700006200. PubMed PMID: 17502368.
1380 37. de Weerd NA, Nguyen T. The interferons and their receptors--distribution and regulation.
1381 Immunol Cell Biol. 2012;90(5):483-91. Epub 20120313. doi: 10.1038/icb.2012.9. PubMed PMID:
1382 22410872; PubMed Central PMCID: PMCPMC7165917.
1383 38. Uze G, Schreiber G, Piehler J, Pellegrini S. The receptor of the type I interferon family.
1384 Curr Top Microbiol Immunol. 2007;316:71-95. doi: 10.1007/978-3-540-71329-6_5. PubMed
1385 PMID: 17969444.
1386 39. Horvath CM, Stark GR, Kerr IM, Darnell JE, Jr. Interactions between STAT and non-STAT
1387 proteins in the interferon-stimulated gene factor 3 transcription complex. Mol Cell Biol.
1388 1996;16(12):6957-64. doi: 10.1128/MCB.16.12.6957. PubMed PMID: 8943351; PubMed Central
1389 PMCID: PMCPMC231699.
1390 40. Veals SA, Schindler C, Leonard D, Fu XY, Aebersold R, Darnell JE, Jr., et al. Subunit of an
1391 alpha-interferon-responsive transcription factor is related to interferon regulatory factor and
1392 Myb families of DNA-binding proteins. Mol Cell Biol. 1992;12(8):3315-24. doi:
1393 10.1128/mcb.12.8.3315-3324.1992. PubMed PMID: 1630447; PubMed Central PMCID:
1394 PMCPMC364572.
1395 41. Darnell JE, Jr., Kerr IM, Stark GR. Jak-STAT pathways and transcriptional activation in
1396 response to IFNs and other extracellular signaling proteins. Science. 1994;264(5164):1415-21.
1397 doi: 10.1126/science.8197455. PubMed PMID: 8197455.
1398 42. Schindler C, Strehlow I. Cytokines and STAT signaling. Adv Pharmacol. 2000;47:113-74.
1399 doi: 10.1016/s1054-3589(08)60111-8. PubMed PMID: 10582086.
1400 43. Levy DE, Darnell JE, Jr. Stats: transcriptional control and biological impact. Nat Rev Mol
1401 Cell Biol. 2002;3(9):651-62. doi: 10.1038/nrm909. PubMed PMID: 12209125.
1402 44. Perng YC, Lenschow DJ. ISG15 in antiviral immunity and beyond. Nat Rev Microbiol.
1403 2018;16(7):423-39. doi: 10.1038/s41579-018-0020-5. PubMed PMID: 29769653; PubMed
1404 Central PMCID: PMCPMC7097117.
1405 45. Speer SD, Li Z, Buta S, Payelle-Brogard B, Qian L, Vigant F, et al. ISG15 deficiency and
1406 increased viral resistance in humans but not mice. Nat Commun. 2016;7:11496. Epub

1407 20160519. doi: 10.1038/ncomms11496. PubMed PMID: 27193971; PubMed Central PMCID:
1408 PMCPMC4873964.
1409 46. Zhang X, Bogunovic D, Payelle-Brogard B, Francois-Newton V, Speer SD, Yuan C, et al.
1410 Human intracellular ISG15 prevents interferon-alpha/beta over-amplification and auto-
1411 inflammation. Nature. 2015;517(7532):89-93. Epub 20141012. doi: 10.1038/nature13801.
1412 PubMed PMID: 25307056; PubMed Central PMCID: PMCPMC4303590.
1413 47. Naka T, Narazaki M, Hirata M, Matsumoto T, Minamoto S, Aono A, et al. Structure and
1414 function of a new STAT-induced STAT inhibitor. Nature. 1997;387(6636):924-9. doi:
1415 10.1038/43219. PubMed PMID: 9202127.
1416 48. Malakhova OA, Kim KI, Luo JK, Zou W, Kumar KG, Fuchs SY, et al. UBP43 is a novel
1417 regulator of interferon signaling independent of its ISG15 isopeptidase activity. EMBO J.
1418 2006;25(11):2358-67. Epub 20060518. doi: 10.1038/sj.emboj.7601149. PubMed PMID:
1419 16710296; PubMed Central PMCID: PMCPMC1478183.
1420 49. Francois-Newton V, Magno de Freitas Almeida G, Payelle-Brogard B, Monneron D,
1421 Pichard-Garcia L, Piehler J, et al. USP18-based negative feedback control is induced by type I and
1422 type III interferons and specifically inactivates interferon alpha response. PLoS One.
1423 2011;6(7):e22200. Epub 20110714. doi: 10.1371/journal.pone.0022200. PubMed PMID:
1424 21779393; PubMed Central PMCID: PMCPMC3136508.
1425 50. Ziegler CGK, Allon SJ, Nyquist SK, Mbano IM, Miao VN, Tzouanas CN, et al. SARS-CoV-2
1426 Receptor ACE2 Is an Interferon-Stimulated Gene in Human Airway Epithelial Cells and Is
1427 Detected in Specific Cell Subsets across Tissues. Cell. 2020;181(5):1016-35 e19. Epub 20200427.
1428 doi: 10.1016/j.cell.2020.04.035. PubMed PMID: 32413319; PubMed Central PMCID:
1429 PMCPMC7252096.
1430 51. Onabajo OO, Banday AR, Stanifer ML, Yan W, Obajemu A, Santer DM, et al. Interferons
1431 and viruses induce a novel truncated ACE2 isoform and not the full-length SARS-CoV-2 receptor.
1432 Nat Genet. 2020;52(12):1283-93. Epub 20201019. doi: 10.1038/s41588-020-00731-9. PubMed
1433 PMID: 33077916; PubMed Central PMCID: PMCPMC9377523.
1434 52. Zhao MM, Yang WL, Yang FY, Zhang L, Huang WJ, Hou W, et al. Cathepsin L plays a key
1435 role in SARS-CoV-2 infection in humans and humanized mice and is a promising target for new
1436 drug development. Signal Transduct Target Ther. 2021;6(1):134. Epub 20210327. doi:
1437 10.1038/s41392-021-00558-8. PubMed PMID: 33774649; PubMed Central PMCID:
1438 PMCPMC7997800.
1439 53. Shang J, Wan Y, Luo C, Ye G, Geng Q, Auerbach A, et al. Cell entry mechanisms of SARS-
1440 CoV-2. Proc Natl Acad Sci U S A. 2020;117(21):11727-34. Epub 20200506. doi:
1441 10.1073/pnas.2003138117. PubMed PMID: 32376634; PubMed Central PMCID:
1442 PMCPMC7260975.
1443 54. Liu T, Luo S, Libby P, Shi GP. Cathepsin L-selective inhibitors: A potentially promising
1444 treatment for COVID-19 patients. Pharmacol Ther. 2020;213:107587. Epub 20200526. doi:
1445 10.1016/j.pharmthera.2020.107587. PubMed PMID: 32470470; PubMed Central PMCID:
1446 PMCPMC7255230.
1447 55. Hoffmann M, Kleine-Weber H, Schroeder S, Kruger N, Herrler T, Erichsen S, et al. SARS-
1448 CoV-2 Cell Entry Depends on ACE2 and TMPRSS2 and Is Blocked by a Clinically Proven Protease
1449 Inhibitor. Cell. 2020;181(2):271-80 e8. Epub 20200305. doi: 10.1016/j.cell.2020.02.052. PubMed
1450 PMID: 32142651; PubMed Central PMCID: PMCPMC7102627.

1451 56. Jackson CB, Farzan M, Chen B, Choe H. Mechanisms of SARS-CoV-2 entry into cells. Nat
1452 Rev Mol Cell Biol. 2022;23(1):3-20. Epub 20211005. doi: 10.1038/s41580-021-00418-x. PubMed
1453 PMID: 34611326; PubMed Central PMCID: PMCPMC8491763.
1454 57. Pellegrini S, John J, Shearer M, Kerr IM, Stark GR. Use of a selectable marker regulated
1455 by alpha interferon to obtain mutations in the signaling pathway. Mol Cell Biol.
1456 1989;9(11):4605-12. doi: 10.1128/mcb.9.11.4605-4612.1989. PubMed PMID: 2513475;
1457 PubMed Central PMCID: PMCPMC363606.
1458 58. Velazquez L, Fellous M, Stark GR, Pellegrini S. A protein tyrosine kinase in the interferon
1459 alpha/beta signaling pathway. Cell. 1992;70(2):313-22. doi: 10.1016/0092-8674(92)90105-l.
1460 PubMed PMID: 1386289.
1461 59. Wang S, Li W, Hui H, Tiwari SK, Zhang Q, Croker BA, et al. Cholesterol 25-Hydroxylase
1462 inhibits SARS-CoV-2 and other coronaviruses by depleting membrane cholesterol. EMBO J.
1463 2020;39(21):e106057. Epub 20201005. doi: 10.15252/embj.2020106057. PubMed PMID:
1464 32944968; PubMed Central PMCID: PMCPMC7537045.
1465 60. Zhu Y, Feng F, Hu G, Wang Y, Yu Y, Zhu Y, et al. A genome-wide CRISPR screen identifies
1466 host factors that regulate SARS-CoV-2 entry. Nat Commun. 2021;12(1):961. Epub 20210211. doi:
1467 10.1038/s41467-021-21213-4. PubMed PMID: 33574281; PubMed Central PMCID:
1468 PMCPMC7878750.
1469 61. Wei LH, Sun Y, Guo JU. Genome-wide CRISPR screens identify noncanonical translation
1470 factor eIF2A as an enhancer of SARS-CoV-2 programmed -1 ribosomal frameshifting. Cell Rep.
1471 2023;42(8):112987. Epub 20230814. doi: 10.1016/j.celrep.2023.112987. PubMed PMID:
1472 37581984.
1473 62. Wei J, Alfajaro MM, DeWeirdt PC, Hanna RE, Lu-Culligan WJ, Cai WL, et al. Genome-wide
1474 CRISPR Screens Reveal Host Factors Critical for SARS-CoV-2 Infection. Cell. 2021;184(1):76-91
1475 e13. Epub 20201020. doi: 10.1016/j.cell.2020.10.028. PubMed PMID: 33147444; PubMed
1476 Central PMCID: PMCPMC7574718.
1477 63. Wang R, Simoneau CR, Kulsuptrakul J, Bouhaddou M, Travisano KA, Hayashi JM, et al.
1478 Genetic Screens Identify Host Factors for SARS-CoV-2 and Common Cold Coronaviruses. Cell.
1479 2021;184(1):106-19 e14. Epub 20201209. doi: 10.1016/j.cell.2020.12.004. PubMed PMID:
1480 33333024; PubMed Central PMCID: PMCPMC7723770.
1481 64. Song J, Chow RD, Pena-Hernandez MA, Zhang L, Loeb SA, So EY, et al. LRRC15 inhibits
1482 SARS-CoV-2 cellular entry in trans. PLoS Biol. 2022;20(10):e3001805. Epub 20221013. doi:
1483 10.1371/journal.pbio.3001805. PubMed PMID: 36228039; PubMed Central PMCID:
1484 PMCPMC9595563.
1485 65. Hossain MS, Kerkvliet JG, Hoppe AD. Whole genome CRISPR screening strategy to
1486 identify genes contributing to SARS-CoV-2 spike and VSV-G mediated entry. J Med Virol.
1487 2023;95(9):e29087. doi: 10.1002/jmv.29087. PubMed PMID: 37707319.
1488 66. Rehfeld F, Eitson JL, Ohlson MB, Chang TC, Schoggins JW, Mendell JT. CRISPR screening
1489 reveals a dependency on ribosome recycling for efficient SARS-CoV-2 programmed ribosomal
1490 frameshifting and viral replication. Cell Rep. 2023;42(2):112076. Epub 20230130. doi:
1491 10.1016/j.celrep.2023.112076. PubMed PMID: 36753415; PubMed Central PMCID:
1492 PMCPMC9884621.
1493 67. Rebendenne A, Roy P, Bonaventure B, Chaves VAL, Desmarets L, Rouille Y, et al.
1494 Bidirectional genome-wide CRISPR screens reveal host factors regulating SARS-CoV-2, MERS-CoV

1495 and seasonal HCoVs. Res Sq. 2021. Epub 20210527. doi: 10.21203/rs.3.rs-555275/v1. PubMed
1496 PMID: 34075371; PubMed Central PMCID: PMCPMC8168385.
1497 68. Pahmeier F, Lavacca TM, Goellner S, Neufeldt CJ, Prasad V, Cerikan B, et al. Identification
1498 of host dependency factors involved in SARS-CoV-2 replication organelle formation through
1499 proteomics and ultrastructural analysis. J Virol. 2023:e0087823. Epub 20231031. doi:
1500 10.1128/jvi.00878-23. PubMed PMID: 37905840.
1501 69. Loo L, Waller MA, Moreno CL, Cole AJ, Stella AO, Pop OT, et al. Fibroblast-expressed
1502 LRRC15 is a receptor for SARS-CoV-2 spike and controls antiviral and antifibrotic transcriptional
1503 programs. PLoS Biol. 2023;21(2):e3001967. Epub 20230209. doi: 10.1371/journal.pbio.3001967.
1504 PubMed PMID: 36757924; PubMed Central PMCID: PMCPMC9910744.
1505 70. Israeli M, Finkel Y, Yahalom-Ronen Y, Paran N, Chitlaru T, Israeli O, et al. Genome-wide
1506 CRISPR screens identify GATA6 as a proviral host factor for SARS-CoV-2 via modulation of ACE2.
1507 Nat Commun. 2022;13(1):2237. Epub 20220425. doi: 10.1038/s41467-022-29896-z. PubMed
1508 PMID: 35469023; PubMed Central PMCID: PMCPMC9039069.
1509 71. Grodzki M, Bluhm AP, Schaefer M, Tagmount A, Russo M, Sobh A, et al. Genome-scale
1510 CRISPR screens identify host factors that promote human coronavirus infection. Genome Med.
1511 2022;14(1):10. Epub 20220127. doi: 10.1186/s13073-022-01013-1. PubMed PMID: 35086559;
1512 PubMed Central PMCID: PMCPMC8792531.
1513 72. Gordon DE, Hiatt J, Bouhaddou M, Rezelj VV, Ulferts S, Braberg H, et al. Comparative
1514 host-coronavirus protein interaction networks reveal pan-viral disease mechanisms. Science.
1515 2020;370(6521). Epub 20201015. doi: 10.1126/science.abe9403. PubMed PMID: 33060197;
1516 PubMed Central PMCID: PMCPMC7808408.
1517 73. Daniloski Z, Jordan TX, Wessels HH, Hoagland DA, Kasela S, Legut M, et al. Identification
1518 of Required Host Factors for SARS-CoV-2 Infection in Human Cells. Cell. 2021;184(1):92-105 e16.
1519 Epub 20201024. doi: 10.1016/j.cell.2020.10.030. PubMed PMID: 33147445; PubMed Central
1520 PMCID: PMCPMC7584921.
1521 74. Chan K, Farias AG, Lee H, Guvenc F, Mero P, Brown KR, et al. Survival-based CRISPR
1522 genetic screens across a panel of permissive cell lines identify common and cell-specific SARS-
1523 CoV-2 host factors. Heliyon. 2023;9(1):e12744. Epub 20221230. doi:
1524 10.1016/j.heliyon.2022.e12744. PubMed PMID: 36597481; PubMed Central PMCID:
1525 PMCPMC9800021.
1526 75. Biering SB, Sarnik SA, Wang E, Zengel JR, Leist SR, Schafer A, et al. Genome-wide
1527 bidirectional CRISPR screens identify mucins as host factors modulating SARS-CoV-2 infection.
1528 Nat Genet. 2022;54(8):1078-89. Epub 20220725. doi: 10.1038/s41588-022-01131-x. PubMed
1529 PMID: 35879412; PubMed Central PMCID: PMCPMC9355872.
1530 76. Baggen J, Persoons L, Vanstreels E, Jansen S, Van Looveren D, Boeckx B, et al. Genome-
1531 wide CRISPR screening identifies TMEM106B as a proviral host factor for SARS-CoV-2. Nat
1532 Genet. 2021;53(4):435-44. Epub 20210308. doi: 10.1038/s41588-021-00805-2. PubMed PMID:
1533 33686287.
1534 77. van der Made CI, Simons A, Schuurs-Hoeijmakers J, van den Heuvel G, Mantere T,
1535 Kersten S, et al. Presence of Genetic Variants Among Young Men With Severe COVID-19. JAMA.
1536 2020;324(7):663-73. doi: 10.1001/jama.2020.13719. PubMed PMID: 32706371; PubMed
1537 Central PMCID: PMCPMC7382021.

78. Shelton JF, Shastri AJ, Ye C, Weldon CH, Filshtein-Sonmez T, Coker D, et al. Trans-ancestry analysis reveals genetic and nongenetic associations with COVID-19 susceptibility and severity. Nat Genet. 2021;53(6):801-8. Epub 20210422. doi: 10.1038/s41588-021-00854-7. PubMed PMID: 33888907.
79. Roberts GHL, Partha R, Rhead B, Knight SC, Park DS, Coignet MV, et al. Expanded COVID-19 phenotype definitions reveal distinct patterns of genetic association and protective effects. Nat Genet. 2022;54(4):374-81. Epub 20220411. doi: 10.1038/s41588-022-01042-x. PubMed PMID: 35410379.
80. Pietzner M, Chua RL, Wheeler E, Jechow K, Willett JDS, Radbruch H, et al. ELF5 is a potential respiratory epithelial cell-specific risk gene for severe COVID-19. Nat Commun. 2022;13(1):4484. Epub 20220815. doi: 10.1038/s41467-022-31999-6. PubMed PMID: 35970849; PubMed Central PMCID: PMCPMC9378714.
81. Latini A, Agolini E, Novelli A, Borgiani P, Giannini R, Gravina P, et al. COVID-19 and Genetic Variants of Protein Involved in the SARS-CoV-2 Entry into the Host Cells. Genes (Basel). 2020;11(9). Epub 20200827. doi: 10.3390/genes11091010. PubMed PMID: 32867305; PubMed Central PMCID: PMCPMC7565048.
82. Horowitz JE, Kosmicki JA, Damask A, Sharma D, Roberts GHL, Justice AE, et al. Genome-wide analysis provides genetic evidence that ACE2 influences COVID-19 risk and yields risk scores associated with severe disease. Nat Genet. 2022;54(4):382-92. Epub 20220303. doi: 10.1038/s41588-021-01006-7. PubMed PMID: 35241825; PubMed Central PMCID: PMCPMC9005345.
83. Garcia-Garcia A, Perez de Diego R, Flores C, Rinchai D, Sole-Violan J, Deya-Martinez A, et al. Humans with inherited MyD88 and IRAK-4 deficiencies are predisposed to hypoxemic COVID-19 pneumonia. J Exp Med. 2023;220(5). Epub 20230303. doi: 10.1084/jem.20220170. PubMed PMID: 36880831; PubMed Central PMCID: PMCPMC9998661.
84. Fallerini C, Daga S, Mantovani S, Benetti E, Picchiotti N, Francisci D, et al. Association of Toll-like receptor 7 variants with life-threatening COVID-19 disease in males: findings from a nested case-control study. Elife. 2021;10. Epub 20210302. doi: 10.7554/eLife.67569. PubMed PMID: 33650967; PubMed Central PMCID: PMCPMC7987337.
85. Severe Covid GG, Ellinghaus D, Degenhardt F, Bujanda L, Buti M, Albillos A, et al. Genomewide Association Study of Severe Covid-19 with Respiratory Failure. N Engl J Med. 2020;383(16):1522-34. Epub 20200617. doi: 10.1056/NEJMoa2020283. PubMed PMID: 32558485; PubMed Central PMCID: PMCPMC7315890.
86. Degenhardt F, Ellinghaus D, Juzenas S, Lerga-Jaso J, Wendorff M, Maya-Miles D, et al. Detailed stratified GWAS analysis for severe COVID-19 in four European populations. Hum Mol Genet. 2022;31(23):3945-66. doi: 10.1093/hmg/ddac158. PubMed PMID: 35848942; PubMed Central PMCID: PMCPMC9703941.
87. D'Antonio M, Nguyen JP, Arthur TD, Matsui H, Initiative C-HG, D'Antonio-Chronowska A, et al. SARS-CoV-2 susceptibility and COVID-19 disease severity are associated with genetic variants affecting gene expression in a variety of tissues. Cell Rep. 2021;37(7):110020. Epub 20211103. doi: 10.1016/j.celrep.2021.110020. PubMed PMID: 34762851; PubMed Central PMCID: PMCPMC8563343.

1580 88. Cruz R, Diz-de Almeida S, Lopez de Heredia M, Quintela I, Ceballos FC, Pita G, et al. Novel
1581 genes and sex differences in COVID-19 severity. Hum Mol Genet. 2022;31(22):3789-806. doi:
1582 10.1093/hmg/ddac132. PubMed PMID: 35708486; PubMed Central PMCID: PMCPMC9652109.
1583 89. Initiative C-HG. A first update on mapping the human genetic architecture of COVID-19.
1584 Nature. 2022;608(7921):E1-E10. Epub 20220803. doi: 10.1038/s41586-022-04826-7. PubMed
1585 PMID: 35922517; PubMed Central PMCID: PMCPMC9352569.
1586 90. Andolfo I, Russo R, Lasorsa VA, Cantalupo S, Rosato BE, Bonfiglio F, et al. Common
1587 variants at 21q22.3 locus influence MX1 and TMPRSS2 gene expression and susceptibility to
1588 severe COVID-19. iScience. 2021;24(4):102322. Epub 20210317. doi:
1589 10.1016/j.isci.2021.102322. PubMed PMID: 33748697; PubMed Central PMCID:
1590 PMCPMC7968217.
1591 91. Zhou S, Butler-Laporte G, Nakanishi T, Morrison DR, Afilalo J, Afilalo M, et al. A
1592 Neanderthal OAS1 isoform protects individuals of European ancestry against COVID-19
1593 susceptibility and severity. Nat Med. 2021;27(4):659-67. Epub 20210225. doi: 10.1038/s41591-
1594 021-01281-1. PubMed PMID: 33633408.
1595 92. Huffman JE, Butler-Laporte G, Khan A, Pairo-Castineira E, Drivas TG, Peloso GM, et al.
1596 Multi-ancestry fine mapping implicates OAS1 splicing in risk of severe COVID-19. Nat Genet.
1597 2022;54(2):125-7. Epub 20220113. doi: 10.1038/s41588-021-00996-8. PubMed PMID:
1598 35027740; PubMed Central PMCID: PMCPMC8837537.
1599 93. Initiative C-HG. Mapping the human genetic architecture of COVID-19. Nature.
1600 2021;600(7889):472-7. Epub 20210708. doi: 10.1038/s41586-021-03767-x. PubMed PMID:
1601 34237774; PubMed Central PMCID: PMCPMC8674144.
1602 94. Pairo-Castineira E, Clohisey S, Klaric L, Bretherick AD, Rawlik K, Pasko D, et al. Genetic
1603 mechanisms of critical illness in COVID-19. Nature. 2021;591(7848):92-8. Epub 20201211. doi:
1604 10.1038/s41586-020-03065-y. PubMed PMID: 33307546.
1605 95. Banday AR, Stanifer ML, Florez-Vargas O, Onabajo OO, Papenberg BW, Zahoor MA, et al.
1606 Genetic regulation of OAS1 nonsense-mediated decay underlies association with COVID-19
1607 hospitalization in patients of European and African ancestries. Nat Genet. 2022;54(8):1103-16.
1608 Epub 20220714. doi: 10.1038/s41588-022-01113-z. PubMed PMID: 35835913; PubMed Central
1609 PMCID: PMCPMC9355882.
1610 96. Payman S-T, Hala A, James DRK, Audrey A, Reuben S, Zhen-Yuan L, et al. A SARS-CoV-2 –
1611 host proximity interactome. bioRxiv. 2020:2020.09.03.282103. doi:
1612 10.1101/2020.09.03.282103.
1613 97. Gordon DE, Jang GM, Bouhaddou M, Xu J, Obernier K, White KM, et al. A SARS-CoV-2
1614 protein interaction map reveals targets for drug repurposing. Nature. 2020;583(7816):459-68.
1615 Epub 20200430. doi: 10.1038/s41586-020-2286-9. PubMed PMID: 32353859; PubMed Central
1616 PMCID: PMCPMC7431030.
1617 98. Estelle MNL, Yorgos S, Anastassia K, Jean-Pascal G, Payman Samavarchi T, Dae-Kyum K, et
1618 al. Global BioID-based SARS-CoV-2 proteins proximal interactome unveils novel ties between
1619 viral polypeptides and host factors involved in multiple COVID19-associated mechanisms.
1620 bioRxiv. 2020:2020.08.28.272955. doi: 10.1101/2020.08.28.272955.
1621 99. St-Germain JR, Astori A, Samavarchi-Tehrani P, Abdouni H, Macwan V, Kim D-K, et al. A
1622 SARS-CoV-2 BioID-based virus-host membrane protein interactome and virus peptide

compendium: new proteomics resources for COVID-19 research. bioRxiv. 2020:2020.08.28.269175. doi: 10.1101/2020.08.28.269175.

100. Liu X, Huuskonen S, Laitinen T, Redchuk T, Bogacheva M, Salokas K, et al. SARS-CoV-2-host proteome interactions for antiviral drug discovery. Mol Syst Biol. 2021;17(11):e10396. doi: 10.15252/msb.202110396. PubMed PMID: 34709727; PubMed Central PMCID: PMCPMC8552907.

101. May DG, Martin-Sancho L, Anschau V, Liu S, Chrisopulos RJ, Scott KL, et al. A BioID-Derived Proximity Interactome for SARS-CoV-2 Proteins. Viruses. 2022;14(3). Epub 20220315. doi: 10.3390/v14030611. PubMed PMID: 35337019; PubMed Central PMCID: PMCPMC8951556.

102. Zhou Y, Liu Y, Gupta S, Paramo MI, Hou Y, Mao C, et al. A comprehensive SARS-CoV-2-human protein-protein interactome reveals COVID-19 pathobiology and potential host therapeutic targets. Nat Biotechnol. 2023;41(1):128-39. Epub 20221010. doi: 10.1038/s41587-022-01474-0. PubMed PMID: 36217030; PubMed Central PMCID: PMCPMC9851973.

103. Stukalov A, Girault V, Grass V, Karayel O, Bergant V, Urban C, et al. Multilevel proteomics reveals host perturbations by SARS-CoV-2 and SARS-CoV. Nature. 2021;594(7862):246-52. Epub 20210412. doi: 10.1038/s41586-021-03493-4. PubMed PMID: 33845483.

104. Li J, Guo M, Tian X, Wang X, Yang X, Wu P, et al. Virus-Host Interactome and Proteomic Survey Reveal Potential Virulence Factors Influencing SARS-CoV-2 Pathogenesis. Med. 2021;2(1):99-112 e7. Epub 20200721. doi: 10.1016/j.medj.2020.07.002. PubMed PMID: 32838362; PubMed Central PMCID: PMCPMC7373048.

105. Davies JP, Almasy KM, McDonald EF, Plate L. Comparative Multiplexed Interactomics of SARS-CoV-2 and Homologous Coronavirus Nonstructural Proteins Identifies Unique and Shared Host-Cell Dependencies. ACS Infect Dis. 2020;6(12):3174-89. Epub 20201202. doi: 10.1021/acsinfecdis.0c00500. PubMed PMID: 33263384; PubMed Central PMCID: PMCPMC7724760.

106. Schmidt N, Ganskih S, Wei Y, Gabel A, Zielinski S, Keshishian H, et al. SND1 binds SARS-CoV-2 negative-sense RNA and promotes viral RNA synthesis through NSP9. Cell. 2023;186(22):4834-50 e23. Epub 20231003. doi: 10.1016/j.cell.2023.09.002. PubMed PMID: 37794589; PubMed Central PMCID: PMCPMC10617981.

107. Schmidt N, Lareau CA, Keshishian H, Ganskih S, Schneider C, Hennig T, et al. The SARS-CoV-2 RNA-protein interactome in infected human cells. Nat Microbiol. 2021;6(3):339-53. Epub 20201221. doi: 10.1038/s41564-020-00846-z. PubMed PMID: 33349665; PubMed Central PMCID: PMCPMC7906908.

108. Labeau A, Fery-Simonian L, Lefevre-Utile A, Pourcelot M, Bonnet-Madin L, Soumelis V, et al. Characterization and functional interrogation of the SARS-CoV-2 RNA interactome. Cell Rep. 2022;39(4):110744. doi: 10.1016/j.celrep.2022.110744. PubMed PMID: 35477000; PubMed Central PMCID: PMCPMC9040432.

109. Kamel W, Noerenberg M, Cerikan B, Chen H, Jarvelin AI, Kammoun M, et al. Global analysis of protein-RNA interactions in SARS-CoV-2-infected cells reveals key regulators of infection. Mol Cell. 2021;81(13):2851-67 e7. Epub 20210524. doi: 10.1016/j.molcel.2021.05.023. PubMed PMID: 34118193; PubMed Central PMCID: PMCPMC8142890.

1666 110. Flynn RA, Belk JA, Qi Y, Yasumoto Y, Wei J, Alfajaro MM, et al. Discovery and functional
1667 interrogation of SARS-CoV-2 RNA-host protein interactions. Cell. 2021;184(9):2394-411 e16.
1668 Epub 20210311. doi: 10.1016/j.cell.2021.03.012. PubMed PMID: 33743211; PubMed Central
1669 PMCID: PMCPMC7951565.
1670 111. Lee S, Lee YS, Choi Y, Son A, Park Y, Lee KM, et al. The SARS-CoV-2 RNA interactome. Mol
1671 Cell. 2021;81(13):2838-50 e6. Epub 20210427. doi: 10.1016/j.molcel.2021.04.022. PubMed
1672 PMID: 33989516; PubMed Central PMCID: PMCPMC8075806.
1673 112. Bouhaddou M, Memon D, Meyer B, White KM, Rezelj VV, Correa Marrero M, et al. The
1674 Global Phosphorylation Landscape of SARS-CoV-2 Infection. Cell. 2020;182(3):685-712 e19.
1675 Epub 20200628. doi: 10.1016/j.cell.2020.06.034. PubMed PMID: 32645325; PubMed Central
1676 PMCID: PMCPMC7321036.
1677 113. Sanchez-Magraner L, Posada IM, Andraka N, Contreras FX, Viguera AR, Guerin DM, et al.
1678 The C-terminal transmembrane domain of human phospholipid scramblase 1 is essential for the
1679 protein flip-flop activity and Ca(2)(+)-binding. J Membr Biol. 2014;247(2):155-65. Epub
1680 20131217. doi: 10.1007/s00232-013-9619-7. PubMed PMID: 24343571.
1681 114. Ricardo-Lax I, Luna JM, Thao TTN, Le Pen J, Yu Y, Hoffmann HH, et al. Replication and
1682 single-cycle delivery of SARS-CoV-2 replicons. Science. 2021;374(6571):1099-106. Epub
1683 20211014. doi: 10.1126/science.abj8430. PubMed PMID: 34648371; PubMed Central PMCID:
1684 PMCPMC9007107.
1685 115. Schmidt F, Weisblum Y, Muecksch F, Hoffmann HH, Michailidis E, Lorenzi JCC, et al.
1686 Measuring SARS-CoV-2 neutralizing antibody activity using pseudotyped and chimeric viruses. J
1687 Exp Med. 2020;217(11). doi: 10.1084/jem.20201181. PubMed PMID: 32692348; PubMed
1688 Central PMCID: PMCPMC7372514.
1689 116. Khan H, Winstone H, Jimenez-Guardeno JM, Graham C, Doores KJ, Goujon C, et al.
1690 TMPRSS2 promotes SARS-CoV-2 evasion from NCOA7-mediated restriction. PLoS Pathog.
1691 2021;17(11):e1009820. Epub 20211122. doi: 10.1371/journal.ppat.1009820. PubMed PMID:
1692 34807954; PubMed Central PMCID: PMCPMC8648102.
1693 117. Thorne LG, Bouhaddou M, Reuschl AK, Zuliani-Alvarez L, Polacco B, Pelin A, et al.
1694 Evolution of enhanced innate immune evasion by SARS-CoV-2. Nature. 2022;602(7897):487-95.
1695 Epub 20211223. doi: 10.1038/s41586-021-04352-y. PubMed PMID: 34942634; PubMed Central
1696 PMCID: PMCPMC8850198.
1697 118. Markov PV, Ghafari M, Beer M, Lythgoe K, Simmonds P, Stilianakis NI, et al. The evolution
1698 of SARS-CoV-2. Nature Reviews Microbiology. 2023;21(6):361-79. doi: 10.1038/s41579-023-
1699 00878-2.
1700 119. Carabelli AM, Peacock TP, Thorne LG, Harvey WT, Hughes J, de Silva TI, et al. SARS-CoV-2
1701 variant biology: immune escape, transmission and fitness. Nature Reviews Microbiology.
1702 2023;21(3):162-77. doi: 10.1038/s41579-022-00841-7.
1703 120. Huang P, Liao R, Chen X, Wu X, Li X, Wang Y, et al. Nuclear translocation of PLSCR1
1704 activates STAT1 signaling in basal-like breast cancer. Theranostics. 2020;10(10):4644-58. Epub
1705 20200325. doi: 10.7150/thno.43150. PubMed PMID: 32292520; PubMed Central PMCID:
1706 PMCPMC7150476.
1707 121. Nanjundan M, Sun J, Zhao J, Zhou Q, Sims PJ, Wiedmer T. Plasma membrane
1708 phospholipid scramblase 1 promotes EGF-dependent activation of c-Src through the epidermal

growth factor receptor. J Biol Chem. 2003;278(39):37413-8. Epub 20030718. doi: 10.1074/jbc.M306182200. PubMed PMID: 12871937.

122. Ben-Efraim I, Zhou Q, Wiedmer T, Gerace L, Sims PJ. Phospholipid scramblase 1 is imported into the nucleus by a receptor-mediated pathway and interacts with DNA. Biochemistry. 2004;43(12):3518-26. doi: 10.1021/bi0356911. PubMed PMID: 15035622.

123. Chen MH, Ben-Efraim I, Mitrousis G, Walker-Kopp N, Sims PJ, Cingolani G. Phospholipid scramblase 1 contains a nonclassical nuclear localization signal with unique binding site in importin alpha. J Biol Chem. 2005;280(11):10599-606. Epub 20041217. doi: 10.1074/jbc.M413194200. PubMed PMID: 15611084.

124. Wiedmer T, Zhao J, Nanjundan M, Sims PJ. Palmitoylation of phospholipid scramblase 1 controls its distribution between nucleus and plasma membrane. Biochemistry. 2003;42(5):1227-33. doi: 10.1021/bi026679w. PubMed PMID: 12564925.

125. Zhao J, Zhou Q, Wiedmer T, Sims PJ. Palmitoylation of phospholipid scramblase is required for normal function in promoting Ca2+-activated transbilayer movement of membrane phospholipids. Biochemistry. 1998;37(18):6361-6. doi: 10.1021/bi980218m. PubMed PMID: 9572851.

126. Dittmann M, Hoffmann HH, Scull MA, Gilmore RH, Bell KL, Ciancanelli M, et al. A serpin shapes the extracellular environment to prevent influenza A virus maturation. Cell. 2015;160(4):631-43. doi: 10.1016/j.cell.2015.01.040. PubMed PMID: 25679759; PubMed Central PMCID: PMCPMC4328142.

127. Burke JM, St Clair LA, Perera R, Parker R. SARS-CoV-2 infection triggers widespread host mRNA decay leading to an mRNA export block. RNA. 2021;27(11):1318-29. Epub 20210727. doi: 10.1261/rna.078923.121. PubMed PMID: 34315815; PubMed Central PMCID: PMCPMC8522697.

128. Zhang K, Miorin L, Makio T, Dehghan I, Gao S, Xie Y, et al. Nsp1 protein of SARS-CoV-2 disrupts the mRNA export machinery to inhibit host gene expression. Sci Adv. 2021;7(6). Epub 20210205. doi: 10.1126/sciadv.abe7386. PubMed PMID: 33547084; PubMed Central PMCID: PMCPMC7864571.

129. Kimura I, Konno Y, Uriu K, Hopfensperger K, Sauter D, Nakagawa S, et al. Sarbecovirus ORF6 proteins hamper induction of interferon signaling. Cell Rep. 2021;34(13):108916. Epub 20210312. doi: 10.1016/j.celrep.2021.108916. PubMed PMID: 33765414; PubMed Central PMCID: PMCPMC7953434.

130. Setaro AC, Gaglia MM. All hands on deck: SARS-CoV-2 proteins that block early anti-viral interferon responses. Curr Res Virol Sci. 2021;2:100015. Epub 20211112. doi: 10.1016/j.crviro.2021.100015. PubMed PMID: 34786565; PubMed Central PMCID: PMCPMC8588586.

131. Ogunjimi B, Zhang SY, Sorensen KB, Skipper KA, Carter-Timofte M, Kerner G, et al. Inborn errors in RNA polymerase III underlie severe varicella zoster virus infections. J Clin Invest. 2017;127(9):3543-56. Epub 20170807. doi: 10.1172/JCI92280. PubMed PMID: 28783042; PubMed Central PMCID: PMCPMC5669568.

132. Zimmer MM, Kibe A, Rand U, Pekarek L, Ye L, Buck S, et al. The short isoform of the host antiviral protein ZAP acts as an inhibitor of SARS-CoV-2 programmed ribosomal frameshifting. Nat Commun. 2021;12(1):7193. Epub 20211210. doi: 10.1038/s41467-021-27431-0. PubMed PMID: 34893599; PubMed Central PMCID: PMCPMC8664833.

1753 133. Klein S, Golani G, Lolicato F, Lahr C, Beyer D, Herrmann A, et al. IFITM3 blocks influenza
1754 virus entry by sorting lipids and stabilizing hemifusion. Cell Host Microbe. 2023. Epub 20230329.
1755 doi: 10.1016/j.chom.2023.03.005. PubMed PMID: 37003257.
1756 134. Guo X, Steinkuhler J, Marin M, Li X, Lu W, Dimova R, et al. Interferon-Induced
1757 Transmembrane Protein 3 Blocks Fusion of Diverse Enveloped Viruses by Altering Mechanical
1758 Properties of Cell Membranes. ACS Nano. 2021;15(5):8155-70. Epub 20210303. doi:
1759 10.1021/acsnano.0c10567. PubMed PMID: 33656312; PubMed Central PMCID:
1760 PMCPMC8159881.
1761 135. Suddala KC, Lee CC, Meraner P, Marin M, Markosyan RM, Desai TM, et al. Interferon-
1762 induced transmembrane protein 3 blocks fusion of sensitive but not resistant viruses by
1763 partitioning into virus-carrying endosomes. PLoS Pathog. 2019;15(1):e1007532. Epub 20190114.
1764 doi: 10.1371/journal.ppat.1007532. PubMed PMID: 30640957; PubMed Central PMCID:
1765 PMCPMC6347298.
1766 136. Desai TM, Marin M, Chin CR, Savidis G, Brass AL, Melikyan GB. IFITM3 restricts influenza
1767 A virus entry by blocking the formation of fusion pores following virus-endosome hemifusion.
1768 PLoS Pathog. 2014;10(4):e1004048. Epub 20140403. doi: 10.1371/journal.ppat.1004048.
1769 PubMed PMID: 24699674; PubMed Central PMCID: PMCPMC3974867.
1770 137. Fadeel B, Gleiss B, Hogstrand K, Chandra J, Wiedmer T, Sims PJ, et al. Phosphatidylserine
1771 exposure during apoptosis is a cell-type-specific event and does not correlate with plasma
1772 membrane phospholipid scramblase expression. Biochem Biophys Res Commun.
1773 1999;266(2):504-11. doi: 10.1006/bbrc.1999.1820. PubMed PMID: 10600532.
1774 138. Zhou Q, Zhao J, Al-Zoghaibi F, Zhou A, Wiedmer T, Silverman RH, et al. Transcriptional
1775 control of the human plasma membrane phospholipid scramblase 1 gene is mediated by
1776 interferon-alpha. Blood. 2000;95(8):2593-9. PubMed PMID: 10753839.
1777 139. Zhou Q, Zhao J, Wiedmer T, Sims PJ. Normal hemostasis but defective hematopoietic
1778 response to growth factors in mice deficient in phospholipid scramblase 1. Blood.
1779 2002;99(11):4030-8. doi: 10.1182/blood-2001-12-0271. PubMed PMID: 12010804.
1780 140. Kusano S, Eizuru Y. Human phospholipid scramblase 1 interacts with and regulates
1781 transactivation of HTLV-1 Tax. Virology. 2012;432(2):343-52. Epub 20120711. doi:
1782 10.1016/j.virol.2012.06.019. PubMed PMID: 22789739.
1783 141. Kusano S, Eizuru Y. Interaction of the phospholipid scramblase 1 with HIV-1 Tat results in
1784 the repression of Tat-dependent transcription. Biochem Biophys Res Commun. 2013;433(4):438-
1785 44. Epub 20130315. doi: 10.1016/j.bbrc.2013.02.098. PubMed PMID: 23501106.
1786 142. Sadanari H, Takemoto M, Ishida T, Otagiri H, Daikoku T, Murayama T, et al. The
1787 Interferon-Inducible Human PLSCR1 Protein Is a Restriction Factor of Human Cytomegalovirus.
1788 Microbiol Spectr. 2022;10(1):e0134221. Epub 2022/02/10. doi: 10.1128/spectrum.01342-21.
1789 PubMed PMID: 35138119; PubMed Central PMCID: PMCPMC8826943.
1790 143. Metz P, Dazert E, Ruggieri A, Mazur J, Kaderali L, Kaul A, et al. Identification of type I and
1791 type II interferon-induced effectors controlling hepatitis C virus replication. Hepatology.
1792 2012;56(6):2082-93. Epub 20121014. doi: 10.1002/hep.25908. PubMed PMID: 22711689.
1793 144. Yang J, Zhu X, Liu J, Ding X, Han M, Hu W, et al. Inhibition of Hepatitis B virus replication
1794 by phospholipid scramblase 1 in vitro and in vivo. Antiviral Res. 2012;94(1):9-17. Epub
1795 20120209. doi: 10.1016/j.antiviral.2012.01.010. PubMed PMID: 22342889.

145. Kusano S, Ikeda M. Interaction of phospholipid scramblase 1 with the Epstein-Barr virus protein BZLF1 represses BZLF1-mediated lytic gene transcription. J Biol Chem. 2019;294(41):15104-16. Epub 2019/08/23. doi: 10.1074/jbc.RA119.008193. PubMed PMID: 31434743; PubMed Central PMCID: PMCPMC6791327.
146. Luo W, Zhang J, Liang L, Wang G, Li Q, Zhu P, et al. Phospholipid scramblase 1 interacts with influenza A virus NP, impairing its nuclear import and thereby suppressing virus replication. PLoS Pathog. 2018;14(1):e1006851. Epub 20180119. doi: 10.1371/journal.ppat.1006851. PubMed PMID: 29352288; PubMed Central PMCID: PMCPMC5792031.
147. Dal Col J, Lamberti MJ, Nigro A, Casolaro V, Fratta E, Steffan A, et al. Phospholipid scramblase 1: a protein with multiple functions via multiple molecular interactors. Cell Commun Signal. 2022;20(1):78. Epub 2022/06/02. doi: 10.1186/s12964-022-00895-3. PubMed PMID: 35650588.
148. Jonathan RS-G, Audrey A, Payman S-T, Hala A, Vinitha M, Dae-Kyum K, et al. A SARS-CoV-2 BioID-based virus-host membrane protein interactome and virus peptide compendium: new proteomics resources for COVID-19 research. bioRxiv. 2020:2020.08.28.269175. doi: 10.1101/2020.08.28.269175.
149. Guo K, Barrett BS, Morrison JH, Mickens KL, Vladar EK, Hasenkrug KJ, et al. Interferon resistance of emerging SARS-CoV-2 variants. Proc Natl Acad Sci U S A. 2022;119(32):e2203760119. Epub 20220722. doi: 10.1073/pnas.2203760119. PubMed PMID: 35867811; PubMed Central PMCID: PMCPMC9371743.
150. Shalamova L, Felgenhauer U, Wilhelm J, Schaubmar AR, Buttner K, Schoen A, et al. Omicron variant of SARS-CoV-2 exhibits an increased resilience to the antiviral type I interferon response. PNAS Nexus. 2022;1(2):pgac067. Epub 20220523. doi: 10.1093/pnasnexus/pgac067. PubMed PMID: 36713328; PubMed Central PMCID: PMCPMC9802332.
151. Shi G, Li T, Lai KK, Johnson RF, Yewdell JW, Compton AA. Omicron Spike confers enhanced infectivity and interferon resistance to SARS-CoV-2 in human nasal tissue. Nat Commun. 2024;15(1):889. Epub 20240130. doi: 10.1038/s41467-024-45075-8. PubMed PMID: 38291024; PubMed Central PMCID: PMCPMC10828397.
152. Willett BJ, Grove J, MacLean OA, Wilkie C, De Lorenzo G, Furnon W, et al. SARS-CoV-2 Omicron is an immune escape variant with an altered cell entry pathway. Nat Microbiol. 2022;7(8):1161-79. Epub 20220707. doi: 10.1038/s41564-022-01143-7. PubMed PMID: 35798890; PubMed Central PMCID: PMCPMC9352574.
153. Peacock TP, Brown JC, Zhou J, Thakur N, Sukhova K, Newman J, et al. The altered entry pathway and antigenic distance of the SARS-CoV-2 Omicron variant map to separate domains of spike protein. bioRxiv. 2022:2021.12.31.474653. doi: 10.1101/2021.12.31.474653.
154. Sette A, Crotty S. Adaptive immunity to SARS-CoV-2 and COVID-19. Cell. 2021;184(4):861-80. Epub 20210112. doi: 10.1016/j.cell.2021.01.007. PubMed PMID: 33497610; PubMed Central PMCID: PMCPMC7803150.
155. Chen S, Francioli LC, Goodrich JK, Collins RL, Kanai M, Wang Q, et al. A genomic mutational constraint map using variation in 76,156 human genomes. Nature. 2024;625(7993):92-100. doi: 10.1038/s41586-023-06045-0.
156. Mar KB, Van Dyke MC, Lopez AH, Eitson JL, Fan W, Hanners NW, et al. LY6E protects mice from pathogenic effects of murine coronavirus and SARS-CoV-2. bioRxiv. 2023. Epub 20230126.

1839 doi: 10.1101/2023.01.25.525551. PubMed PMID: 36747632; PubMed Central PMCID:
1840 PMCPMC9900800.
1841 157. Pfaender S, Mar KB, Michailidis E, Kratzel A, Boys IN, V'Kovski P, et al. LY6E impairs
1842 coronavirus fusion and confers immune control of viral disease. Nat Microbiol. 2020;5(11):1330-
1843 9. Epub 20200723. doi: 10.1038/s41564-020-0769-y. PubMed PMID: 32704094; PubMed
1844 Central PMCID: PMCPMC7916999.
1845 158. Consortium GT. The Genotype-Tissue Expression (GTEx) project. Nat Genet.
1846 2013;45(6):580-5. doi: 10.1038/ng.2653. PubMed PMID: 23715323; PubMed Central PMCID:
1847 PMCPMC4010069.
1848 159. Blight KJ, McKeating JA, Rice CM. Highly permissive cell lines for subgenomic and
1849 genomic hepatitis C virus RNA replication. J Virol. 2002;76(24):13001-14. doi:
1850 10.1128/jvi.76.24.13001-13014.2002. PubMed PMID: 12438626; PubMed Central PMCID:
1851 PMCPMC136668.
1852 160. Zhang L, Bukreyev A, Thompson CI, Watson B, Peeples ME, Collins PL, et al. Infection of
1853 ciliated cells by human parainfluenza virus type 3 in an in vitro model of human airway
1854 epithelium. J Virol. 2005;79(2):1113-24. doi: 10.1128/JVI.79.2.1113-1124.2005. PubMed PMID:
1855 15613339; PubMed Central PMCID: PMCPMC538579.
1856 161. Hoffmann HH, Schneider WM, Rozen-Gagnon K, Miles LA, Schuster F, Razooky B, et al.
1857 TMEM41B Is a Pan-flavivirus Host Factor. Cell. 2021;184(1):133-48 e20. Epub 20201209. doi:
1858 10.1016/j.cell.2020.12.005. PubMed PMID: 33338421; PubMed Central PMCID:
1859 PMCPMC7954666.
1860 162. Benboudjema L, Mulvey M, Gao Y, Pimplikar SW, Mohr I. Association of the herpes
1861 simplex virus type 1 Us11 gene product with the cellular kinesin light-chain-related protein PAT1
1862 results in the redistribution of both polypeptides. J Virol. 2003;77(17):9192-203. doi:
1863 10.1128/jvi.77.17.9192-9203.2003. PubMed PMID: 12915535; PubMed Central PMCID:
1864 PMCPMC187382.
1865 163. Lee D, Le Pen J, Yatim A, Dong B, Aquino Y, Ogishi M, et al. Inborn errors of OAS-RNase L
1866 in SARS-CoV-2-related multisystem inflammatory syndrome in children. Science.
1867 2023;379(6632):eabo3627. Epub 20230210. doi: 10.1126/science.abo3627. PubMed PMID:
1868 36538032.
1869 164. Mendoza EJ, Manguiat K, Wood H, Drebot M. Two Detailed Plaque Assay Protocols for
1870 the Quantification of Infectious SARS-CoV-2. Curr Protoc Microbiol. 2020;57(1):ecpmc105. doi:
1871 10.1002/cpmc.105. PubMed PMID: 32475066; PubMed Central PMCID: PMCPMC7300432.
1872 165. Polo JM, Davis NL, Rice CM, Huang HV, Johnston RE. Molecular analysis of Sindbis virus
1873 pathogenesis in neonatal mice by using virus recombinants constructed in vitro. J Virol.
1874 1988;62(6):2124-33. doi: 10.1128/JVI.62.6.2124-2133.1988. PubMed PMID: 2835514; PubMed
1875 Central PMCID: PMCPMC253309.
1876 166. Bick MJ, Carroll JW, Gao G, Goff SP, Rice CM, MacDonald MR. Expression of the zinc-
1877 finger antiviral protein inhibits alphavirus replication. J Virol. 2003;77(21):11555-62. doi:
1878 10.1128/jvi.77.21.11555-11562.2003. PubMed PMID: 14557641; PubMed Central PMCID:
1879 PMCPMC229374.
1880 167. Atasheva S, Kim DY, Akhrymuk M, Morgan DG, Frolova EI, Frolov I. Pseudoinfectious
1881 Venezuelan equine encephalitis virus: a new means of alphavirus attenuation. J Virol.

2013;87(4):2023-35. Epub 20121205. doi: 10.1128/JVI.02881-12. PubMed PMID: 23221545; PubMed Central PMCID: PMCPMC3571482.
168. Dalton KP, Rose JK. Vesicular stomatitis virus glycoprotein containing the entire green fluorescent protein on its cytoplasmic domain is incorporated efficiently into virus particles. Virology. 2001;279(2):414-21. doi: 10.1006/viro.2000.0736. PubMed PMID: 11162797.
169. Dobin A, Davis CA, Schlesinger F, Drenkow J, Zaleski C, Jha S, et al. STAR: ultrafast universal RNA-seq aligner. Bioinformatics. 2013;29(1):15-21. Epub 20121025. doi: 10.1093/bioinformatics/bts635. PubMed PMID: 23104886; PubMed Central PMCID: PMCPMC3530905.
170. Liao Y, Smyth GK, Shi W. The R package Rsubread is easier, faster, cheaper and better for alignment and quantification of RNA sequencing reads. Nucleic Acids Res. 2019;47(8):e47. doi: 10.1093/nar/gkz114. PubMed PMID: 30783653; PubMed Central PMCID: PMCPMC6486549.
171. Love MI, Huber W, Anders S. Moderated estimation of fold change and dispersion for RNA-seq data with DESeq2. Genome Biol. 2014;15(12):550. doi: 10.1186/s13059-014-0550-8. PubMed PMID: 25516281; PubMed Central PMCID: PMCPMC4302049.
172. Korotkevich G, Sukhov V, Budin N, Shpak B, Artyomov MN, Sergushichev A. Fast gene set enrichment analysis. bioRxiv. 2021:060012. doi: 10.1101/060012.
173. Liberzon A, Subramanian A, Pinchback R, Thorvaldsdottir H, Tamayo P, Mesirov JP. Molecular signatures database (MSigDB) 3.0. Bioinformatics. 2011;27(12):1739-40. Epub 20110505. doi: 10.1093/bioinformatics/btr260. PubMed PMID: 21546393; PubMed Central PMCID: PMCPMC3106198.
174. Fabregat A, Jupe S, Matthews L, Sidiropoulos K, Gillespie M, Garapati P, et al. The Reactome Pathway Knowledgebase. Nucleic Acids Res. 2018;46(D1):D649-D55. doi: 10.1093/nar/gkx1132. PubMed PMID: 29145629; PubMed Central PMCID: PMCPMC5753187.
175. Kanehisa M, Goto S. KEGG: kyoto encyclopedia of genes and genomes. Nucleic Acids Res. 2000;28(1):27-30. doi: 10.1093/nar/28.1.27. PubMed PMID: 10592173; PubMed Central PMCID: PMCPMC102409.
176. Agrawal A, Balci H, Hanspers K, Coort SL, Martens M, Slenter DN, et al. WikiPathways 2024: next generation pathway database. Nucleic Acids Res. 2024;52(D1):D679-D89. doi: 10.1093/nar/gkad960. PubMed PMID: 37941138; PubMed Central PMCID: PMCPMC10767877.
177. Schaefer CF, Anthony K, Krupa S, Buchoff J, Day M, Hannay T, et al. PID: the Pathway Interaction Database. Nucleic Acids Res. 2009;37(Database issue):D674-9. Epub 20081002. doi: 10.1093/nar/gkn653. PubMed PMID: 18832364; PubMed Central PMCID: PMCPMC2686461.
178. Nishimura D. BioCarta. Biotech Software & Internet Report: The Computer Software Journal for Scient. 2001;2(3):117-20.
179. Schmittgen TD, Livak KJ. Analyzing real-time PCR data by the comparative C(T) method. Nat Protoc. 2008;3(6):1101-8. doi: 10.1038/nprot.2008.73. PubMed PMID: 18546601.
180. Dittmann M, Hoffmann HH, Scull MA, Gilmore RH, Bell KL, Ciancanelli M, et al. A serpin shapes the extracellular environment to prevent influenza A virus maturation. Cell. 2015;160(4):631-43. doi: 10.1016/j.cell.2015.01.040. PubMed PMID: 25679759; PubMed Central PMCID: PMC4328142.
181. Majdoul S, Compton AA. Lessons in self-defence: inhibition of virus entry by intrinsic immunity. Nat Rev Immunol. 2022;22(6):339-52. Epub 20211013. doi: 10.1038/s41577-021-00626-8. PubMed PMID: 34646033; PubMed Central PMCID: PMCPMC8511856.

1926 182. Bruchez A, Sha K, Johnson J, Chen L, Stefani C, McConnell H, et al. MHC class II
1927 transactivator CIITA induces cell resistance to Ebola virus and SARS-like coronaviruses. Science.
1928 2020;370(6513):241-7. Epub 20200827. doi: 10.1126/science.abb3753. PubMed PMID:
1929 32855215; PubMed Central PMCID: PMCPMC7665841.
1930 183. Doyle T, Moncorge O, Bonaventure B, Pollpeter D, Lussignol M, Tauziet M, et al. The
1931 interferon-inducible isoform of NCOA7 inhibits endosome-mediated viral entry. Nat Microbiol.
1932 2018;3(12):1369-76. Epub 20181126. doi: 10.1038/s41564-018-0273-9. PubMed PMID:
1933 30478388; PubMed Central PMCID: PMCPMC6329445.
1934

Figure 1

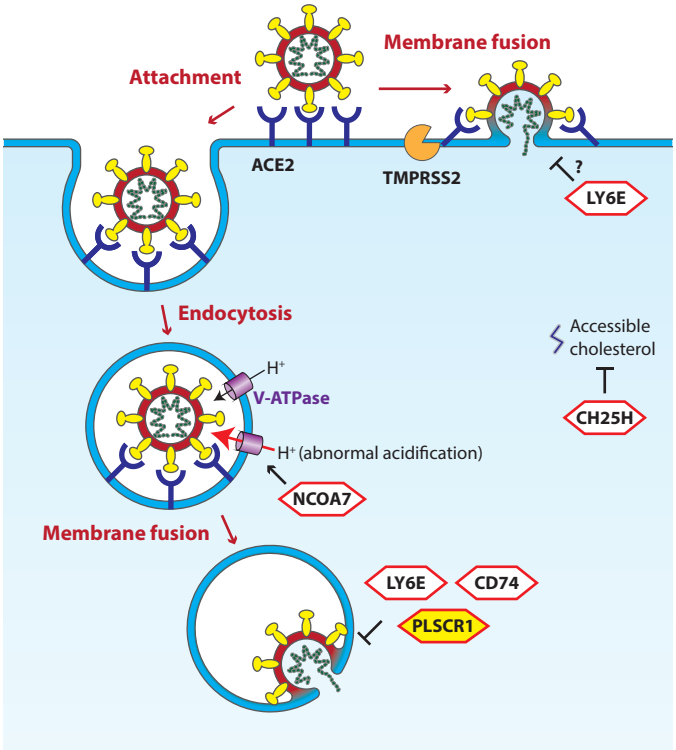
Attachment
Membrane fusion
ACE2
TMPRSS2
?
LY6E
Endocytosis
Accessible cholesterol
H+
V-ATPase
CH25H
H+ (abnormal acidification)
NCOA7
Membrane fusion
LY6E
CD74
PLSCR1

Figure 2

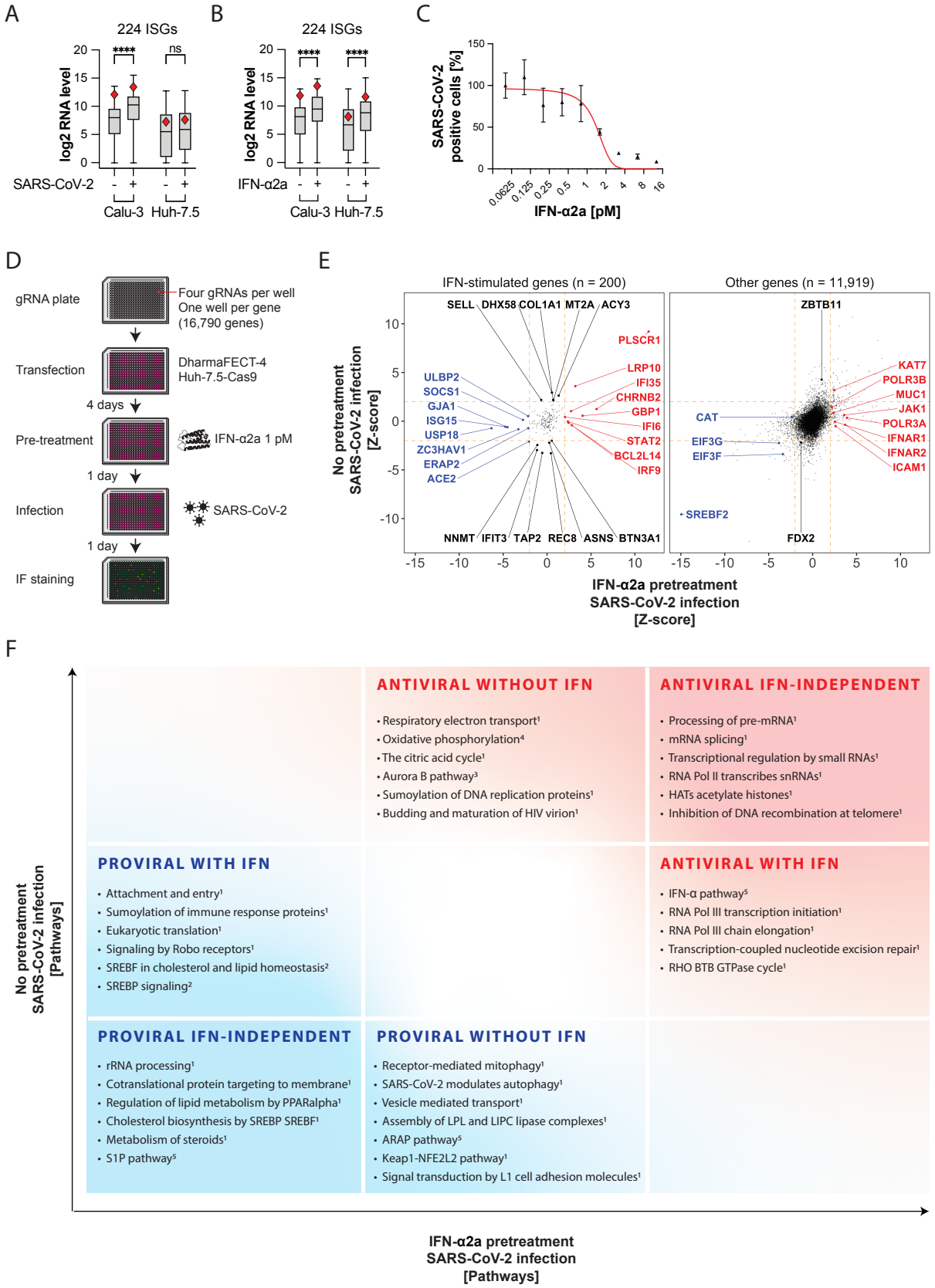
A
224 ISGs
log2 RNA level
****
ns
SARS-CoV-2
Calu-3
Huh-7.5
B
224 ISGs
log2 RNA level
****
****
IFN-α2a
Calu-3
Huh-7.5
C
SARS-CoV-2 positive cells [%]
IFN-α2a [pM]
D
gRNA plate
Four gRNAs per well
One well per gene
(16,790 genes)
Transfection
DharmaFECT-4
Huh-7.5-Cas9
4 days
Pre-treatment
IFN-α2a 1 pM
1 day
Infection
SARS-CoV-2
1 day
IF staining
E
IFN-stimulated genes (n = 200)
Other genes (n = 11,919)
No pretreatment SARS-CoV-2 infection [Z-score]
IFN-α2a pretreatment SARS-CoV-2 infection [Z-score]
SELL
DHX58
COL1A1
MT2A
ACY3
PLSCR1
LRP10
IFI35
CHRNB2
GBP1
IFI6
STAT2
BCL2L14
IRF9
ULBP2
SOCS1
GJA1
ISG15
USP18
ZC3HAV1
ERAP2
ACE2
NNMT
IFIT3
TAP2
REC8
ASNS
BTN3A1
ZBTB11
KAT7
POLR3B
MUC1
JAK1
POLR3A
IFNAR1
IFNAR2
ICAM1
CAT
EIF3G
EIF3F
SREBF2
FDX2
F
No pretreatment SARS-CoV-2 infection [Pathways]
IFN-α2a pretreatment SARS-CoV-2 infection [Pathways]
ANTIVIRAL WITHOUT IFN
• Respiratory electron transport¹
• Oxidative phosphorylation⁴
• The citric acid cycle¹
• Aurora B pathway³
• Sumoylation of DNA replication proteins¹
• Budding and maturation of HIV virion¹
ANTIVIRAL IFN-INDEPENDENT
• Processing of pre-mRNA¹
• mRNA splicing¹
• Transcriptional regulation by small RNAs¹
• RNA Pol II transcribes snRNAs¹
• HATs acetylate histones¹
• Inhibition of DNA recombination at telomere¹
PROVIRAL WITH IFN
• Attachment and entry¹
• Sumoylation of immune response proteins¹
• Eukaryotic translation¹
• Signaling by Robo receptors¹
• SREBF in cholesterol and lipid homeostasis²
• SREBP signaling²
ANTIVIRAL WITH IFN
• IFN-α pathway⁵
• RNA Pol III transcription initiation¹
• RNA Pol III chain elongation¹
• Transcription-coupled nucleotide excision repair¹
• RHO BTB GTPase cycle¹
PROVIRAL IFN-INDEPENDENT
• rRNA processing¹
• Cotranslational protein targeting to membrane¹
• Regulation of lipid metabolism by PPARalpha¹
• Cholesterol biosynthesis by SREBP SREBF¹
• Metabolism of steroids¹
• S1P pathway⁵
PROVIRAL WITHOUT IFN
• Receptor-mediated mitophagy¹
• SARS-CoV-2 modulates autophagy¹
• Vesicle mediated transport¹
• Assembly of LPL and LIPC lipase complexes¹
• ARAP pathway⁵
• Keap1-NFE2L2 pathway¹
• Signal transduction by L1 cell adhesion molecules¹

Figure 3

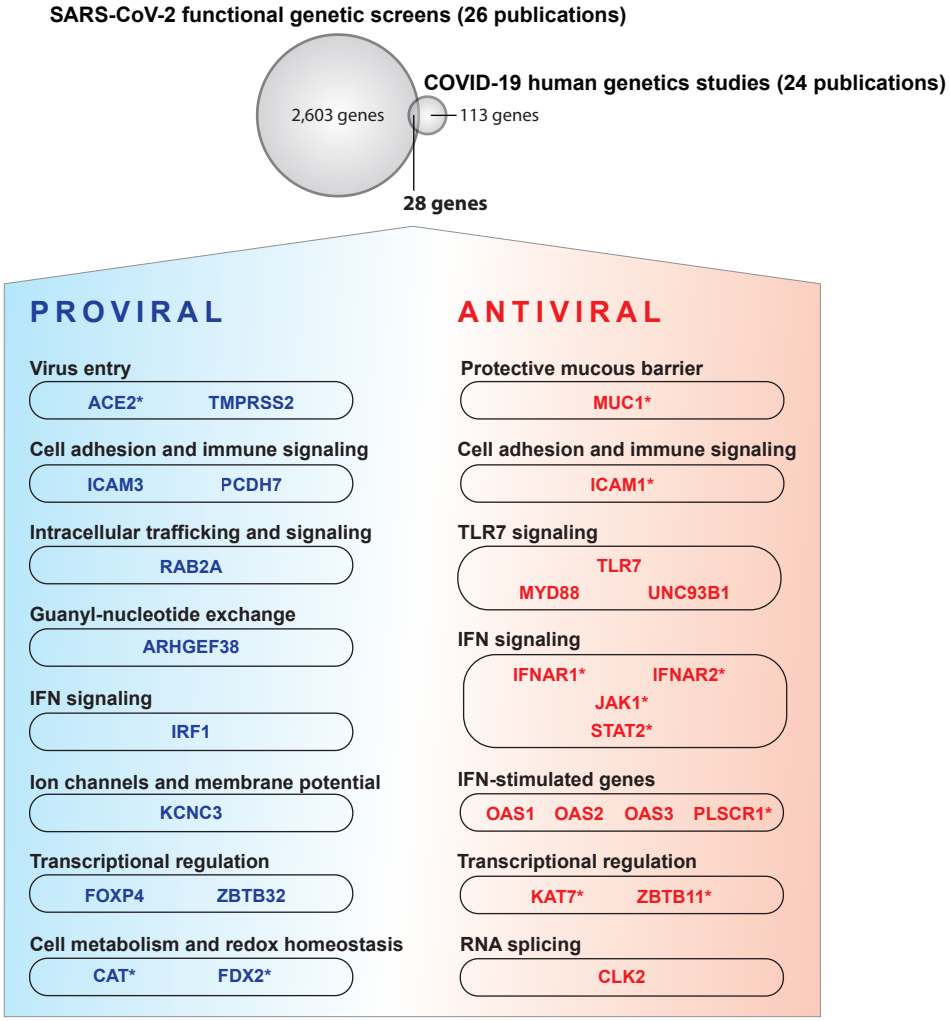

* Hit in arrayed CRISPR KO screen.

Figure 4

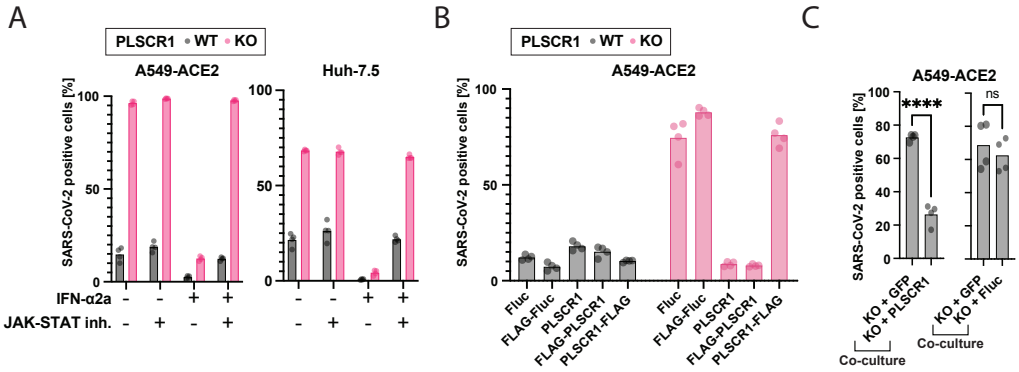
A
PLSCR1 WT KO
A549-ACE2
Huh-7.5
SARS-CoV-2 positive cells [%]
100
50
0
IFN-α2a - - + +
JAK-STAT inh. - + - +
B
PLSCR1 WT KO
A549-ACE2
Fluc
FLAG-Fluc
PLSCR1
FLAG-PLSCR1
PLSCR1-FLAG
C
A549-ACE2
****
ns
KO + GFP
KO + PLSCR1
KO + Fluc
Co-culture

Figure 5

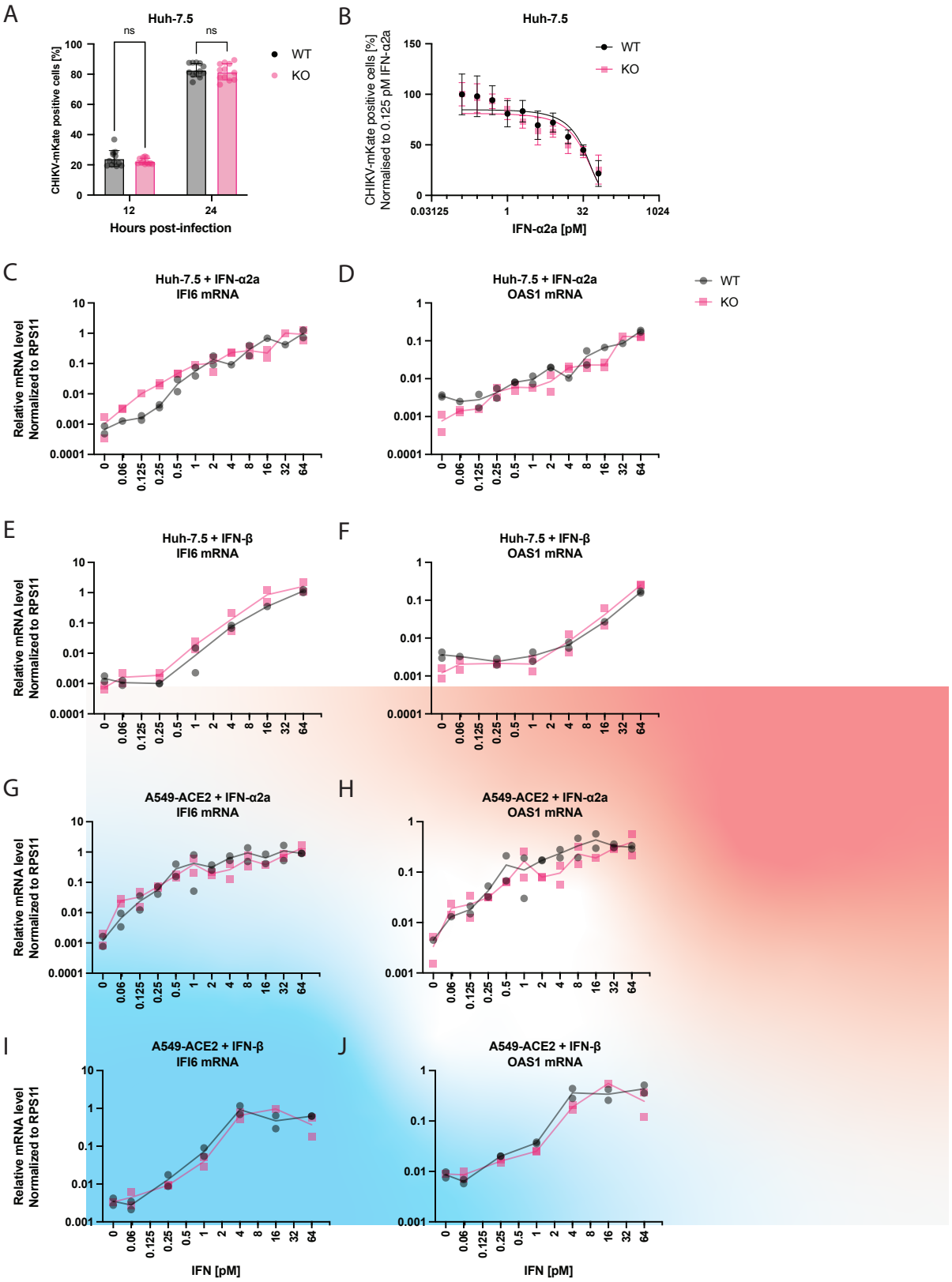
A
Huh-7.5
ns
ns
CHIKV-mKate positive cells [%]
WT
KO
Hours post-infection
B
Huh-7.5
CHIKV-mKate positive cells [%]
Normalised to 0.125 pM IFN-α2a
IFN-α2a [pM]
C
Huh-7.5 + IFN-α2a
IFI6 mRNA
Relative mRNA level
Normalized to RPS11
D
Huh-7.5 + IFN-α2a
OAS1 mRNA
E
Huh-7.5 + IFN-β
IFI6 mRNA
F
Huh-7.5 + IFN-β
OAS1 mRNA
G
A549-ACE2 + IFN-α2a
IFI6 mRNA
H
A549-ACE2 + IFN-α2a
OAS1 mRNA
I
A549-ACE2 + IFN-β
IFI6 mRNA
J
A549-ACE2 + IFN-β
OAS1 mRNA
IFN [pM]

Figure 6

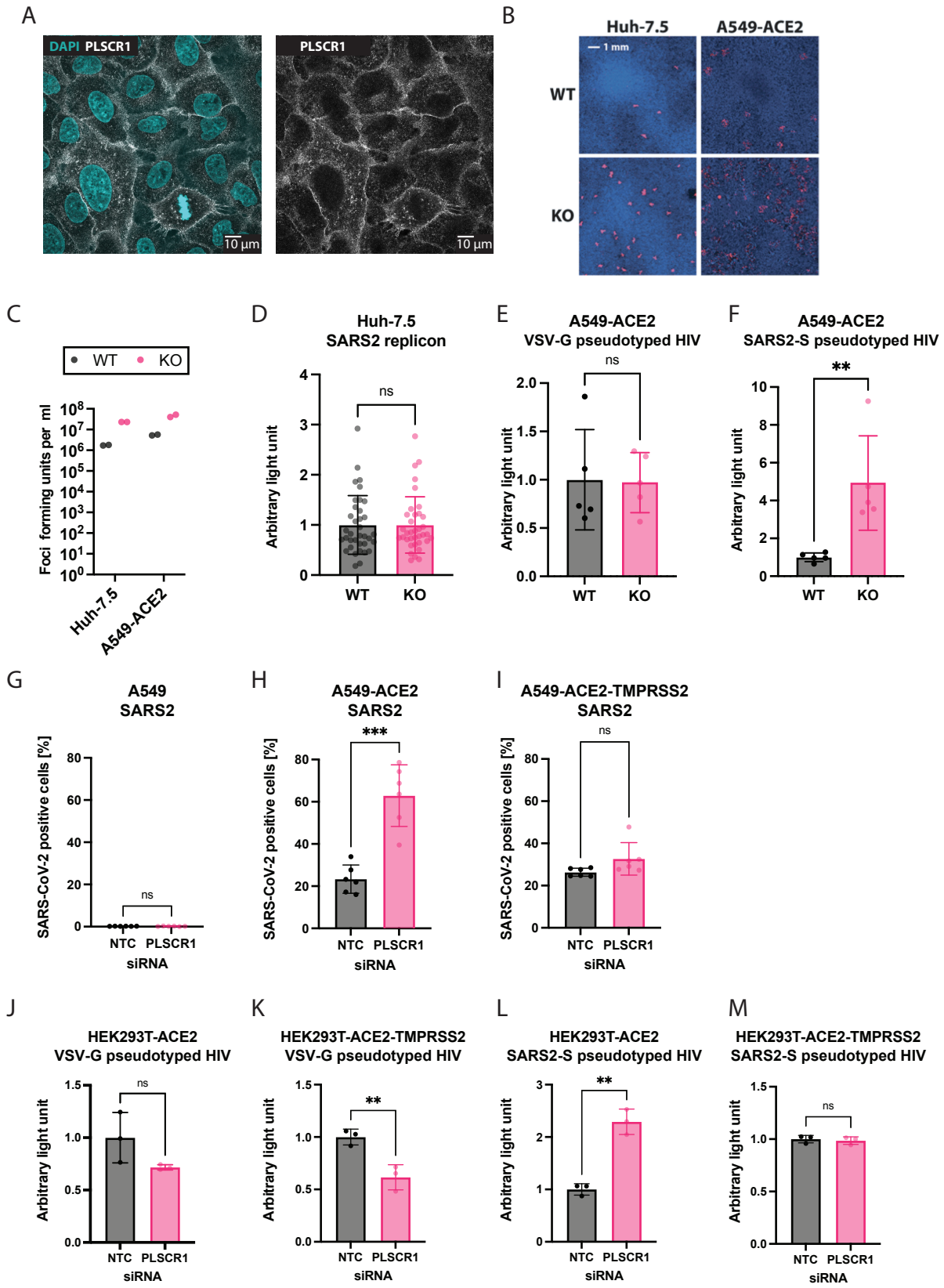
A
DAPI PLSCR1
10 µm
PLSCR1
10 µm
B
Huh-7.5
A549-ACE2
1 mm
WT
KO
C
WT
KO
Foci forming units per ml
Huh-7.5
A549-ACE2
D
Huh-7.5
SARS2 replicon
Arbitrary light unit
ns
WT
KO
E
A549-ACE2
VSV-G pseudotyped HIV
ns
F
A549-ACE2
SARS2-S pseudotyped HIV
**
G
A549
SARS2
SARS-CoV-2 positive cells [%]
ns
NTC
PLSCR1
siRNA
H
A549-ACE2
SARS2
***
I
A549-ACE2-TMPRSS2
SARS2
J
HEK293T-ACE2
VSV-G pseudotyped HIV
K
HEK293T-ACE2-TMPRSS2
VSV-G pseudotyped HIV
L
HEK293T-ACE2
SARS2-S pseudotyped HIV
M
HEK293T-ACE2-TMPRSS2
SARS2-S pseudotyped HIV

Figure 7

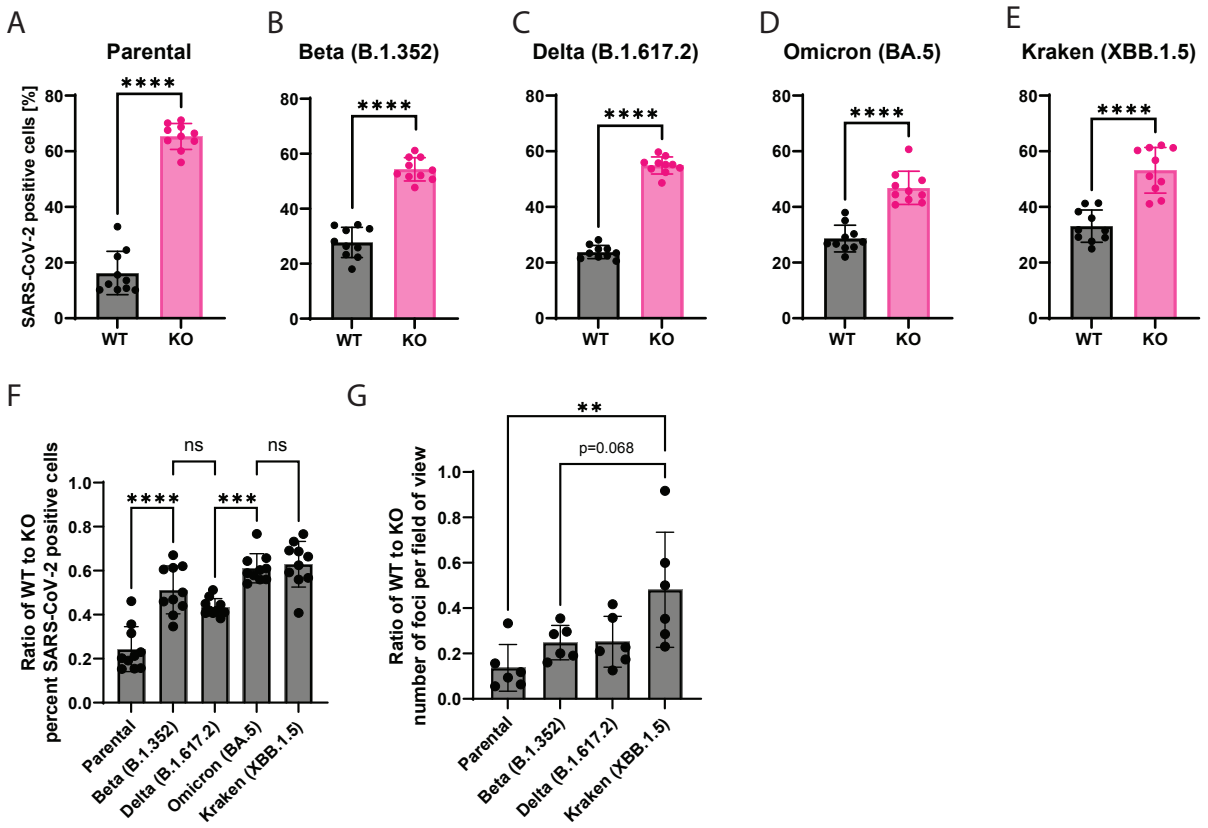
A
Parental
B
Beta (B.1.352)
C
Delta (B.1.617.2)
D
Omicron (BA.5)
E
Kraken (XBB.1.5)
SARS-CoV-2 positive cells [%]
****
WT
KO
F
Ratio of WT to KO
percent SARS-CoV-2 positive cells
****
***
ns
ns
Parental
Beta (B.1.352)
Delta (B.1.617.2)
Omicron (BA.5)
Kraken (XBB.1.5)
G
Ratio of WT to KO
number of foci per field of view
**
p=0.068

Figure 8

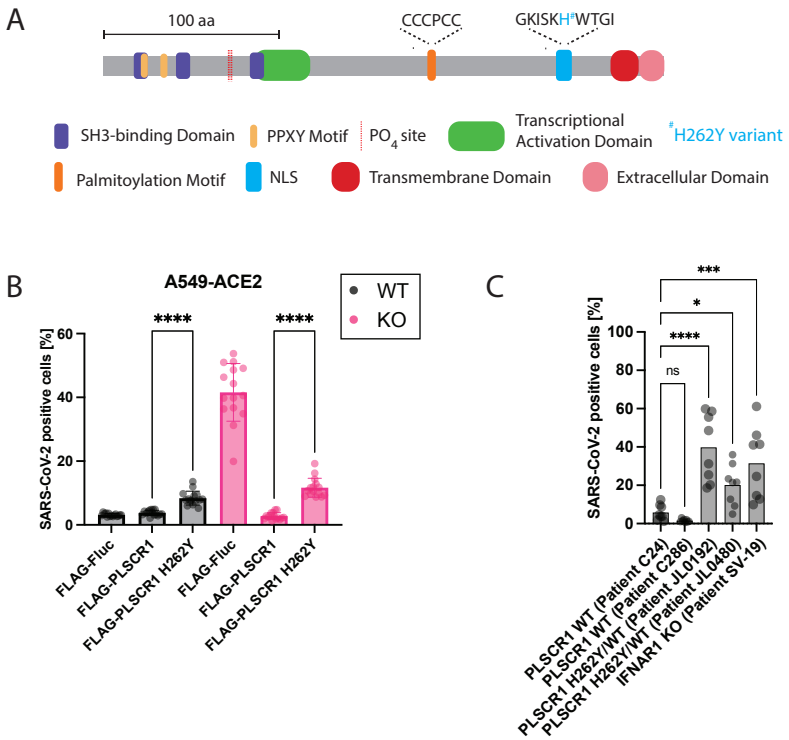
A
100 aa
CCCPCC
GKISKH#WTGI
SH3-binding Domain
PPXY Motif
PO4 site
Transcriptional Activation Domain
#H262Y variant
Palmitoylation Motif
NLS
Transmembrane Domain
Extracellular Domain
B
A549-ACE2
WT
KO
SARS-CoV-2 positive cells [%]
****
****
FLAG-Fluc
FLAG-PLSCR1
FLAG-PLSCR1 H262Y
FLAG-Fluc
FLAG-PLSCR1
FLAG-PLSCR1 H262Y
C
SARS-CoV-2 positive cells [%]
***
*
****
ns
PLSCR1 WT (Patient C24)
PLSCR1 WT (Patient C286)
PLSCR1 H262Y/WT (Patient JL0192)
PLSCR1 H262Y/WT (Patient JL0430)
IFNAR1 KO (Patient SV-19)

Supplementary figure 1

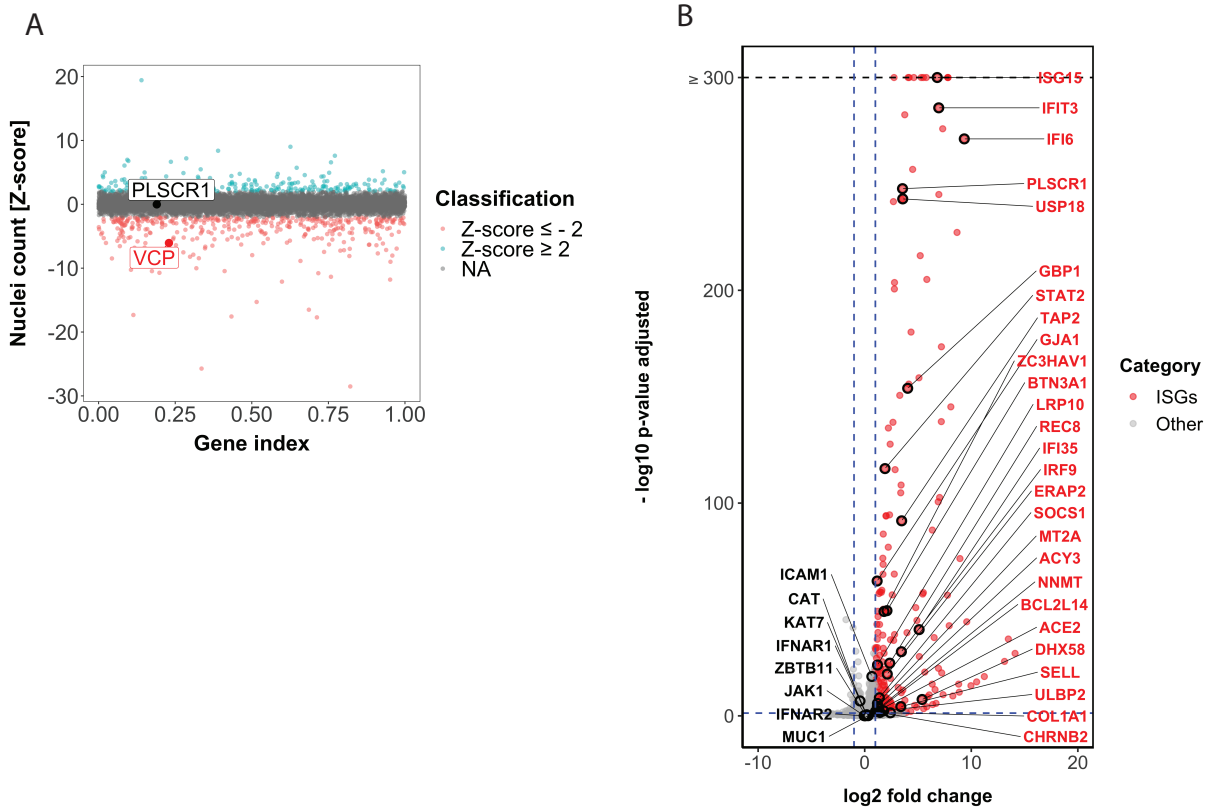

Supplementary figure 2

A

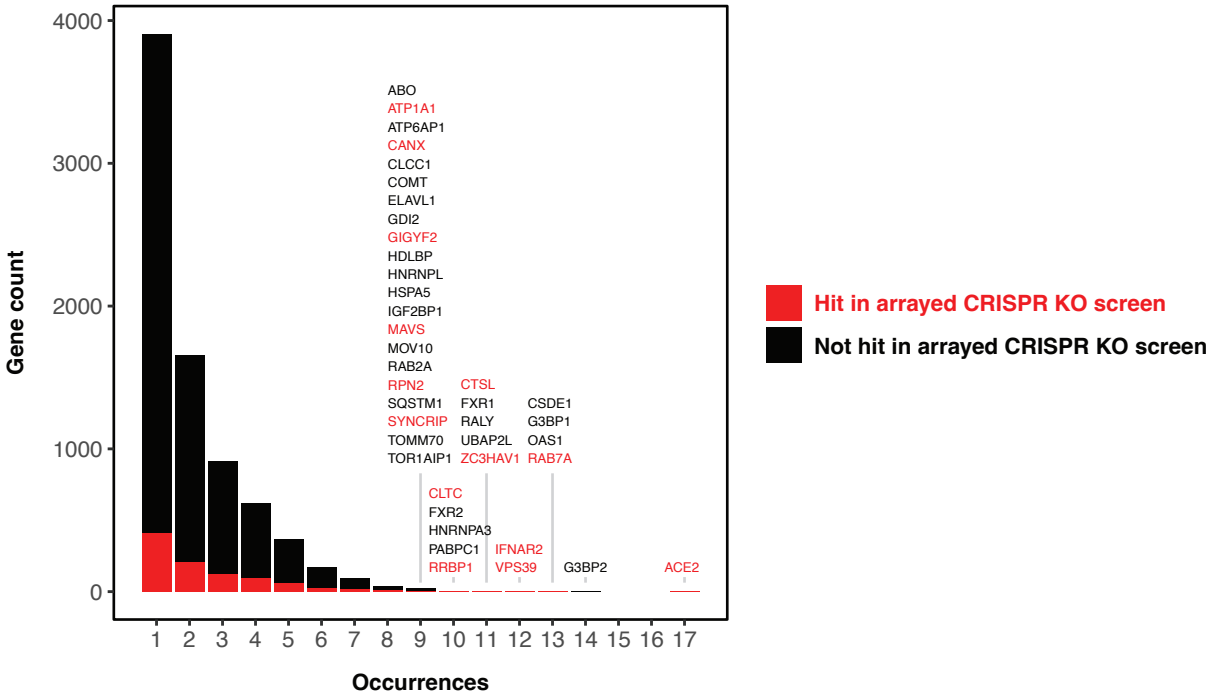

B

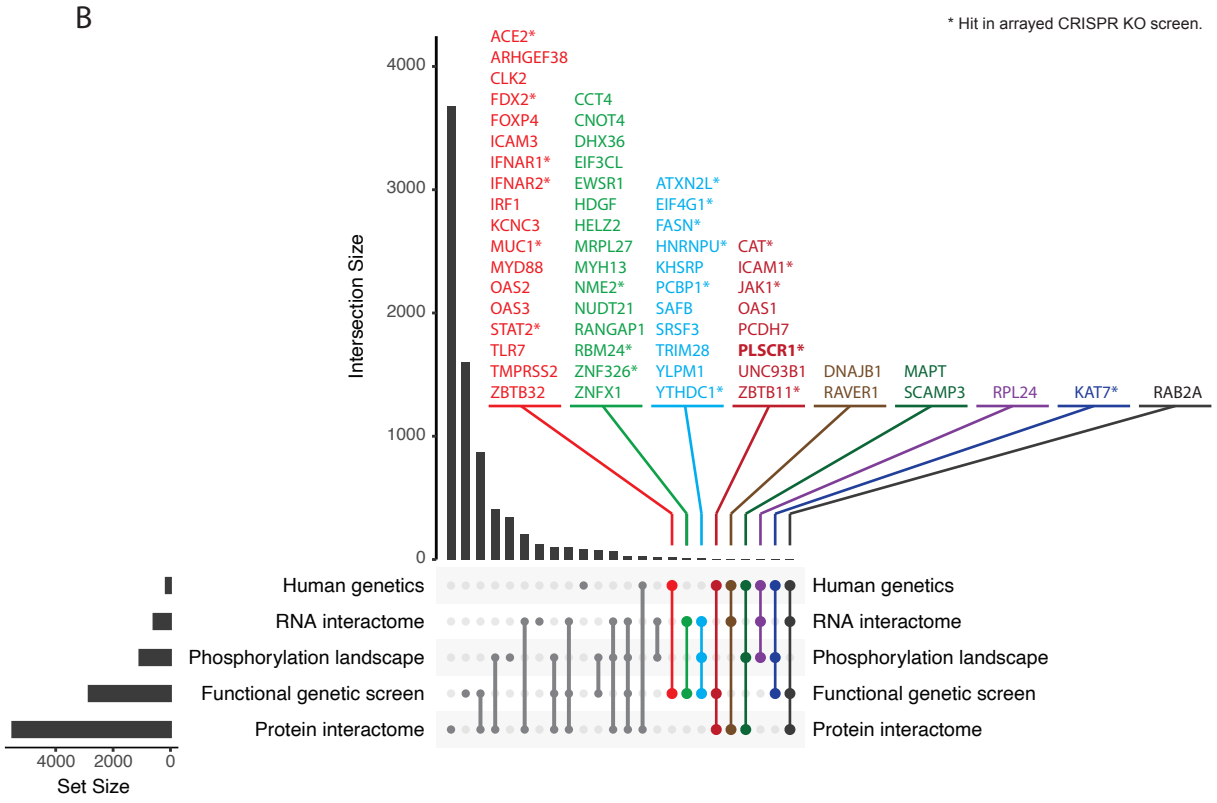

Supplementary figure 3

A

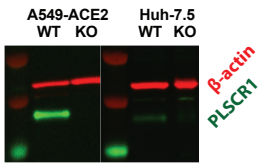

B

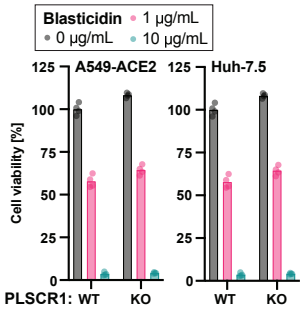

C

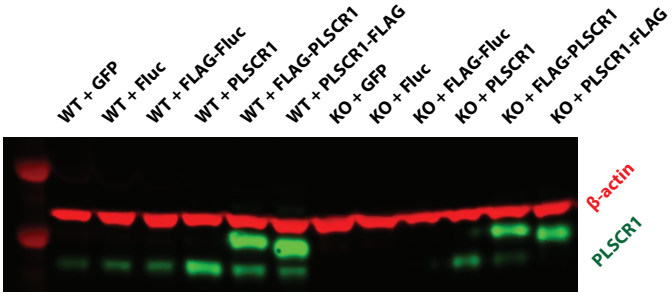

Supplementary figure 4

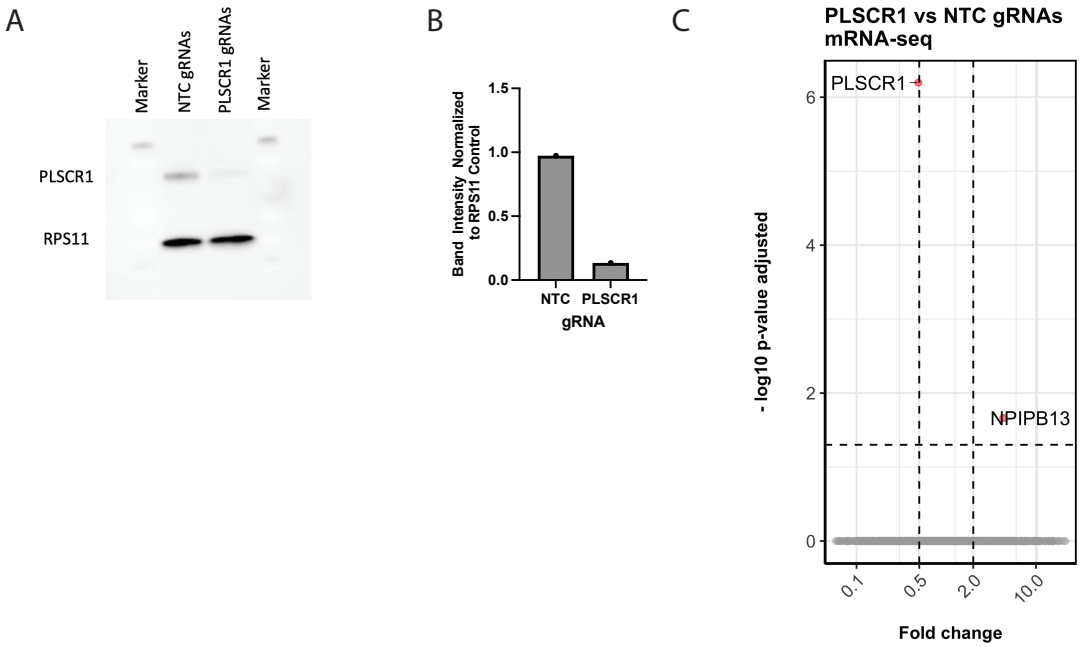

Supplementary figure 5

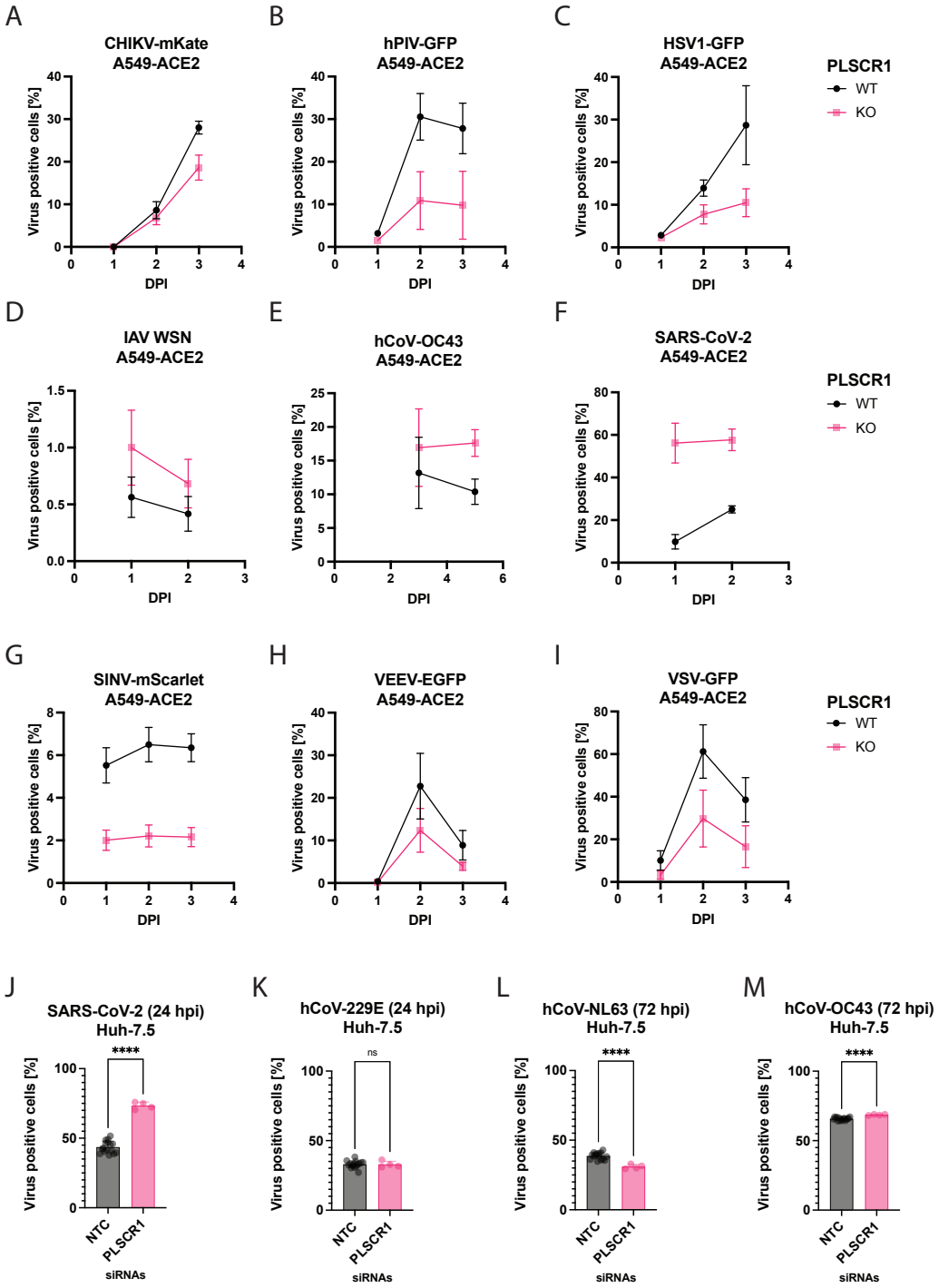

Supplementary figure 6

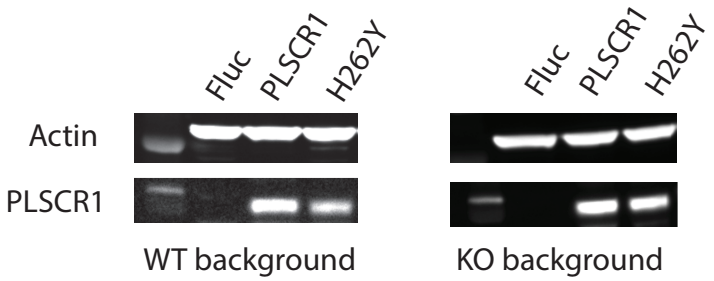

Supplementary figure 7

A

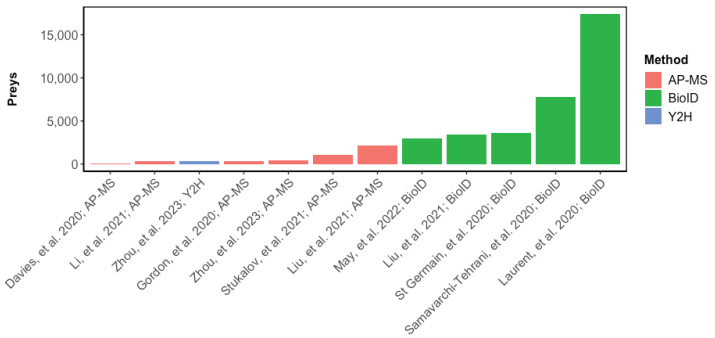

B

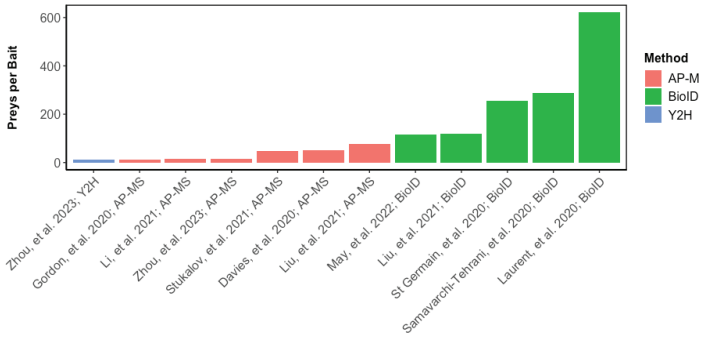
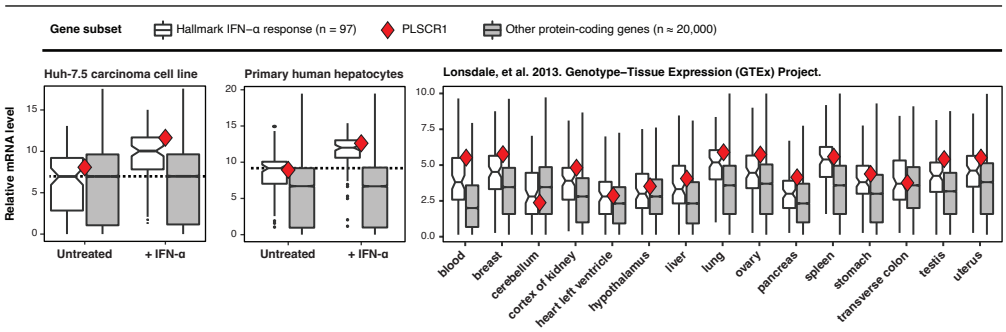
Supplementary figure 8